Using 3D reconstruction to analyse early mouse development

Renske M. Brune

Thesis submitted for the degree of

Doctor of Philosophy

University of Edinburgh

2001

ABSTRACT

Our current description of mouse developmental anatomy has mainly been based on studies using SEM, confocal, light or dissecting microscopy and, as the resulting picture gives an incomplete understanding of 3D morphological relationships within the embryo, it is inadequate for current molecular and genetic studies. The work reported here sets out to improve the situation by describing novel aspects of mouse developmental anatomy obtained from the analysis of 3D digital reconstructions of serial sections of mouse embryos at embryonic days 1-9 (E1-9) within which all anatomically defined tissues were delineated. These embryos were carefully selected for being representative of their developmental stage and reconstructions were checked for normal representation of tissues. The reconstructions contain histological detail accessible at any angle through the reconstruction within the reconstructions, while surface rendering software can display 3D tissue organisation.

These reconstructions have been used to examine three particular aspects of mouse development: geometric relationships in the early stages of mouse development, the morphological events that accompany turning, and the relative growth rates of the key tissues during early embryogenesis and organogenesis.

The geometric relationships of the reconstructions of E1-9 were analysed and compared to the existing description of mouse anatomy. New anatomical features could be described for nearly all stages. For example, there is evidence that axis formation occurs earlier than hitherto reported, namely at E5-6.5. Two blastocysts are bilaterally symmetric but only the earlier stage shows a tilt in the inner cell mass with respect to the embryonic-abembryonic axis. The tilt in the ectoplacental cone with respect to the latter axis is not at a consistent angle, but does coincide with an asymmetry in the extraembryonic ectoderm that could be explained by the tilt of the cone. During early organogenesis, the myocardial walls, cardiac jelly and endothelial lining are congruent. The vascular system develops in isolated sacs that are inline and link up later. There is no obvious morphological asymmetry between left and right components of structures.

Recent work on turning has, because of its link with the establishment of visceral organ laterality, generated a considerable amount of genetic and molecular data associated with these processes. Nevertheless, the mechanism by which the early rodent embryo acquires the normal foetal position remains unknown. The morphological analysis of turning

presented here provides new data. It appears that turning starts at the tail and hindbrain region and progresses medially. The medial region is also the last region to complete the process of turning. It is shown that not only the direction of turning is opposite to that of the rat, but also that the process is different. The data as a whole are more compatible with turning being driven by a global process such as growth rather than a local process such as tissue condensation.

There is currently no quantitative data on the growth of the mouse embryo and its constituent tissues over the entire age range studied. Because the tissue delineation process defines each tissue as a digital volume composed of voxels, it is relatively easy to obtain a direct measure of the volume of each tissue present in each developmental stage and so to obtain direct data on mouse growth, albeit in fixed material. The observations show that during egg cylinder stages there is a strong growth emphasis on mesodermal structures and the ectoplacental cone, and that, during early organogenesis, there is an overall slowing down of growth in the embryo. During the latter period the fastest growing tissue in the embryo is the cardiovascular system and the slowest the gut. There is no difference in volumes of left and right hand components of structures for the stages investigated.

The most important limitation of these models is that they are based on single, fixed embryos and that there is only one model per Theiler stage, albeit that each is typical of its stage. Nevertheless, these reconstructions have allowed us to obtain information about anatomy not readily obtainable using conventional approaches as well as being useful for teaching, for exploring anatomical relationships and for the graphical storage of gene-expression data. Perhaps most important, however, is the fact that the advance in our description of tissue geometry helps better define the anatomical problems to be solved by molecular analysis.

DECLARATION

I declare that:

(a) this thesis was composed by myself;

(b) the work presented here is my own, except where stated; and

(c) the work has not been submitted for any other degree or professional qualification

Renske M. Brune

ACKNOWLEDGEMENTS

I would like to thank my supervisors Dr. Jonathan Bard for his great inspiration and flexibility, good sense of humour and never ending energy to challenge the good and the bad I had written: and Prof. Matt Kaufman for his limitless knowledge and for his incredible willingness to proof-read even the worst of English, his fast turnover rate an his rock-steady belief in the good of anatomy.

I would like to thank the people in the MRC without whom I could never have done this work in the first place: Dr. Duncan Davidson for many helpful discussions; Dr. Richard Baldock and Margaret Stark for reconstructing, warping and normalising the reconstructions; Bill Hill for writing the digitisation and reconstruction software Allyson Ross for making the wonderful plastic sections; Duncan, Richard, Jonathan and Matt for creating the project in which I could produce this work

I would like to thank all my friends and family and in particular: Lorna, Cecilia, Amanda and Annick for preceding me through this fire. Amanda also thanks for proofreading while you only just got rid of your thesis! Annick thanks for being at the other end of the email line and empathising, the craft-clubbers thanks for providing me with mind-saving distraction. Thanks to my family: Richard, Tim, Jo and Mike, for providing this warm home in which I could be myself and keep sanity and thanks for putting up with my no doubt impossible behaviour without getting back to me (yet). Tim thanks for endless giggles and Rich for endless support, scientifically, practically and most of all, emotionally.

Finally, I would like to dedicate this work to the baby in my belly: thanks for being there all the time.

Table of Contents

CHAPTER 1: INTRODUCTION

1.1 GENERAL INTRODUCTION

A much better description of the morphology of normal embryonic development is needed in order to make full use of the large amounts of data that are becoming available from molecular and genetic experiments in developmental biology. The principal advantage to be gained from the availability of this additional information is that the tendency to look for answers to biological questions in a reductionist way is unlikely to lead to optimal understanding. Biological patterns are not hierarchical but closely entangled and interwoven. For example, the activity of a gene has an impact on the anatomical configuration of a component of the embryo, while this affects subsequent gene activity. Constant interaction between the genotype and the phenotype is therefore of critical importance. This is especially the case in the field of developmental biology where systems are studied over time during which anatomical changes evolve. This reason, plus the scale and quantity of the data being produced, creates a need to improve our current knowledge of mouse developmental anatomy.

There are numerous reasons why research is undertaken on the mouse as a model for humans, the most important ones being to facilitate the understanding of: tissues that evolve with a complicated geometry during development, tissues that play a key role in embryonic development, tissues that exhibit (gene related) functions in diseases or in the genesis of malformations, or a combination of the former three. A thorough and detailed knowledge of anatomy is therefore necessary when undertaking and interpreting all these types of research. In the case of complex geometrical development, it is essential to understand the 3D anatomical changes that occur over time, in order to be able to interpret and assess molecular data. Detailed anatomical knowledge is also required to gain information about topological organisation and the relationship between a tissue and its environment, particularly for transgenic animals. For an understanding of (gene related) diseases or malformations a detailed description of normal development is needed for establishing changes that may be observed that coincide with the onset of the disease state.

Early aspects of developmental anatomy have traditionally been studied using SEM or by the analysis of material under the dissecting microscope or by light microscopy for the analysis of histological features of the material under analysis. Although these approaches have certainly facilitated our understanding of developmental processes,

SEM and dissecting microscopy in themselves cannot give histological detail of the stages being studied. Equally, light microscopy of histological material cannot provide the necessary degree of 3D understanding because it is extremely difficult for most observers to make sense of data from more than a few sections without computational aid. Confocal microscopy is equally of very limited use in bridging the gaps between the two previously described methods, since it is principally used for fluorescent antibody labeling. The visual output is different from that obtained following gene expression labeling of histological sections: only a relatively small proportion of the cell contents and/or surroundings are stained, while the remainder of the embryo remains unstained.

One possible complementary approach involves the use of computer-aided three dimensional reconstruction of serially sectioned material. Computer-reconstructed embryos have now been produced for the Edinburgh Mouse Atlas (EMAP) project (Baldock et al., 1992; Ringwald et al., 1994; Davidson et al., 1997) and will form the spatial part of the framework. This work has also contributed to the development of the anatomy nomenclature (Bard *et al*, 1998) and a number of published papers (Kaufman *et al* 1997, Kaufman *et al* 1998). Some of the results have already been published (Brune *et al* 1999) and the reconstructions E5.5-E9, with mapped anatomy, are available on the EMAP CD-ROM volume 1 (Baldock *et al*, 2001), included at the back of this thesis. The CD-ROM currently has a distribution of about 4-5000. This framework is currently in use in a number of databases, including the Jackson Laboratory MGI and the MRC gene-expression database in Edinburgh. All required software has been developed specifically for the project and enabled hand-driven delineation of the anatomical domains by labeling voxels (volume elements) in the reconstruction. This allows separate tissues to be viewed in three dimensions using commercial software (in our case Advanced Visualisation System (AVS)) with the ability to refer back to the underlying histology where necessary. As well as being a tool for labeling anatomical domains in the reconstructions, the software also shows the histology together with transparent segmentation overlays at any arbitrary angle through the reconstruction.

This combination of reconstruction and segmentation of morphologically discrete anatomical domains and structures enables the viewer to review existing descriptions

of mouse developmental anatomy in greater detail than has hitherto been possible. The histological detail is preserved and can be viewed at arbitrary orientation. Moreover, with the visualising software, 3D overview of complicated geometry is now possible. The reconstructions of anatomically defined structures will aid the analysis of detailed histological relationships within an embryo, and, simultaneously, the delineated anatomy on the histological sections facilitates a detailed analysis of a given area within the embryo. By the use of these models, a more accurate descriptive account of mouse developmental anatomy can be provided than has hitherto been possible.

1.2 WORK PLAN

Embryos ranging from E1 - E9 were reconstructed after fixation, embedding, sectioning and staining using digitisation, alignment and warping software developed for the Mouse Atlas Project (http//:genex.gu.mrc.ac.uk). For embryos older than E8 the resolution provided by paraffin sections of 7μm was considered adequate for the reconstructions of these embryos, and the same serial sections that had been used in The Atlas of Mouse Development (Kaufman, 1992) were studied in order to ensure consistency between different reference sources. For the developmentally less advanced embryos a higher resolution was required, and therefore additional embryos were embedded in plastic and sectioned at a thickness of 2 μm. Resolution of the reconstructions was considered to be sufficient to view the morphological features of groups of cells but not, in general, provide information on cellular detail. Due to limitations in time only, one embryo per Theiler stage was reconstructed.

Computer-aided segmentation of these reconstructions, or digital models, into anatomical domains provided sets of anatomical (sub-) components which could then be viewed as transparent overlays on the 2-D histological background of these components, or in any arbitrary combination with other components in a 'pseudo'-3D view. The range of segmented components was guided by the anatomical database of mouse development (Bard *et al.*, 1998) and limited by the features visible within these reconstructions. In principle only tissues that were morphologically distinct when looking down a light microscope using magnification x100, were segmented.

These reconstructions were then used in various ways. Firstly, to compare the set of prepared 3D reconstructions with the existing description of developmental anatomy for these stages. In this way, it was possible to highlight discrepancies and to provide a description of novel anatomical features that have not hitherto been described. Second, to give a detailed description on the process of 'turning' in the mouse, particularly by observing the internal and external configuration of the embryo during this process. Such a study has not been done before, because hitherto it has not been possible to get 3D insight into the internal geometry during this process. Third, to give an account of growth during all reconstructed stages by measuring the volumes of delineated tissues. Since no measure is available for variance between embryos within stages, tissue sizes were presented in absolute terms as well as relative to the total volume of the embryo. This has enabled me to highlight trends of growth that could not have been achieved without reconstructing tissues throughout consecutive stages of development.

1.3 LAYOUT OF THESIS

All embryonic ages are given as 'gestational age'. For a table linking these to the appropriate Theiler stage, see chapter 2

The next section in this chapter will provide a literature review of mouse developmental anatomy from E1 to E9. The subsequent section will give an account of other modeling techniques that have been used to visualise anatomical relationships, and their advantages and drawbacks will be investigated. Chapter 2 will give an account of materials and methods that are applicable to all the chapters in this thesis. Two appendices (1 and 2), give an account of histology artefacts in the reconstructions and how decisions were made on arbitrary anatomical boundaries. Chapter 3 will compare the E1 - E9 3D reconstructions to the existing literature and will fill in obvious gaps in anatomical accounts of these stages of development. Chapter 4 gives an account of the process of 'turning' that investigates the consensus on this process. Chapter 5 describes relative and absolute tissue volumes in the reconstructions from E1 - E9. Chapter 6 provides an overall discussion of the thesis as a whole.

1.4 MOUSE ANATOMY E1 - E9

General note

The basis for the following literature review is the standard text of Kaufman (1992) and Kaufman and Bard (1999), and to a lesser extent Theiler (1972) and Rugh (1966). To avoid repetition, these sources have not been quoted verbatim whenever cited, although they are cited whenever critical statements were made.

This literature review deals with available descriptions of mouse development during E1 - E9 insofar as these descriptions could be checked against the reconstructions focusing on some of the more contentious points. Some background literature on developmental mechanisms is provided in order to make the text more readable. This work concentrates on the data available from the histological analysis of these stages of development, and does not review information from molecular biology or genetical analysis. The purpose of this essentially standard description is to provide the baseline data for considering the reconstructions discussed in the subsequent chapters.

1.4.1 Egg and first cleavage divisions

1.4.1.1 Maturation of the egg

Maturation of the egg occurs within the ovary when FSH (follicle stimulating hormone) and later LH (luteinising hormone) stimulate ovarian follicles to undergo folliculogenesis. This allows the egg to mature from prophase of the first meiotic division until metaphase of the second meiotic division where it undergoes arrest at metaphase of the second meiotic division shortly before ovulation. The first polar body is extruded at the completion of the first meiotic division. The stimulus to complete the second meiotic division is usually provided by the sperm-egg interaction at fertilisation.

1.4.1.2 First cleavage divisions

Within a few hours after the spermatozoon has entered the egg cell and induced activation, the second meiotic division is completed and the second polar body is

extruded. Shortly afterwards, the male and female pronuclei are formed. As the fertilised egg is about to enter the first cleavage division, the outlines of the two pronuclei gradually disappear. All the events associated with the first cleavage division (from the disappearance of the outlines of the pronuclei to cytoplasmic cleavage) are completed in approximately 2 hours (Kaufman, 1973). The total duration of the first cell cycle (from fertilization to first cleavage division inclusive) is normally about 16-18 hours.

1.4.2 Morula

After about a further 36 hrs and two not necessarily synchronous cell divisions, the 8-cell stage is achieved. The individual cells are now called blastomeres. Normally by this stage the embryo has reached the utero-tubal junction and will shortly pass into the lumen of the uterus.

The next event to occur in the embryo is the morula stage, associated with compaction of the blastomeres, which causes the loss of their macroscopic individuality. The distribution of microvilli over the cell surface changes during the process of compaction from a roughly even distribution to a more localised distribution restricted to the apical region of the cell and to the basal zone of intercellular contact, a condition termed polarisation (Ducibella, 1977). The outer layer of cells are morphologically distinct from the cells that they surround (the future ICM, or inner cell mass). The outer cells are larger, have more microvilli on their surface, while the inner cells have less microvilli and are more adhesive (Johnson and Ziomek, 1981). Compaction starts taking place after about 8 cells which is equivalent to approximately E2.

1.4.3 Blastocyst

1.4.3.1 General appearance

At about 28-33 cells (approximately E3-3.5) (Smith, 1980; Smith and McLaren, 1977), fluid starts to accumulate in the embryo between the inside layer and the outside layer of cells. When this happens the embryo has transformed from the

morula-stage into the blastocyst-stage. The inside group of cells which are located all to one side of the cavity are the inner cell mass (ICM), which will eventually give rise to the embryo proper (and a few extraembryonic structures). The second group of cells, which form an epithelial layer around the ICM and blastocoelic cavity (Enders and Schlafke, 1965), are called the trophectoderm cells; these will eventually form the embryo-derived component of the placenta (figure 1.1). Trophoblast cells that border the ICM are called the polar trophectoderm and those that border the blastocoelic cavity are mural trophectoderm cells. The blastocyst expands because the

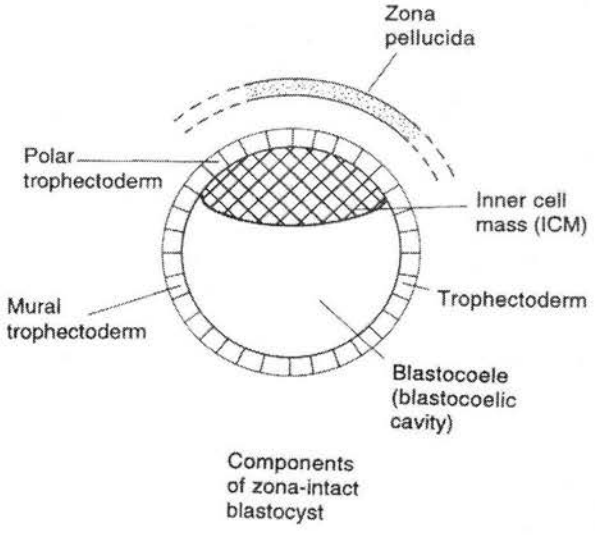

Figure 1.1: Diagram illustrating the typical features seen in the zona-intact balstocyst.

trophectoderm cells pump fluid into the blastocoelic cavity. The fluid is largely retained in the cavity because of the presence of tight junctions between the trophectoderm cells.

The ICM cells are more rounded and likewise have more limited contact surfaces than the trophectoderm cells, which have a flat and elongated shape and form an epithelium (Kaufman, 1983).

Nadijcka and Hillman, (1974) classified the developmental status of blastocysts into four stages: Stage 1 has a non-expanded blastocoelic cavity, and microvilli on the trophectoderm of the abembryonic and embryonic poles. Stage 2 has an expanded cavity and homogenous ICM, whose cells have squamous morphology. The trophectoderm cells are elongated. Stage 3 has a differentiated ICM. The lateral mural

(as opposed to those at the abembryonic pole) and polar trophectoderm cells are elongated, and trophectoderm cells at the abembryonic pole are varied but normally spindle-shaped. Primary endoderm cells overlap, and there are spaces present between the ICM cells. Stage 4 displays the first evidence of parietal endoderm, and only the polar trophectoderm cells are elongated; others are of varied shape or spindle-shaped. The ICM cells have large intercellular spaces. Stage 4 always occurs after shedding the zona pellucida, and stages 1 and 2 always occur before 'hatching'.

Gardner (1997) reports that polar bodies are present up to about 70% in early blastocysts, and that this rate goes down to 40% in very late blastocysts. The polar body is invariably situated close to halfway down the embryonic-abembryonic (EM-AB) axis and on the long axis of the oval shape of the blastocoelic cavity. The length of blastocysts is more indicative of age than of developmental status and ranges from an average of 96 μm for blastocysts that still have a zona pellucida, via an average of 108 μm for those without zona pellucida and giant cells, via an average of 151 μm for those halfway through giant cell transformation, to an average of 185 μm for those with completed giant cell transformation (Dickson, 1966).

1.4.3.2 Asymmetry of blastocysts.

Difference of opinion exist in the literature regarding the symmetry along the embryonic-abembryonic (EM-AB) axis of the blastocyst. Gardner(1997) states that there is a radial symmetry along the EM-AB axis while Smith (1980,1985) reports a plane of bilateral symmetry and a tilt of the ICM relative to the EM-AB axis. The tilted ICM has a blunt edge and a sharp edge, and the sharp edge is pointed towards the narrower and pointed side of the cavity at the AB-pole (see below). Moreover, Smith reports in the same studies that this tilt of the ICM coincides with the future anterior-posterior (AP) axis, the lowest point of the tilted ICM being the posterior region and the highest point the anterior region of the embryonic axis.

Another difference in opinion is about the symmetry of the cavity: Dickson (1966) reports a flattening of the cavity in the direction mutually perpendicular to the length and the breadth of the blastocyst in all embryos between E4 and E6. Smith (1980), in contrast, reports that the lumen is flattened and wider and rounded on one side, narrower and pointed on the other side of the AB-pole at E3.5. Although the

characteristics around the AB-pole remain the same, the lumen becomes spherical before E4.5 and stays that way until egg cylinder formation. Gardner (1997) reports cavities that are oval in the same plane as Smith describes, but the oval shape becomes more rounded as the blastocysts mature, and that, by E6, almost all cavities are round.

1.4.3.3 Differentiation of ICM

At about E3.5 - E4 the ICM splits into two groups of cells (Gardner, 1997; Smith, 1980). The group bordering the blastocoelic cavity can contain up to two cell layers, and is called the primitive endoderm. These cells are more loosely packed than the next cell layer and the pre-differentiating ICM. The other cell layer borders the trophoblast and is called the epiblast and consists of embryonic ectoderm cells. Primitive endoderm cells start delaminating and migrating along the trophoblast cells until they eventually line the entire blastocoelic cavity. Once this has happened the blastocoelic cavity is then termed the primary yolk sac cavity (E5). The endodermal cells bordering the trophoblastic cells are termed parietal endoderm and those bordering the epiblast are termed visceral endoderm.

1.4.3.4 Implantation

Just before implantation (at appr. E4.5) the zona pellucida is shed (Dickson, 1966; Cole, 1967). This process starts with the blastocyst contracting at appr. 4-hourly intervals, until the zona pellucida breaks. The contractions keep occurring, and increasingly large cytoplasmic 'blebs' that are fluid-filled but not continuous with the blastocyst cavity, start coming through the gap in the zona until the entire blastocyst has escaped (Cole, 1967). The blastocyst became attached to the uterus before hatching from the zona at the AB-pole, with the AB-EM axis situated horizontally in the lumen. After shedding of the zona, the EM-pole makes contact with the uterus and the trophoblast cells that are in touch with the wall of the uterus became less flattened and more vacuolated (Smith, 1980). The polar trophectoderm of the embryo plays an active role in implantation by inducing a decidual reaction (Gardner, 1972). The blastocyst now contains appr. 100 cells and 75% of these consist of trophectoderm, and are no longer involved in the production of the embryo.

1.4.3.5 Giant cell transformation

At about E5-E5.5 (Dickson, 1966; Copp, 1978) the mural trophectoderm starts transforming into 'primary' giant cells. These cells have giant nuclei with replicated DNA that occurred through endoreduplication rather than fusion of cells (Gardner and Papaioannou, 1975). The consensus is that the attachment of the blastocyst at the EM-pole to the uterus stops a further influx (Copp, 1978) of polar trophectoderm cells into the mural zone, thereby triggering giant cell transformation, although this effect is delayed (Gardner, 1972; Copp, 1981). This transformation starts at the abembryonic pole after shedding of the zona pellucida and progresses toward the embryonic pole where the transformation of the polar trophoblast cells is called 'secondary' giant cell transformation. These secondary giant cells are morphologically indistinguishable from the primary giant cells (Gardner *et al.*, 1973).

1.4.4 Egg cylinders

1.4.4.1 Formation of egg cylinder

Implantation of the blastocyst blocks sideways migration of polar trophoblast cells into the mural region (Copp, 1981). This event and a high proliferation rate in the polar trophoblast, combined with an inhibition to form giant cells triggered by contact with the ICM (Gardner, 1972; Gardner *et al.*, 1973), results in the formation of the egg cylinder at E5. This cylinder grows into the yolk sac cavity and consists of two cell layers: the inside of the cylinder consists of ectoderm, which is covered by a layer of visceral endoderm. This ectoderm contains epiblast cells at the embryonic pole (distal part of the egg cylinder) and trophoblast cells at the abembryonic pole (proximal part) of the cylinder. The extraembryonic ectoderm of the egg cylinder originates from polar trophectoderm (Papaioannou, 1982). There is no morphological distinction between the cellular arrangement in the extraembryonic ectoderm and the ectoplacental cone (Kaufman, 1983).

Within the egg cylinder another cavity becomes apparent called the proamniotic canal. This is first seen in the embryonic region but it later expands into the extra-embryonic region. This cavity forms under the influence of two signals: one from the visceral endoderm that induces apoptosis in the ectoderm and another from the cells in contact with the basement membrane between endoderm and ectoderm that inhibits apoptosis.

In this way, a layer of ectoderm that consists of one cell layer, which is pseudo stratified by E6, lines the newly formed proamniotic cavity (Coucouvanis and Martin, 1995 and 1999).

1.4.4.2 Visceral and parietal endoderm

As in the blastocyst, a single cell layer of endoderm termed visceral endoderm and parietal endoderm soon covers the egg cylinder and lines the mural trophectoderm. At approximately E6 (Kaufman, 1992), the parietal endoderm secretes an acellular membrane, called Reichert's membrane, between the parietal endoderm and mural trophectoderm (figure 1.2). The morphologies of the two types of endoderm are quite distinct: the parietal endoderm cells which are evenly scattered over the primary yolk sac (Gardner, 1984) have a long and pointed shape and are smooth, while visceral endoderm cells have numerous microvilli and form part of a continuous epithelial layer. Cells at the junction of parietal and visceral endoderm are elongated with branched filopodial extensions. There is a marginal zone of approximately 20 cells wide where cells have ruffled membranes, marked from the rest of the visceral endoderm by a ridge (Hogan and Newman, 1984).

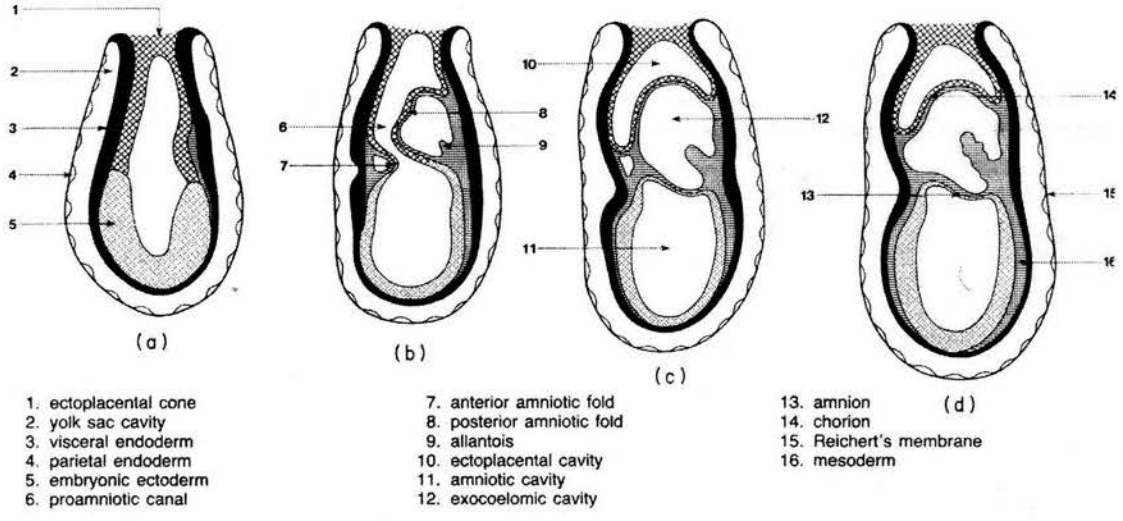

Figure 1.2: Stages in the conversion of the egg cylinder into the primitive streak stage embryo. (a) egg cylinder, (b) proamniotic canal present, (c) during closure of proamniotic canal, (d) after closure (from Kaufman 1992).

There are strong suggestions that the cells of the visceral endoderm migrate over Reichert's membrane: there are the filopodial extensions on the junctional cells, intermediate filaments in the parietal endoderm (Lehtonen *et al.*, 1983), observations from marker studies (Lawson *et al.*, 1986) while visceral endoderm can transform into parietal endoderm *in vitro* (Hogan and Tilly, 1981). It has been suggested that the direction of differentiation of these endoderm cells depends on interactions with non-endoderm cells (Gardner,1982). Both cell types originate from primitive endoderm formed in the blastocyst (Lawson *et al.*, 1986, Gardner, 1978 and 1982, Gardner and Papaioannou, 1975), although there is one contradicting publication that suggests that visceral endoderm derives from the epiblast, but this study has only been based on ICM studies *in vitro* (Dziadek, 1979).

1.4.4.3 Axes and asymmetry formation

It is generally thought that the morphology of the AP-axis does not get established until gastrulation when the primitive streak forms. However, some attempts have been made to find earlier morphological signs of axis formation. The earliest asymmetry that breaks the radial asymmetry is the tilt of the ICM in the blastocyst and the tilt of the ectoplacental cone in the egg cylinder. The ectoplacental cone is often tilted with respect to the egg cylinder, much as the ICM tilts with respect to the EM-AB axis (Smith 1980,1985). Gardner *et al.* (1992) reports an angle between 0° and 45° between the direction of the tilt of the cone and the AP axis while Smith (1980, 1985) reports that these directions coincide. According to Gardner *et al.*, the cone is as often tilted towards the anterior end as it is to the posterior end, and the tilt, whether pointing posterior or anterior, is more often located on the left hand side of the embryo. Unfortunately, neither Gardner *et al.* nor Smith have unambiguously established that the tilt in the ICM is the same as that in the ectoplacental cone. Both assumed this on the grounds of morphology. Although Gardner *et al.* did mark cells, they only did so in the visceral endoderm of the yolk sac and not in the ICM, trophectoderm or ectoplacental cone. Interestingly, Smith (1980) reports that the ectoplacental cone becomes symmetrical between E6.75 and E7.25, which is at, or just after, the primitive streak appears (see below).

While this review focuses on the morphological data, there is also gene-expression data in the earliest stages of axis development. Varlet *et al.*, 1997 report *nodal* as the

earliest posterior marker at the future site of the primitive streak, noting that its expression is 'opposite the heightened endoderm cells at the anterior side of the embryo'. These cells are situated approximately 1/3 of the way distal from the embryonic/extraembryonic border of the egg cylinder. What is not mentioned but the pictures show, is that the proamniotic cavity is squashed in the AP direction. Obviously if this narrowing is consistent among embryos it only indicates an axis and not a polarity. Another publication on a neuralizing factor in the endoderm (Belo *et al.*, 1997) confirms the cavity morphology in the presteak stage, and also shows the same heightened cells at the anterior end of the embryo. Additionally, Belo *et al.* show an off-axis orientation of the proamniotic cavity at the early streak stage.

1.4.4.4 Primitive streak

Until about E6.5 the embryo is cup-shaped and consists of two cell layers; the ectodermal epiblast and the endodermal hypoblast. At E6, the primitive groove and streak start forming at the posterior end of the embryonic axis on the border between embryo and extra-embryonic region (Beddington and Robertson, 1998). The groove is not as morphologically clear as in the chick and has an overlying primitive streak through which epiblast cells migrate laterally and cranially, forming the mesoderm, which separates the ectoderm from the endoderm, except in the areas of the buccopharyngeal and cloacal membranes. During and soon after the formation of the primitive streak, the embryo mainly grows in the posterior region, thus allowing the streak to extend to the most distal end of the egg cylinder by E7.5 (Poelmann, 1981; Lawson and Pedersen, 1987), after which the anterior region catches up in growth and pushes the streak caudally. The streaks lengthens to 400-500 μm at E7.5, then shortens to 200-300 μm at E8, to 150-170 μm at E8.5 (Tam, 1981).

The mesoderm deposited up to the midstreak stage will all become extraembryonic mesoderm, after which time the embryonic mesoderm is laid down (Parameswaran and Tam, 1995). There are two schools of thought about the migration of the mesoderm: Poelmann (1981) believes that the spread of the mesoderm is passive, based on the anatomy of the cells. The differential growth of mesoderm and the rest of the embryo takes account of the spread of the mesoderm. However, Nakatsuji *et al.*, 1986 and Tam *et al.*, 1993 have shown that the movement is active and that the mesoderm cells move in a cohesive sheet as well as individually.

1.4.4.5 Node and notochord

At the time of the fusion of the anterior and posterior amniotic folds and just before the appearance of the allantois (appr. E7-7.5), the node forms at the anterior end of the streak. The node is continuous with the streak and is distinguished from the latter by a discontinuity in the endoderm under the node, which forms a 'pit' in the most distal aspect of the embryo. There are two aspects of the node: a dorsal aspect which is contiguous with the surrounding epiblast, and a ventral region, which itself has two aspects: the central part, the pit, with ciliated cells, and around it a horse-shoe shaped ring, 2 - 3 cells wide, which is open anteriorly, with less cilia (Bellomo *et al.*, 1996). There are two publications that contradict this detailed study: Poelmann (1981 a+b) describe the morphology of the anterior streak and the head process but in neither paper mentions the node. The area described as the node by Bellomo, he describes as the head process. Wilson *et al.*, 1995 gives an illustration of the nodal region to illustrate gene-expression and points to the node just anterior to the 'dip' in the endoderm, described by Bellomo *et al.* as the central pit of the ventral node.

The node is the origin of the head process, notochord, axial mesendoderm and the definitive endoderm of the gut (Lawson and Pedersen, 1987, Tam *et al.*, 1993). Since the ventral node has a very low (Bellomo *et al.*, 1996; Lawson *et al.*, 1986), and the dorsal node a very high mitotic rate (Snow, 1977) it was concluded that the dorsal node is the precursor population and the ventral node the organiser, a view supported by the fact that descendants of the ventral node, the head process and the notochord, similarly have low mitotic rates. The head or notochordal process (or axial mesendoderm), which consists of conical cells, forms anterior to the node and is initially associated with the axial endoderm but later separates from it (Beddington and Robertson, 1998). The conical cells of the head process are initially flattened, cuboidal, then conical and are initially not readily distinguished from endoderm cells. When the head process does separate from the endoderm, it is called the notochord.

1.4.4.6 Neurectoderm formation

Correct formation of the neurectoderm depends on signals from the visceral endoderm before gastrulation (Beddington and Robertson, 1998; Thomans and Beddington, 1996; Biben *et al.*, 1998). The neural axis is induced by the node (Beddington, 1994) and the precursor population of the neurectoderm is contained within the distal cap

epiblast at the early-streak embryo (Quinlan *et al.*, 1995; Tam, 1989). The posterior region of this cap gives rise to the caudal spinal cord, the distal region of the cap gives rise to all brain structures and the spinal cord and the most anterior region of the cap gives rise to the fore- and midbrain.

1.4.4.7 Extraembryonic membranes

Posterior amniotic fold

During the process of gastrulation two cell types, one ectodermal and one mesodermal, start to grow across the proamniotic cavity starting from the posterior end of the embryo. Initially this bulge is completely filled with mesoderm cells, but lacunae soon appear among the mesoderm cells that coalesce to form the central cavity of the proamniotic fold. Slightly later, a similar process happens at the anterior end of the embryo (Kaufman, 1992). The mesoderm cells in these folds are irregular in shape, and the cells in the centre of the fold have longer and thinner cytoplasmic processes, some of which enclose small lacunae. When the anterior and posterior amniotic folds coalesce they form the exocoelomic cavity (Ellington, 1987).

These anterior and posterior folds fill the entire proamniotic canal and fuse, separating former proamniotic cavity into 3 smaller cavities. The upper (*i.e.* abembryonic) cavity is called the ectoplacental cavity, the middle cavity the exocoelomic cavity and the cavity bordering the embryo the amniotic cavity. The two cell layers between the two proximal cavities are called the chorion and the cell layers between the middle and the distal cavity the amnion.

Yolk sac

The wall of the egg cylinder that extends proximal from the embryonic region and borders the exocoelomic cavity is called the secondary or visceral yolk sac. The wall of the egg cylinder bordering the ectoplacental cavity consists of endoderm and extra-embryonic ectoderm (Ellington, 1987). The primary yolk sac is bounded by Reichert's membrane with mural trophectoderm on the external and parietal endoderm on the luminal side.

The visceral yolk sac has a absorptive function; preplacental nutrition is achieved by the uptake and catabolism of maternal macromolecules which constitue the so-called histiotroph. This form of nutrition continues alongside the chorio-allantoic placenta

until birth. Visceral yolk sac endoderm has a significantly larger volume of vacuoles than embryonic endoderm (Gupta *et al.*, 1982), and these are mainly membrane-bound (Kaufman, 1983). This theory is supported by the observation by Kaufman (1984, 1992) of a yolk sac canal associated with cell death in the yolk sac. These canals are lined with microvilli and observed in nearly half the embryos around the first appearance of the allantois. The canals are invariably situated at the anterior end of the embryo just proximal to the embryonic-extraembryonic boundary. Kaufman suggests that these holes may allow rapid ingress of substances from the yolk sac or excretion of toxic metabolites.

Allantois and chorion

The development of the allantois starts with a clustering of extra-embryonic mesoderm cells near the caudal end of the embryo at the late streak stage. The allantois grows rapidly particularly during the initial phase, and its component cells proliferate very rapidly. Another contributing factor to its rapid expansion is a relatively high hydrostatic pressure as compared to the surrounding exocoelom (Ellington, 1985). The allantois fuses with the chorion where the extra-embryonic ectoderm is exposed to the exocoelomic cavity. This exposure is due to the fact that the mitotic index of the chorion is twice as high in the ectoderm as it is in the mesoderm (Ellington, 1987). As soon as the chorion fuses with the allantois and the ectoplacental cone, the hydrostatic pressure is released and the overall diameter of the allantois decreases in size (Ellington, 1985).

1.4.5 Early organogenesis

As will be discussed later, the extra-embryonic tissues were removed from the specimen prior to histology. The discussion here will thus focus on the embryonic tissues.

Over the period between E7.5-E9 when the major organs start developing, significant shape changes take place in the embryo. Since the extraembryonic tissues were not analysed during the embryonic reconstructions, the description of anatomical development for these stages will only deal with the embryo proper. Sections are divided according to the organ systems studied, and are in no particular order.

1.4.5.1 Neural tube and its derivatives

Neurectoderm

At approximately E7.5, the epiblast differentiates into neurectoderm and surface epithelium and this process progresses craniocaudally. The former tissue has heightened through columnarisation while the latter flattens as its cells become cuboidal. As the process of neurulation progresses, the boundary between the two tissues becomes increasingly evident and marks the future source of neural crest cells.

Headfold

Between E7.5 and E8 the headfold, or cranial flexure, starts to form. This is the first event that is evident within the cup shape of the embryo. These folds first form at the most rostral part of the axis and move caudally towards the mesencephalon (midbrain), where it is first evident between E9 and E10. The progress of the cranial flexure (*i.e.* the angle of flexure) pauses while neural tube formation occurs (Jacobson and Tam, 1982).

Tube formation

By E8 two lateral folds have formed that bulge laterally, with there being a deep (neural) groove in the midline (Jacobson and Tam, 1982). Soon after E8, the neural folds start to elevate and become apposed, they then fuse across the dorsal midline, initially at the border between future rhombomere 4 and 5 (Kaufman and Bard, 1999). The curvature of the embryo at this level reflects the folds dorsally and may thus assist the closure of the folds. From here, closure progresses both rostrally and caudally, and during this process the lateral edges of the neural folds extend more along the axis than the midline of the neural tissue, which may assist the process of tube formation. After the first evidence of neural fold fusion in the mid- to caudal cervical region the next point is in the prosencephalon from where closure also extends rostrally and caudally. The last sites to close are the rostral and caudal neuropore, and the latter closes later, by approximately E9 –E9.5.

Brain compartments

The future brain region of the neural tube becomes divided into fore-, mid- and hindbrain, or pros-, mes, and rhombencephalon, and this division is normally evident by E8. Later, the prosencephalon splits in to tel- and diencephalon, the telencephalon

forms the telencephalic vesicles, while the rhombencephalon forms eight rhombomeres which comprise the met- and myelencephalon. At E8.5 the presumptive diencephalon can be recognized in the forebrain, while the first rhombomeres A and B become apparent in the hindbrain. No information is available on the appearance of the rhombomeres in the mouse, apart from that by E9.5 there are a total of six rhombomeres present (Murphy *et al.*, 1989). In human, chick and rat embryos, only 7 rhombomeres form after three initial rhombomeres A, B and C (Fraser *et al.*, 1990; Adelmann, 1925). The segmentation of the brain into neuromeres occurs in neural plates overlying already segmented mesenchyme (see *Somites and somitomeres*) and the boundaries of the neuromeres adhere to the boundaries of the segmentation of the mesenchyme (Jacobson and Tam, 1982).

Factors involved in shaping the brain

The expansion and shaping of the brain roof is assisted by at least two mechanical factors. There is an expanding force, deriving from intraventricular pressure, and there is a resistance to this expansion from the overlying surface epithelium. Obstructing either of these factors leads to an abnormal shape of the brain (Coulombre and Coulombre, 1958). A factor contributing to intraventricular pressure is occlusion of the neural lumen that, in humans occurs over up to 60% of the total length of the neural axis (Kaufman, 1983). In mouse, this occlusion occurs before tube closure at about the 10 –12 somite stage (E8.5). The extent of occlusion varies widely between embryos of the same litter and otherwise similar developmental stage.

Topography

The closed neural tube is bordered ventrally by the gut, mesenchyme and notochord; laterally by mesenchyme; dorsally and cranially the surface epithelium; and caudally the neural tube is still continuous with the primitive streak.

Optic and otic structures

Optic placodes are first evident soon after E8, when the embryo has about 4 pairs of somites (Kaufman, 1979), as heightened cells in the diencephalon. By E8.5 they have turned into optic evaginations, and it is at this time that the neural folds fuse over the top of these evaginations. The rostral neuropore which is situated under the optic structures closes approximately when the embryo has about 20 pairs of somites.

The otic placode is first seen when the embryo has about 5 – 6 pairs of somites (Kaufman, 1979). Before this, the preotic sulcus can be seen as an indentation in the lateral edge of the neural folds at the level of rhombomere3. In the rat, when the embryo has about 9 pairs of somites, the otic placode covers rhombomere 4 and part of rhombomere 5. When the embryo has about 14 pairs of somites, the otic placode has become level with rhombomere 5 (Adelmann, 1925).

Ganglia

Up till E9, only two ganglia can be distinguished from the surrounding mesenchyme: the trigeminal (V) ganglion and the still merged facioacoustic (VII and VIII) ganglion complex. By this stage, the trigeminal ganglion makes up the largest part of the mesenchyme of the first branchial arch (Kaufman and Bard, 1999). Both the facioacoustic and trigeminal ganglia in the rat originate from the rhombomeres: the trigeminal from rhombomere 1 and the facioacoustic from rhombomere 4 (Adelmann, 1925).

1.4.5.2 Heart

Formation of heart tube

At E7.5, during the late presomite stage, cavitation starts in the presumptive pericardial mesoderm to form the pericardiac cavity. Slightly later, the cardiogenic plate appears as heightened cells in the ventral wall of the pericardiac cavity of the intraembryonic coelom. Simultaneously, when the embryo has about 1-2 pairs of somites, in the region subjacent (*i.e.* ventral) to the cardiogenic plate, two endothelial tubes form that soon coalesce to form a single tube when the embryo has about 4 pairs of somites (Kaufman and Navaratnam, 1980). The endocardial tube that runs craniocaudally becomes surrounded by the former cells of the cardiogenic plate which has then become the myocardial wall. Early cardiogenic mesoderm can give rise to both myocardial and endocardial structures (Eisenberg and Bader, 1996). There are two endothelial heart primordia present which fuse to become a single entity (Kaufman and Navaratnam, 1980). The myocardial wall is still connected with the mesothelial lining of the pericardiac cavity via the wide dorsal mesocardium. The dorsal mesocardium stays intact rostrally and caudally, but will rupture in the middle, at or soon before E9 to formed the transverse pericardial sinus.

The heart, that started off as the cardiogenic plate, which then rounded up and surrounded the endocardial tubes at the ventral side of the pericardiac cavity is now located at the dorsal part of this cavity. The heart has turned 180° over a virtual transverse axis, and this rotation was mainly caused by the headfold or cranial flexure in the neurectoderm. Before rotation, the pericardiac cavity was situated proximal to the buccopharyngeal membrane and neurectoderm; after folding, it has become situated ventral to the neurectoderm. Because of tissue connections, this folding has caused the former ventral aspect of the pericardiac cavity to become dorsally located (Kaufman and Bard, 1999).

Differentiation of myocardial cells

The differentiation of the cardiogenic plate into the myocardial cells is marked by the formation of thick myosin type filaments. The development of cardiac muscle cells is most advanced in the future ventricular area and the process spreads both cranially and caudally. The ventrocaudal wall of the sinus venosus differentiates from the loose mesenchymal clls of the septum transversum (Viragh and Challice 1973). It is likely that the hepatocyte growth factor plays a role in the coordination of the programme of growth or differentiation (Rappolee *et al.*, 1996). Epicardial cells are not derived from the myocardium but migrate onto it from the septum transversum and are first seen at approximately E9.5 (Viragh and Challice, 1973). The cardiac valves which start developing at approximately E11 are formed by the myocardium and endocardium (Moorman and Lamers, 1994) and the same is true for the trabeculae which develop earlier (Fishman and Chien, 1997). The maturing human heart, and it is assumed that the same arrrangement is present in the mouse heart, has three layers of muscle tissue: a subepicardial, middle and subendocardial layer. The middle layer is only present in the left ventricle and has a circumferential pattern. The other layers are oblique and more or less perpendicular to each other and are anchored in the orifices of the heart (Sanchez-Quintana *et al.*, 1995)

Cardiac jelly

Between the endothelial tube and the myocardial wall a layer of very loosely packed cells forms that mainly consist of extracellular material, called cardiac jelly. This jelly is possibly derived from the myocardial, excluding the atrial, walls of the heart (Manasek, 1979), and is formed before the endocardial tubes are enclosed by the

myocardium. Although the jelly is transient, it has a distinct function. It allows the primitive heart tube to close during contraction without the presence of valves. Since the diameter of the heart tube can only be reduced to approximately 60% by contraction, it therefore needs a 'padding', if there are no valves present to prevent a dead volume of blood blocking a healthy blood flow (Moorman and Lamers, 1992)

Contractions of the early heart

In the human, the heart first starts contracting at the stage when the embryo has about 4 – 6 pairs of somites (Goss, 1938), pumping at the stage when the embryo has about 8 – 10 pairs of somites (just before a continuous blood flow is established with the vasculature of the yolk sac) and is beating regularly and powerfully when the embryo has about 15 – 20 somites. It is clear that the heart works initially without any external innervation (Navaratnam, 1965) and indeed contractility is an intrinsic property of cardiac cells (Harary and Farley, 1963). The sinus venosus region, that consitutes the inlet of the heart, acts as the initial 'pacemaker' of the primitive heart, and the peristaltic contraction is propogated rostrally along the heart tube. The atrial inlet region contracts quickly and briefly, whereas the more downstream regions contract for a longer time, thus preventing blood from the outflow area being sucked back into the inlet area (Moorman and Lamers, 1992). It has been proposed that acetylcholine-esterase is responsible for delaying the depolarisation time of the outlet region of the heart (Lamers *et al.*, 1987).

Segmentation and looping of the heart

Before 'looping' of the heart, during which the shape of the heart transforms from a straight tube into a 'S'-shape, between E8 - E8.5, the initially primitive heart tube forms three main regions that can be distinguished by their bulging morphology. Rostral is the bulbus cordis and outflow tract that will form the right ventricle and outflow tract; medial is the primitive ventricle that will form the left ventricle; and caudal is the common atrial (or primitive) chamber that will later be separated into the left and right atria. After looping of the heart, there is a relatively deep groove between the two future ventricles (Vuillemin and Pexeider, 1989) but there is no clear demarcation between the future right ventricle and the outflow tract.

Soon after its initial segmentation the heart tube starts to 'loop' to form an 'S'-shape, and this causes the vascular system to loose its symmetry. The initially caudally situated atrium 'ascends' and becomes located dorsal to the primitive ventricle and bulbus cordis. The boundary between the ventricle and bulbus cordis 'descends'. There appears to be an intrinsic capacity of the heart tube to loop (Manning and McLachlan, 1990), as it even loops in the absence of its surrounding tissues and without contractions (Manasek and Monroe, 1972). This is believed to be facilitated by axial growth of the primitive heart tube and the establishment of the transverse pericardial sinus (Patten, 1922).

A multitude of theories have been put forward to explain and describe the events during the looping of the heart in the chick (Stalsberg, 1970) and cover both intrinsic and extrinsic factors. Intrinsic factors include differential growth in different parts of the heart, differential redistribution of cells and early asymmetric contractility (Davis, 1927; Van Praagh and De Haan; Wilens, 1955; Lepori, 1966; Stalsberg, 1969 and Patten, 1949). All of these could be contributory but are not main factors in the process of 'looping'. Other intrinsic factors that have been proposed but are unlikely to contribute, are cell death, differential regional cell proliferation and a differential size and segmentation of the two halves of the heart (Manasek, 1969; Stalsberg, 1969 and Lepori, 1967).

Extrinsic factors include several asymmetries in the embryo such as the head process and the caudal axis of the embryo not being in a straight line, an uneven course of the primitive streak etc. These are however also unlikely to be contributing factors since they do not appear to be consistent between embryos (Stalsberg, 1970) and since they are the same in *situs inversus* embryos, in which hearts loop in the opposite direction to that observed normal hearts. Damage done to the pericardial cavity to investigate its role in looping, has been shown to influence the direction of looping (ref).

The most compelling evidence for intrinsic factors causing looping come from observations on change of cell shape in the myocardium during the process of looping (Manasek and Monroe, 1972), combined with the fact that there is no signifant change in forces on the epicardial region of the heart at different times or different places during looping. This evidence, of course, in combination with the previously mentioned experiments of Manning and McLachlan (1990) in which heart tubes were

explanted before the onset of looping and were shown to loop *in vitro*. The overall conclusion is that the main factor for looping is intrinsic with some contributing external factors.

1.4.5.3 Vascular system

Arterial system

At E8, the cranial pole of the primitive heart tube bifurcates to form the first branchial arch arteries. These pass dorsally on either side of the rostral extension of the foregut pocket to unite with the paired dorsal aortae. From these arch arteries another five pairs of arteries sprout that also pass dorsally to the dorsal aortae. The fifth pair is said not to develop in vertebrates. Only the first and second pair that form by about E8.5 (Theiler, 1972) are relevant here, since the other pairs differentiate after E9. The dorsal aortae form initially as angioblasts that coalesce around the time that the first arch arteries join up with these vessels, and more caudally, the paired dorsal aortae fuse in the midline. The dorsal aortae extend rostrally and ramify in the cephalic region to form the internal carotid arteries by E10 (Kaufman and Bard, 1999). Caudally, the dorsal aorta gives off the vitelline artery that supplies the visceral yolk sac. Even more caudally, the aortae give off the paired umbilical arteries, which pass through the umbilical cord (E8.5).

Venous system

The endothelial lining of the primitive atrium bifurcates caudally to give rise to the caudal parts of the right and left endocardial tubes that form the horns of the sinus venosus. The venous drainage of the rostral and caudal parts of the embryo are through the posterior and anterior cardinal veins that fuse to form the common cardinal vein that drains into the sinus venosus. The sinus venosus has two more inlets: the vitelline veins which bring blood back from the yolk sac and the paired umbilical veins, carrying oxygenated blood from the umbilical cord. Until E9 – 9.5 the left and right umbilical veins are of equal size after which the right branch regresses, to leave the left as the only branch to carry oxygenated blood from the placenta into the embryonic heart (Kaufman and Bard, 1999).

1.4.5.4 Primitive gut and its derivatives

At about E7.5 the foregut diverticulum forms as a blind pocket in the endoderm at the rostral end of the embryo. Somewhat later, a similar process occurs at the caudal end of the embryo, which forms the hindgut pocket. As noted previously, the gut consists of definitive endoderm formed by the dorsal node. Moreover, the borderline between definitive and primitive gut defines the lateral edge of the gut (Lamers *et al.*, 1987). After the formation of the fore- and hindgut pockets most of the gut remains open until after the process of turning.

The endothelium of the gut is thin and squamous at first but becomes more columnar after closure of the gut tube. It is not known whether the shape changes that occur during the development of the gut are due to mitotic activity or are due to cell shape changes.

The hepatic diverticulum forms from about E8.5 due to differential growth of the endodermal plate combined with a fixed contact with the endothelial lining of the heart (Godlewski *et al.*, 1992). In rat at TS14 (mouse equivalent E9), the hepatic diverticulum is separated by the septum transversum caudally from the sinus venosus and ventrally from the developing heart. In the midline however there remains a contact with the endothelium of the heart. When the embryo has about 18 pairs of somites, the lumen of the hepatic diverticulum is T-shaped.

1.4.5.5 Somites and somitomeres

Somites

The somites are formed in a craniocaudal direction from the presomitic mesoderm at the cranial end of the paraxial mesenchyme which is deposited by the primitive streak lateral to the axial mesoderm. A removal of cells from the cranial end and a deposition of cells from the caudal end by the primitive streak therefore govern the presomitic mesoderm. In the mouse embryo, somites form at a rate of about 1 pair of somites per 1-2 hours, and the most advanced embryo can be about 6 – 8 hours ahead of its slowest littermate with regard to somite formation. The volume of somites varies along the body axis: lumbar and sacral somites are about twice the volume of upper trunk and tail somites (Tam, 1981). Somite formation is typically defined by a radial organisation of cells around the cavity in the middle of the somite, the myocoele. Cell clusters of approximately the same amount have been shown to be present in the

presomitic mesoderm (Tam, 1981). Tam (1981) indicates that the level of the cranial border of the first somite is just below the otic placode.

Somitomeres

In mid and late streak stage embryos, a pattern has been shown in the cranial region of the presomitic mesoderm of cells arranged in concentric circles, and these are named somitomeres. At the midstreak stage, two such somitomeres can be distinguished in the lateral wings of the mesoderm, and at the late streak stage, 4 to 6 somitomeres can consistently be seen (Tam and Meier, 1982). In chick, segmented mesoderm has been shown in the mesoderm underlying the otic placode that can be traced back to the above described somitomeres (Meier, 1984).

1.4.5.6 Notochord

As seen in the section on the egg cylinders, the notochord cells are derived from the node. They then move in the cephalic direction to be incorporated into the roof of the foregut. At E9, the notochord is for its entire length attached to the roof of the gut and starts detaching at E9.5 (Jurand, 1974). The separation of the notochord from the gut starts caudally (Lamers *et al.*, 1987), and after this separation the development of the notochord develops craniocaudally. This development consists of vacuolisation of the notochord cells and a detachment from the neural tissue to adopt a position in the mesenchyme (E11-12). Caudally, the notochord is continuous with the primitive streak at E9.

1.4.5.7 Mesoderm segmentation

The intraembryonic mesoderm forms three columns of tissue: the paraxial, the intermediate-plate and the lateral-plate-mesenchyme (thus called after the invasion of neural crest cells), while the axial mesoderm forms the notochord. The paraxial mesmesenchyme segments into somites (see above). The intermediate mesoderm (no neural crest cells collect here) running between the paraxial and lateral plate mesenchyme also segments and forms the nephrogenic cord and presumptive nephric duct. The lateral-plate mesoderm does not segment but is split into two layers by the formation of the intraembryonic coelom. The ventral plate is the splanchnopleure and the dorsal plate is the somatopleure. Tam (1981) has claimed that the head

mesenchyme is segmented in theory, but this is not observed to be the case when examined histologically or by other means.

The mesodermal component of the visceral yolk sac forms the blood islands, which make the blood vessels and cells. It is not until approximately E8.5 that the vascular system of the embryo connects with the islands in the yolk sac, and, therefore, it is not until then, that the embryo can attract nutrients from the vascular system. The mesodermal component of the yolk sac is also the location where the primordial germ cells are first seen. From there they migrate along the base of the allantois, along the wall of the hindgut and its dorsal mesentery into the urogenital ridge.

1.4.5.8 The process of turning

At about E8.5, when the embryo has about 8-14 pairs of somites, the embryo turns around its length axis, so the embryo adopts the characteristic 'fetal' position in which the ectodermally-derived tissues occupy the outside of the curve, while the endodermal tissues become located on the inside of the curve. During the process of turning, the embryo rolls into its extraembryonic membranes and becomes completely surrounded by its amnion and yolk sac. This process takes only about half a day. A full description of the process of turning is given in chapter 4.

1.5 3D EMBRYONIC VISUALISATION TECHNIQUES

From relatively early on there has been the need to create a 3D oversight of anatomical detail. This has been done either by different visualisation techniques either or not using reconstruction methods.

1.5.1 3D visualisation techniques not requiring reconstruction

The oldest technique for showing normally inaccessible 3D anatomy in mouse embryos is to inject ink into parts of the vascular system or other orifices (Moffat, 1959), and this is followed by latex or vinyl acetate (Halpern, 1953), followed by coloured perfusion fixative (Effman, 1982), contrast fluid (Smith, 2001) or polymerisation compound (Clark *et al*, 1979). The surrounding tissue then has to be 'cleared' to make it transparent, or in the case of polymerisation compound, can simply

be removed. The method of Smith is non-destructive and therefore does not involve the clearing away of the surrounding tissue.

All of these techniques have the drawback that they only show continuous cavities, and not surrounding histology. Therefore, for our purposes, the techniques are not sufficient because the vascular system is not yet continuous and other lumina are either still open or we wish to know about the surrounding tissues, more so, than about the lumina.

Other techniques are scanning electron microscopy, magnetic resonance microscopy (Smith *et al.*, 1994) and ultrasound scanning (Allan *et al.*, 1997). The first gives an excellent degree of resolution and texture of the viewed surface but unfortunately, can only view surfaces, leaving underlying tissues unknown. Magnetic resonance microscopy gives reasonable views of internal histology of embryos but unfortunately the resolution is limited to approximately 20 μm and the view of the histology is far poorer than when looking at conventional histological sections. Cell arrangement and tissue boundaries cannot be clearly distinguished. Ultrasound scanning is another way of viewing internal structures, but, as has been extensively tested, is too crude to give morphological detail at the developmental age range covered in this thesis (Allan *et al.*, 1997).

1.5.2 3D visualisation techniques requiring reconstruction

For a very long time, people have been reconstructing tissues from microscopic slides using tracing paper and cardboard or millimeter graph paper (*e.g.* Padget, 1948). The early version of this technique was inexact in the sense that the drawing on paper was an interpretation of what was seen down the microscope, in the sense that there was no transferal of the exact shape that was viewed down the microscope. Later, when projection microscopes became available this problem was solved because the slide was then projected at the required dimensions so the tissues could be traced without personal interpretation.

This technique (tracing individual tissues from projection microscopes) became the basis for an array of computer-aided reconstruction methods in which the surface of one or more tissues together were 3D-rendered. This provided insight in 3D relationships of the heart (Whiten *et al.*, 1998; Scarborough *et al.*, 1997; Verbeek *et*

al., 1995; Ito *et al.*, 1992; Sumida *et al*, 1989) and other organs or gene expression patterns (David *et al.*, 1998; Sherwood *et al.*, 1999; Streicher *et al.*, 2000).

Most of these reconstructions show anatomical boundaries only; others show migrating cells or gene-expression patterns in conjunction with the underlying anatomy. Most of these reconstructions are just shown as 2D pictures in publications, which reduces the value of the 3D organisation that was gained by making the reconstruction. Other reconstructions are actually downloadable with their appropriate viewing software from the World Wide Web (Whiten *et al.*, 1998; Scarborough *et al.*, 1997) which has the great advantage of bringing the 3D oversight to the viewer's desk. The resolution of these types of reconstructions varies widely: from 2μm (Hiruma and Hirakow, 1989) to 50μm (Whiten *et al.*, 1998).

The majority of computer reconstruction techniques indicated above have the great advantages that they are relatively quick and require relatively little computer power, but their disadvantage is that the link with the underlying histology has been broken (except for Streicher *et al* who use fiducial marks), and only a fixed number of tissues can be presented. The technique employed in this thesis covers these drawbacks since at any point of time any combination of tissues can be rendered together in 3D or can be referred back to the underlying histology should the viewer wish to do so. Because of the reconstruction, this underlying histology has now become available at any arbitrary angle (Kaufman *et al.*, 1997; 1998; Brune *et al.*, 1999). Moreover, the reconstructions are, via the Mouse Atlas Project, available partly on CD-ROM and partly via the World Wide Web, at http://genex.mrc.ac.uk. and these reconstructions, complemented by additional anatomical information, are accessible using a wide variety of computers.

CHAPTER 2: RECONSTRUCTION, SEGMENTATION AND VISUALISATION OF THE EMBRYO MODELS

2.1 BIOLOGICAL MATERIAL

2.1.1-Selection of embryos

One embryo per Theiler stage (with a few exceptions, see table 2.1) was selected for reconstruction. Serial sections for embryos from E8.5 and E9 were already available and were the same as those used for the Atlas of Mouse Development (Kaufman, 1992). These embryos were selected to be representative for their Theiler stage at the time of production of the paper Atlas, and are now the *de facto* standard for mouse development. The benefit of using the reference material, plus the fact that these series of sections are nearly complete and contain limited shrinkage, distortion or other damage made them the optimal choice for reconstruction of these stages when the project was initiated. However, the section thickness of these sections is approximately 7 μm, and for the younger stages it was decided that, for the purposes of the Edinburgh Mouse Atlas Project, a higher resolution was needed. Therefore new embryos from the same strain were obtained and sectioned in plastic to section-thickness of a nominal 2 μm (by Allyson Ross). The new embryos were selected to be representative for their stages, including sub-stages, and in optimal condition by Dr. K. Lawson, Hubrecht Laboratory in Utrecht. A table of the stages, their defining features and approximate age (dpc) is shown below (Bard *et al.*, 1998). The Theiler staging has been extended to include sub-stages to match the Downs and Davies criteria, as modified by K. Lawson to take account of the developmental differences to the PO strain.

Number of embryos reconstructed	Theiler Stage	Embryo-nic age (range)	Somite No. (range)	Cell num-ber	(C57BLxCBA)F2 embryos	P-O mice
0	1	0-0.9 (0 -2.5)		1	**One cell egg**	
1	2	1 (1 -2.5)		1-4	**2 cell stage**	
2	3	2 (1-3.5)		2-16	**Morula**	
1	4	3 (2-4)		18-40	**Blastocyst**, Inner cell mass apparent	
1	5	4 (3-5.5)			**Blastocyst** (zona-free)	
0	6	4.5 (4-5.5)			**Attachment of blastocyst**, primary endoderm covers blastocoelic surface of inner cell mass	
1	7	5 (4.5-6)			**Implantation and formation of egg cylinder** Ectoplacental cone appears, enlarged epiblast, primary endoderm lines mural trophectoderm	
1	8	6 (5-6.5)			**Differentiation of egg cylinder**, implantation sites, 2x3mm ectoplacental cone region invaded by maternal blood, Reichert's membrane and proamniotic cavity form	
0	9	6.5 (6.25-7.25)			**Pre-streak (PS)**, advanced endometrial reaction, ectoplacental cone invaded by blood, extraembryonic ectoderm, embryonic axis visible,	PS
1	9a				**Early streak (ES)**, gastrulation starts, first evidence of mesoderm	ES
0	10	7 (6.5-7.75)			**Mid streak (MS)**, amniotic fold starts to form	MS
1	10a				**Late streak, no bud (LSOB)** , exocoelom	LS
0	10b				**Late streak, early bud (LSEB),** allantoic bud first appears, node, amnion closing	
0	11	7.5 (7.25-8)			**Neural plate (NP)**, head process developing, amnion complete	OB
1	11a				**Late neural plate (LNP),** elongated allantoic bud	EB/ LB
0	11b				**Early head fold (EHF)**	EHF
0	11c				**Late head fold (LHF),** foregut invagination	LHF

0	12	8 (7.5-8.75)	1-4		**1-4 somites**, allantois extends, 1st branchial arch, heart starts to form, foregut pocket visible, preotic sulcus (at 2-3 somite stage)	
1	12a		4-9		**5-7 somites**, allantois contacts chorion at the end of TS12 ***Absent*** *2nd arch, >7 somites*	
1	13	8.5 (8-9.25)	8-16		**Turning of the embryo**, 1st branchial arch has maxillary and mandibular components, 2nd arch present ***Absent*** *3rd arch, >12 somites*	
1	14	9 (8.5-9.75)	12-24		**Formation & closure of ant**. neuropore, 13-20 somite pairs, otic pit indented but not closed, 3rd branchial arch visible ***Absent*** *forelimb bud*	

Table 2.1: Selected embryos and their developmental stages

All embryos were obtained by crossing (C57BLxCBA) F1 mice in a reversed day-night rhythm. The morning that the vaginal plug was found is being defined as 0.75 days of gestation, assuming that both ovulation and conception occur at about the mid-point of the dark phase.

2.1.2 Fixation, sectioning and staining

2.1.2.1 Paraffin embedded embryos

E8.5 and E9 embryos were fixed using Bouin's fixative (saturated aqueous picric acid, 75 ml; 40% formaldehyde, 25 ml; glacial acetic acid, 75 ml) for 2-24 hours, depending on the size of the embryo, then stored in 70% alcohol until needed. Dehydration was carried out by progressing the embryos through successively 80%, 90%, 96% and absolute alcohol, then into a 50:50 mixture of absolute alcohol : benzene. The duration of exposure was, again, dependent on the size of the embryo. Embryos were kept in benzene, until they cleared, then removed immediately into wax, with three changes of wax needed to allow full penetration. Blocks were made and transverse sections cut at a nominal thickness of 7 μm. Prior to staining, sections were dewaxed in xylene for 5 minutes, then rehydrated through absolute alcohol, 96%, 90% and finally 70% alcohol (five minutes each stage), then washed in running tap water. Sections were stained for 10 minutes in either Delafield's or Ehrlich's haematoxylin, washed in running tap water, and differentiated in acid-alcohol for 15-30 seconds. The sections were washed in running tap water, then counterstained with eosin for 5

minutes. After a final wash in running tap water, sections were dehydrated through ascending alcohol, cleared in xylene, then coverslipped using Dammar xylene mounting medium.

2.1.2.2 Plastic embedded embryos

Embryos were fixed using glutaraldehyde (2.5% in 0.1M Cacodylate buffer pH7.3 +0.1M sucrose) for 2 hours for E1-E5.5 and overnight for E6-E8, then rinsed (2x10 minutes) and stored in 0.1M Cacodylate buffer +0.1M sucrose until needed. Embryos were then treated with 1% osmium tetroxide in 0.1M Cacodylate buffer for 30 minutes - 1 hour depending on size, and rinsed in the same buffer as above 2 x 10 minutes. Dehydration was carried out by progressing the embryos through successively 10%, 30%, 50%, 70%, 95% and absolute alcohol, 2x5 minutes + 10 minutes for E1-E5.5 and 30 minutes for E6-E8; each successive step was then 10 minutes for E1-E5.5 and 30 minutes for E6-E8, apart from the last step which was 3 x 10 minutes for E1-E5.5 and 3 x 30 minutes for E6-E8. Subsequently, the embryos were transferred to a thin layer of araldite overnight, heated at 60°C for 35 minutes and then polymerised at 60°C for 3 days. The final embedding happened on a layer of araldite left to harden in the mould overnight. The araldite used was resin CY212 10ml, DDSA 10 ml and dibutyl phtalate 0.5ml. This was mixed for 1 hour, 0.5 ml DMP 30 was added and allowed to mix for 1 hour on a rotator. The resin blocks of the E2, E3, E4, E5.5, E7.5 and E8 were trimmed to have straight edges to facilitate the reconstruction process. Sections were cut at a nominal thickness of 2 μm and subsequently stained with toluidine blue.

2.2 Reconstruction

The grey-level (i.e. digital photographic) voxel model was reconstructed from digital images of the full sets of serial sections. This was performed by capturing a digital image of each section; sectioning and mounting artifacts were then corrected with 'Photoshop' in appropriate sections. The images were then image aligned, image warped stacked to form a 3D grey-level digital model. All stages of these processes, except for the image correction using 'Photoshop', used software and hardware systems developed at the MRC Human Genetics Unit and were based on the woolz image processing system (Piper & Rutovitz, 1986). After final reconstruction, the models were checked to confirm that they displayed normal shape and histology using 'The Atlas of Mouse Development' (Kaufman, 1992).

2.2.1 Image capture and alignment

A digital image of each section was recorded using a Zeiss Axioplan microscope fitted with a Xillix 1400 (Optimum Vision Ltd., Petersfield, Hampshire, UK) digital camera linked to a Sun Microsystems Sparc 10 workstation via an MRC-designed image capture interface card The objective lens used for each embryo were x5 (paraffin embedded embryos), x10 (plastic embedded, E1, E2.5, E5.5-E8) and x20 (plastic embedded, E2, , E3 & E4). This resulted in pixel-sizes (separation of sampling points in the digital image) of 1.36 μm for the paraffin sections and 0.68 or 0.34 μm for the plastic sections. These dimensions were checked by comparing them with a digital image of a 1 mm graticule with divisions every 100 μm that was captured using the same objectives. The Xillix camera provides a digital image with a 12-bit grey-value (4096 values) for each pixel which was automatically converted to 8-bits (256 values) through a hardware look-up table under programmatic control, using a gamma transfer function. The images were optimised using glass and microscopic filters as well as tools within the capture software for optimising the spread of grey-levels (*i.e.* contrast) in the images. Images of sections on view were brought into register by rotating the microscope stage and translating the image using the computer mouse. Each image was captured and shade-corrected (Baldock & Poole, 1993) to remove the effects of uneven illumination and camera sensitivity.

2.2.1.1 Alignment of older embryos, dividing egg and blastomeres

The image of each paraffin or plastic section was aligned with the previous images using a transparent overlay provided by a 1-bit dithered image of the preceding, section in the series. Figure 2.1 shows a screen shot of section images both out of alignment and aligned with the overlay. After the manual alignment, the images were automatically aligned using the MRC HGU computer program "Reconstruct". This alignment allows both rotation and translation (iterated if necessary) until the translation is over less than half a pixel (Guest, 1994). This automatic alignment uses grey-level correlation as a measure of similarity to determine the best alignment. The first embryo reconstructed was the E9 embryo which was not automatically aligned after manual alignment.

2.2.1.1 Alignment of egg cylinder stages and blastocysts

For the early embryos, this manual alignment during capture and subsequent automatic alignment caused rotation errors because many of the egg-cylinder sections are symmetrically

ring-shaped and the correlation matching often fails especially when artifacts are present. It

Figure 2.1: Screen shot of the XMGrab program used to capture the digital images. In this view the use of a dithered overlay (red) is shown. The underlying grey-level image can be aligned using the cursor (dragging) or by the arrow button provided.

was therefore decided that the best option was to align to the edge of the block to fix the angle of capture. Although these blocks were re-trimmed on a few occasions during the process of sectioning, the method of edge-alignment could be still be used because sudden shifts in angle of the edge of the block could be corrected by manual tie pointing between matching cells in adjacent sections "across the gap". This was done using the MRC 'Reconstruct' software.

Images from sections of the egg-cylinder and blastocyst embryos were thus aligned for the correct angle by matching the edge of the block in which the embryos were embedded with a graticule in the eyepiece of the microscope. In these cases the dithered image of the earlier image in the series was not used. The section images were then automatically aligned allowing

translation only. This method is justified since none of the edges of the block 'spirals' around the main axis of the block and can therefore act as a good angle reference.

2.2.2 Correction of artifacts in individual sections

After capturing and alignment (both manual and automatic) the images were reviewed. Registration errors were corrected manually and badly distorted or torn sections were substituted with adjacent ones. If there was a series of such sections, the stack was replaced with computer-generated interpolated images between the neighbouring sections at either end of the stack.

Some images suffered from air bubbles under the sections, which had been included during the mounting process. These artifacts were removed using 'Photoshop' and image structure was restored using cloned areas from the surrounding (same) tissue. Other artifacts such as tears in sections could not be restored using 'Photoshop', since these artifacts were not restricted to the area of the cut: the artifact caused a displacement of tissue throughout most of the section.

A full list of artifacts occurring during sectioning and mounting is provided in appendix 1. The list comprises the section numbers involved for each reconstruction and the tissues affected by the artifact as well as the course taken during the process of delineation of the anatomy in the reconstruction.

2.2.3 Warping

Sectioning and histological processing introduce both systematic and random distortions to each section which need correcting in order to permit arbitrary sectioning through the model embryo. For this purpose, a technique was developed for warping each image so that digital sections through the stack do not show ragged edges resulting from misaligned image features (Guest & Baldock, 1996). The method treats each digital image as a thin elastic plate linked at corresponding points on the upper and lower adjacent sections and imposes "forces" that warp each image to match those adjacent. The basic assumption is that the biological structures visible within the grey level images are smooth on the scale of section thickness (see figure 2.2)

By treating each section as an elastic plate, and applying forces to deform the plate (arising from automatic matching between sections), the problem is transformed to a physical model with a mathematical formulation. The set of mathematical equations is solved using the *Finite*

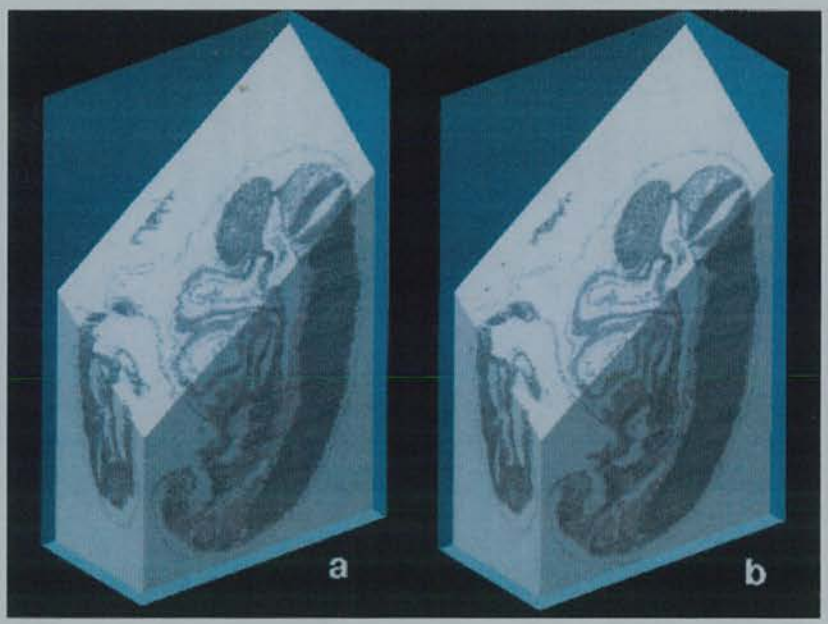

Figure 2.2: Two views of the E9 embryo showing the effect of warping. (a) before warping and (b) after warping.

Element Method (FEM) which divides the image into small triangular regions (elements) within which the equations are easier to solve (linearised). The FEM solution will be a good approximation to the true solution if the elements are small. The software developed to solve the warping problem uses smaller elements over the dark areas of the image which correspond to the embryo and larger ones elsewhere. This is a compromise to get the most accurate warping where it is needed and still be able to solve the resulting set of equations.

2.2.4 Subsampling and normalisation

While the two-dimensional images of successive sections are composed of 1.36 x 1.36μm pixels in the paraffin sections and 0.68 x 0.68 or 0.34 x 0.34 μm in the plastic sections, the depth of the voxels in the volume image is governed by the thickness of the sections *i.e.*7μm for the paraffin sections and 2μm for the plastic sections. To enable re-sectioning of the models without varying resolution in the resulting section image it is desirable to have isotropic voxel sizes, i.e. the same in all directions. It was therefore necessary to make the voxel dimensions more nearly uniform by re-sampling the images in the original section planes with a consequent loss of resolution in that plane. Though a cubic voxel for the paraffin reconstruction would be 7 x 7 x 7 μm, it was compromised by re-sizing to 4.08 x 4.08 x 7 μm: this allows the retention of adequate resolution without significantly affecting the appearance of the resectioned model. For the plastic reconstructions compromise was not necessary since

re-sizing by factor 3 for x10 or factor 6 for x20 in the original plane of sectioning resulted in cuboidal voxels and kept an adequate resolution. For all reconstructions, re-sizing was done after warping by Gaussian subsampling by a factor of three or six in the original plane.

Finally the grey-values in each image were normalised to remove differences in stain intensity between sections arising from variation in section thickness and the staining process. This was done by assuming a similar distribution of grey-values in every plane and adjusting each plane to this averaged distribution.

2.3 Segmentation – Anatomy Delineation

2.3.1 General philosophy

After reconstruction of the digitised sections into a 3D grey-level image (known as a *woolz object* when in the MRC image format), separate voxels (volume elements) can be interactively labeled with the MAPaint program, thus enabling each of the anatomical tissues to be defined. This labeling can be done at any arbitrary section through the reconstruction. Five different domains can be labeled at the same time using a transparent colour 'wash' so that the underlying grey level image, representing the histology, remains visible under the applied colour. All voxels in the reconstruction were labeled, and the ideal would be to do this to the level of detail of the anatomy nomenclature database used within the Mouse Atlas project (Bard *et al.*, 1998). However, in practice, the only tissues that were labeled were those discernible on the sections used for reconstruction, using a normal light microscope and the histology stains used.

2.3.2 Segmentation strategy

Each section of each reconstruction was printed out on A4 size paper in the original resolution, onto which all anatomical boundaries were drawn. All decisions on boundaries were made using the original sections and a light microscope. Once all delineations were drawn on the prints, these were transferred to the reconstruction. To perform the segmentation or delineation, several interactive "paint" tools are available within the program, e.g. tools to draw, to paint, to propagate the labeled domain to another section, as well as options for filling regions and cleaning ragged edges and filling holes. In addition a number of image-processing support tools to automatically label connected voxels with a similar grey value, to

delineate sudden changes in grey level in a section or to propagate boundaries from previous sections onto similar grey level alterations on the next section where available. The use of all these semi-automatic tools did however require checking with occasional manual editing. All boundaries were implemented to an accuracy of one pixel.

2.3.4 Special case boundaries

The delineation of tissue boundaries is based on cell shape and configuration as seen in the original sections under a microscope. Where it was not possible to base boundaries on these grounds, boundaries were sought in other planes in the digital model. In a few cases, this led to an unambiguous boundary e.g. for the somites. However, in the majority of the cases in which boundaries could not be determined in the original sections, decisions had to be based on criteria other than cell shape and configuration; these were termed 'arbitrary' boundaries. The nature of arbitrary boundaries is a 3-dimensional shape change with no specific change in cell shape or configuration; an example is the division between the optic vesicles and the forebrain. A full list of tissues with arbitrary boundaries in each reconstruction and the grounds on which the boundary was based, is given in appendix 2.

2.4 Visualisation

2.4.1 Two-Dimensional

The reconstructed anatomy can be viewed in 2-D using the same software as that used for delineation of the anatomy. This software can give (reconstructed) 2D images at any arbitrary angle through the reconstruction. These images can be overlaid with all delineated anatomy in transparent colour 'washes', but only five different colours can be used to show the histology underlying the anatomical domain (see figure 2.3). In addition to five transparent colours, a further twenty-seven solid colours can be used for displaying domains that will not show the underlying histology.

2.4.2 Three-Dimensional

After labeling, the tissues can be visualised using the commercial software package 'Advanced Visualisation System' (AVS). This software displays a surface rendering of the volume of the selected tissue. With accompanying 3-D glasses, a realistic three dimensional view can be achieved. The system allows tissues to be represented in isolation or in

Figure 2.3: Selected section views of the E9 embryo as displayed using MAPaint. The left hand images show just the histology and the right-hand images show the same sections with coloured overlays representing the anatomical domains.

combination with other tissues, solidly or transparently coloured allowing structures within other structures to be visible. The surface visualisations can be interactively rotated to get a quick overview of the 3D structure, while re-scaling provides the possibility of then looking at the structures in more detail.

2.5 Discussion

2.5.1 Image normalisation

The grey-level normalisation method makes the assumption that the distribution of grey levels (the histogram) is similar in all sections throughout a reconstruction. This is of course an approximation and sections with very little tissue in them (towards the crown and the bottom of the embryo) end up with a dark histology. This could affect automatic delineation, *e.g.* the software tool that connects voxels with a similar grey level throughout the reconstruction. However, all delineation, whether automatic or manual, was thoroughly checked in all three dimensions. The normalisation would affect apparent condensations in the reconstruction and therefore checking for tissue condensations was done on the original histology.

2.5.2 Spatial resolution

What is the resolution of the embryo models? This can be answered in a number of ways depending on use to which the models are put. For the purposes of delineating anatomical structures recognisable in the reconstruction then the resolution is determined by the minimum distance two features in the model need to be apart for the boundary to be visible. If the features have the same grey-level appearance i.e. the same grey-value and grey-value texture then they can only be distinguished if they are at least one pixel apart. This is analogous to the Rayleigh citierion used in physics, e.g. to establish if a bright spot is one or two stars. This is the worst case scenario in which the two features would otherwise share a long common boundary. In the situation that the two features/structures have a well-defined shape, e.g. two circular regions, then even if their respective edges touch it will still be possible to define the common boundary (this of course is a model-based assumption). This analysis implies a worst-case resolution of twice the pixel size, this in turn implies that different resolution in different directions because voxel sizes are not isotropic. This resolution can be termed the *object-separation* resolution.

The resolution to which the boundary can be placed is given by the voxel size and in this work, the constraint imposed by the object-separation resolution discussed above is avoided by using higher resolution images and in many cases the actual histological sections to determine the boundary position. Therefore the anatomy for this thesis has been delineated to a resolution determined by the voxel size. This is termed the *object-placement* resolution.

A third definition of resolution is the smallest size of an object that can be detected. This is dependent on the characteristics of the imaging system (especially background noise) as well as the optical density and contrast of the object with respect to its immediate surroundings. This *minimum-object* resolution is not of significance for this work since the original histological sections were available for detecting small objects. In any case this resolution will have an upper-bound given by the voxel size. With this analysis the resolutions for the different reconstructions are given in table 2.2.

Embryo Type	Object-separation	Object-placement
Plastic embedded: 2x2x2 μm	Worst case: 7 μm Best case: 4 μm	Worst case: 3.5 μm Best case: 2 μm
Wax embedded: 4x4x7 μm	Worst case: 18 μm Best case: 8 μm	Worst case: 9 μm Best case: 4 μm

Table 2.2: Resolutions in reconstructions of plastic and wax embedded embryos

CHAPTER 3: THE ANATOMY OF THE E1-E9 RECONSTRUCTIONS

3.1 INTRODUCTION

The aim of this chapter is to compare the embryo models from E1 – E9 with the existing descriptions as represented in the literature review on mouse developmental anatomy, as found in chapter 1.4, and thus to test the value of the reconstructions for descriptive anatomy. The way that this is done is by extracting statements from the review related to each topic that can be checked in the models, and then indicating whether my own descriptions obtained from the analyses of the models deviate from or agree with the descriptions in the literature. In addition, but this has not been the main focus of the study, any unexpected features observed in the models are described that have not hitherto been noted in the literature.

It is believed that this comparison will form a valuable supplement to the existing anatomical knowledge that may not in all regards be correct or complete. While it would be optimal to have a complete description of each tissue within each model, this is technically not possible in this thesis. Such descriptions are, however, possible but only when the models are viewed digitally using appropriate computer graphics. Therefore, in the back of this thesis a copy of the CD-ROM that was specifically created for the Edinburgh Mouse Atlas Project (http://genex.hgu.mrc.ac.uk) with reconstructions of 8 embryos ranging from E5.5-E9 (egg cylinder stages and early organogenesis) has been included, for those that want to have a look at more anatomy of most of the embryos discussed in this chapter.

The models provide a 3D insight into the internal geometry of the embryos because tissue surfaces of one or more anatomical domains can be 3D-rendered simultaneously. This provides insight in otherwise inaccessible regions in the embryo. The models also provide histological sections at any arbitrary plane through the digitally reconstructed embryos that can be presented with or without the transparent overlays of all the anatomically delineated structures. This provides the possibility of analysing the histological features underlying the 3D surface renderings, to check appropriate tissue detail. The anatomical descriptions in this chapter are presented in text accompanied by images of the above mentioned anatomical representations.

The results section has been divided in four sections based on developmental stages: the models of the cleavage divisions, the different stages of blastocyst differentiation, the egg cylinder stages and the embryos at the early stages of organogenesis. At the

beginning of each of these sections, a list of statements extracted from the literature review (chapter 1.4) is presented against each of which the group of models will be compared. Following this comparison any anatomical features that were unexpectedly observed in the models will be discussed.

3.2 MATERIALS AND METHODS

3.2.1 biological methods

For this study, 13 embryos of ages ranging from E1 (TS2) to E9 (TS14) were used. For the full list of embryos that were used for reconstruction and their staging characteristics, see table 1, chapter 2. The embryos that are less developmentally advanced than E8.0 were embedded in plastic and cut to a nominal section thickness of 2 μm. The E8.5 and E9 embryos were embedded in paraffin and cut to a nominal thickness of approximately 7 μm.

3.2.2 tissues considered in this study

For all stages of development studied, all delineated tissues were compared to the existing anatomical descriptions available in the literature and observed for the presence of novel characteristics.

For 'processing' artefacts in the original sections that appear in the reconstructions that affect the delineation of tissues, see appendix 1.

For discussion regarding decisions on the delineation of arbitrary anatomical boundaries, see appendix 2.

3.2.3 computer methods

For the figures, 3D surface renderings of individual tissues were created using the commercial software package 'AVS'. For more details, see chapter 2. The histological views displayed are histological sections taken from the reconstructions, either in the original plane of sectioning or from a reconstructed plane. When additional detail was required, images were made of the original sections that were used to make the reconstructions, since they have a higher resolution than the histological sections from the reconstructions.

3.2.4 all other methods

For more in depth descriptions of above methods as well as all other methods (biological and computer) see chapter 2.

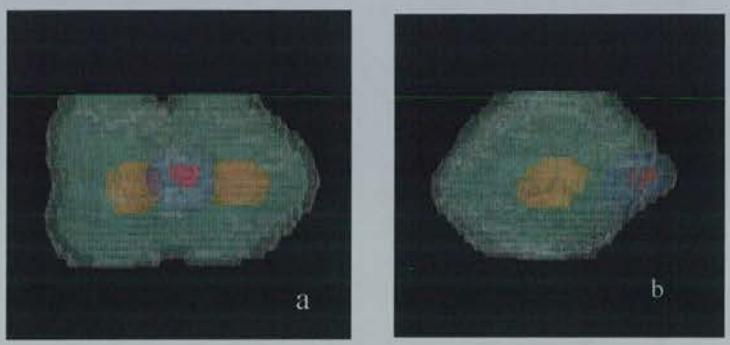

Figure 3.1: 'Frontal' view (a) and 'side' view (b) of the E1 embryo showing the two cells (green transparent) of the embryo, polar body (blue transparent), nuclei: polar body (red), blastomeres (orange) and zona pellucida (white transparent).

3.3 RESULTS

3.3.1 Cleavage divisions and Morulae (E1, E2, E2.5)

3.3.1.1 Descriptions from the literature to be checked in the models

How many cells (*i.e.* blastomeres) are there in each of the embryos? Are they compacted or not? Is there any obvious difference between the morphology of inside

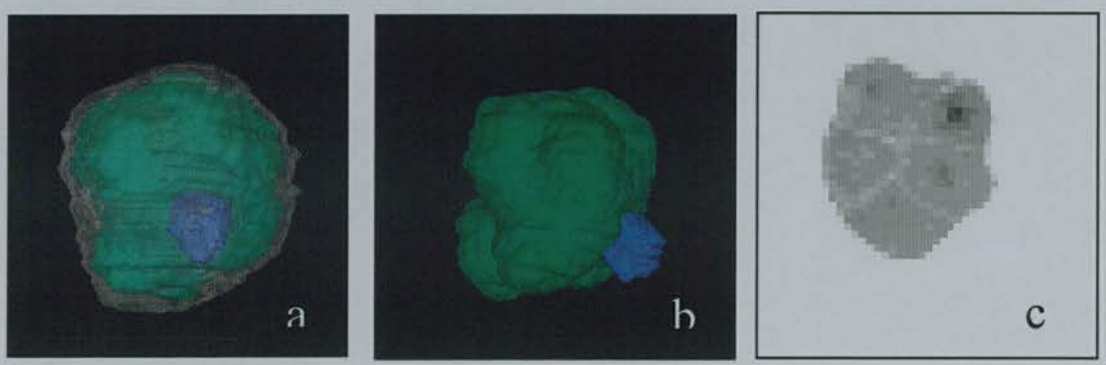

Figure 3.2: 'Frontal' (a) and 'side' (b (no zona pellucida)) view of the E2 embryo. Blastomeres (green), polar body (blue) and zona pellucida (white transparent).

(c) - Section through the E2 embryo reconstruction.

and outside cells in the morulae? Are there one or more polar bodies retained?

3.3.1.2 Comparison with the literature

The E1 embryo

The E1 (TS2) embryo model has two cells and a second polar body (note the top and bottom sections are missing). The cells have an elliptical shape and are not compacted (figure 3.1), which is according to the literature (Kaufman and Bard, 1999).

The E2 embryo

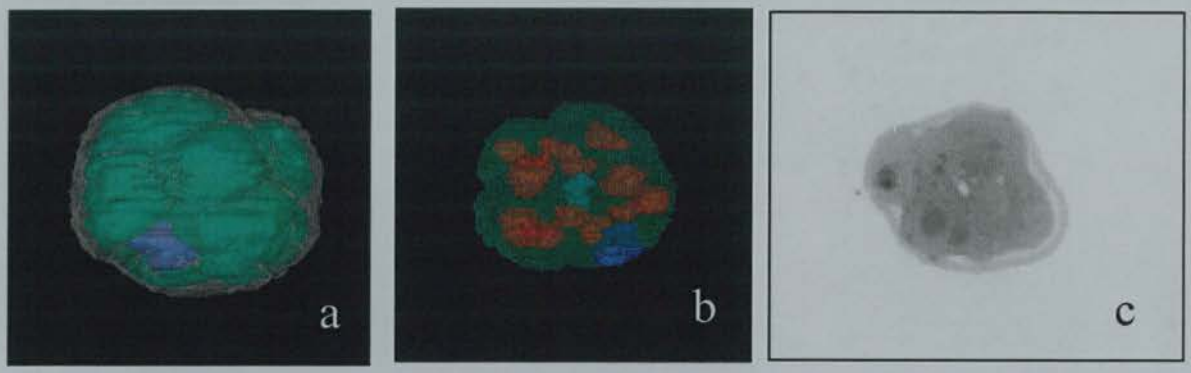

Figure 3.3: E2.5 embryo: (a) - Blastomeres (green), polar body (blue) and zona pellucida (white transparent). (b) - different viewing angle. Blastomeres (green transparent), nuclei (red), extracellular spaces (turquoise), polar body (blue). (c) - Original histological section.

The E2 (TS3) embryo has 8 cells, which are compacted on the inside of the morula (figure 3.2c), but the cells still form bulges on the outside of the morula (figure 3.2a and b), so the compaction is only partial. It also has a second polar body. This morphology is according to the literature (Kaufman and Bard, 1999).

The E2.5 embryo

The E2.5 (TS3) embryo has 12 cells and one polar body (figure 3.3a and b). This embryo has some extracellular spaces around the inner cells (figure 3.3b and c). This is presumably because of the different morphology of the inside and outside cells (Ducibella, 1977) and not because of the onset of cavitation (Smith, 1980; Smith and McLaren, 1977). The degree of compaction is similar to the previous embryo, and the morphology of the embryo is in accordance with the literature.

3.3.1.3 Unexpected anatomical features

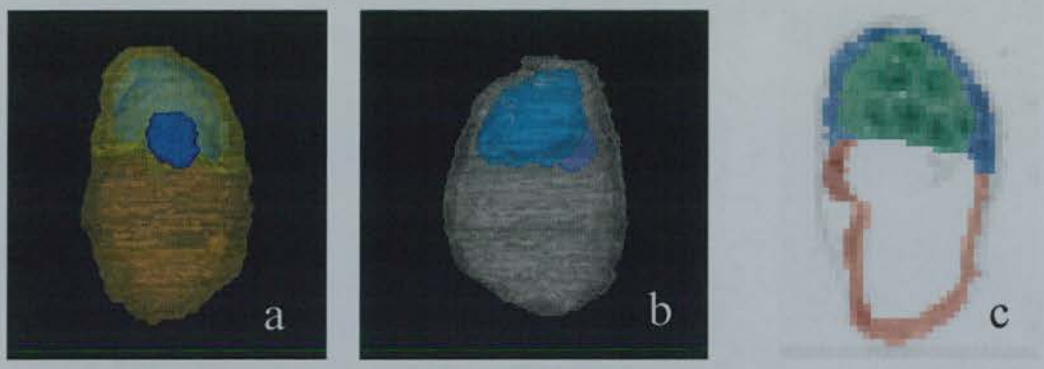

Figure 3.4: (a) - View parallel to the long (transverse) axis of the blastocoelic cavity of the E3 embryo. Polar trophectoderm (yellow transparent), mural trophectoderm (orange transparent), inner cell mass (light blue) and polar body (dark blue); (b) - View parallel to the shortest (transverse) axis axis of the blastocoelic cavity of the E3 embryo, showing the ICM sloping towards the back of the figure. Zona pellucida (white transparent), inner cell mass (light blue) and polar body (dark blue). (c) - Section through the reconstruction of the E3 embryo. Mural trophectoderm (pink), polar trophectoderm (blue) and inner call mass (green).

The processing must have affected the rigidity of the zona pellucida somewhat as in both the E2 and E2.5 the zona follows the contours of the morulae and their polar bodies, rather than form a globular structure around both embryo and polar body as observed in fresh material (figures 3.1a, 3.2a and 3.3a) (Kaufman, 1992, plate 1b). The other interesting feature is that the polar body in the 2-cell embryo is in touch with both of the two cells of the embryo (figure 3.1a and b).

3.3.2 Blastocysts (E3 and E4)

3.3.2.1 Descriptions from the literature to be checked in the models

Are there zona pellucidae (Cole, 1967; Dickson, 1966) present? What is the morphology of the ICM and trophectoderm cells and therefore, at which of the four stages, are the two blastocysts used for this study according to Nadijcka and Hillman (1974)? If the zona pellucida was lost, can a change in cell shape at the abembryonic pole be noted (Gardner, 1980)?.

Does the length of the AB-EM (abembryonic-embryonic) axis of the blastocysts comply with Dickson's (1966) measurements of blastocysts? The blastocysts should not have started undergoing giant cell transformation (Dickson, 1966, Copp, 1978).

Are the polar bodies still present (Gardner, 1977)? Is the latter situated somewhere at the level of the middle of the AB-EM axis and on the plane of longest transverse axis through the blastocoelic cavity (Gardner, 1992)? Is the shape of the blastocoelic cavity rounded on one side and more pointed at the opposite side (Smith 1980, 1985) or elliptical Gardner (1996, 1997)? Is the ICM (inner cell mass) tilted with respect to the AB-EM axis (Smith, 1980, 1985; Gardner, 1992)

3.3.2.2 Comparison with the literature

Blastocyst stages

Two blastocysts have been studied, the developmentally earlier is E3 and the more advanced embryo at E4. The E3 embryo has a zona pellucida, polar body, and expanded blastocoelic cavity, elongated polar and trophectoderm cells and a homogeneous ICM, which classifies it according to Nadijcka *et al.* (1974) as a stage 2 blastocyst. However, Nadijcka's description of this stage does not appear to be consistent with the reconstruction, in that the ICM cells do not have a squamous morphology. Instead, they have a rounded morphology with limited cell contacts (figure 3.4c).

The E4 blastocyst has no zona pellucida, and a spindle-shaped mural trophectoderm at the abembryonic pole (figure 3.5b). However, one particular feature makes it difficult to classify this embryo as a stage 3: the ICM has not yet differentiated into epiblast

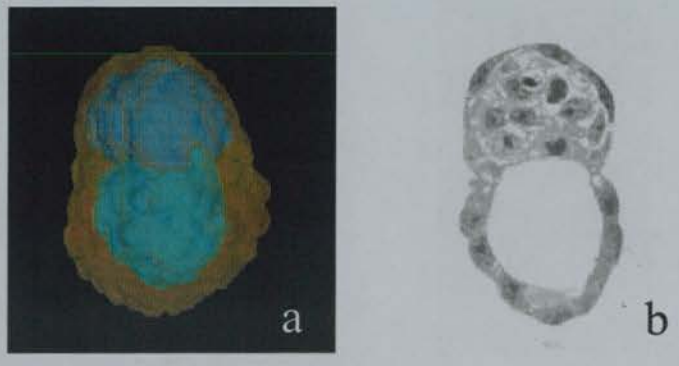

Figure 3.5: (a) View parallel to the shortest (transverse) axis of the blastocoelic cavity of the E4 embryo, showing the ICM sloping towards the back of the figure. Trophectoderm (orange transparent), inner cell mass (light blue) and blastocoelic cavity (turquoise); (b) - Original section of the E4 embryo; (c) .

and primary endoderm. The staging system however states that stages 1 and 2 are always zona-intact, so therefore stage 3 would appear to be the best fit for this

embryo. The 'collapsed' lateral mural trophectoderm in the younger blastocyst is most likely to be a handling artefact (figure 3.4d).

Giant cell transformation and length

Neither of the embryos shows a sign of giant cell transformation which is consistent with their age (Dickson, 1966; Copp, 1978) (figures 3.4d and 3.5b). The length of the AB-EM axis of the earlier embryo is 100μm and of the later embryo is 90μm. Given the average of 10% shrinkage during processing (chapter 5), this makes the younger embryo slightly on the large side of Dickson's (1966) scale, and the older embryo slightly on the small side of his scale.

Asymmetry in the blastocyst

The younger embryo has a zona pellucida and second polar body present which is consistent with Dickson's (1966) and Cole's (1967) timing of shedding of the zona. The older one has no zona or polar body. This means that according Dickson and Cole, the zona was shed at a slightly early stage. The polar body of the E3 blastocyst is situated in the middle half of the AB-EM axis, according to Gardner (1992), and in the plane of symmetry parallel to the longest transverse axis of the blastocoelic cavity (figure 3.4a).

The shapes of the cavities in both embryos comply with Smith's (1980) description of having a more pointed side on one side of the long axis through the cavity (figures 3.4b and 3.5a; right hand side) and a more rounded side on the other side of the long axis (figures 3.4b and 3.5a; left hand side). The feature that does not agree with the existing description is that the slope of the ICM in the young embryo is not parallel with the long axis through the cavity but at an angle of about 60° with it (figure 3.4b) (Smith, 1980, 1985; Gardner, 1992, 1997). However, in this embryo the ICM is tilted and has a sharp edge and blunt edge as described by Smith (1980) (figure 3.4a). The older embryo does not have a tilted ICM, again unlike the descriptions provided by Gardner (1996, 1997) and Smith (1980, 1985) (figure 3.5a).

3.3.2.3 Unexpected anatomical features

In the older blastocyst the lateral mural trophectoderm has a similar morphology to that of the mural trophectoderm at the abembryonic pole and this trophectoderm is less flattened and elongated than the polar trophectoderm. This has not been described

previously. Nadijcka *et al.* (1974) only described less flattened and elongated cells at the AB-pole where presumably the trophoblast has been in touch with the uterus. The same embryo also appears to have a circumferential constriction (figure 3.5b) at the border between the polar and mural trophectoderm.

3.3.3 Egg cylinders (E5.5, E6, E6.5, E7 and E7.5)

3.3.3.1 Descriptions from the literature to be checked in the models

Egg cylinder formation

Is there any sign of apoptosis in relation to cavity formation in the egg cylinder as described by Coucouvanis and Martin (1996, 1999)?

Visceral and parietal endoderm

Is the marginal zone of 20 cells width in visceral endoderm at the junction with the parietal endoderm as described by Hogan and Newman (1984) detectable in the reconstructions? Is the distribution of the parietal endoderm over the visceral yolk sac as even as in the embryos in Gardner's (1984) paper?

Asymmetry formation and axes

Is it possible to find any evidence of asymmetry in the egg cylinder that may indicate a morphological establishment of an anterior-posterior axis before the first evidence of primitive streak formation? If there is, then how does the lumen of the proamniotic cavity and the slope of the tilt in the ectoplacental cone relate to this? Do the slopes of the cones after definitive establishment of the anterior-posterior axis agree with Gardner's (1992) or Smith's (1980, 1985) description?

Primitive streak and node

According to Tam (1981), the primitive streak reaches its maximum length of 400 – 500 μm at approximately E7.5 after which the streak regresses to 200 – 300 μm at E8 and 150 – 170 μm at E8.5. Is the length of the primitive streak at E7.5 (TS11) consistent with this description?

Does the node appear after fusion of the proamniotic folds (Bellomo *et al.*, 1996)? Is it possible to distinguish a ventral aspect (forming a 'pit' in the embryo) and a dorsal aspect to the node, the dorsal component of which has more mitotic figures? Is there

axial mesendoderm or a head process in the E7.5 and, if so, how far does this structure extend?

Neurectoderm

Is the anterior neurectoderm in the E7.5 embryo organised in a single-cell, columnar epithelium as Jacobson and Tam (1981) describe for the E7.5 – E8 embryo?

Extraembryonic membranes

Do the cavities in the posterior amniotic fold start off as lacunae that coalesce to form a single cavity as described by Ellington (1987) and is there an anterior amniotic fold (Kaufman, 1992) Do the mesodermal cells in the centre of the fold have longer and thinner cytoplasmic processes than those at the periphery?

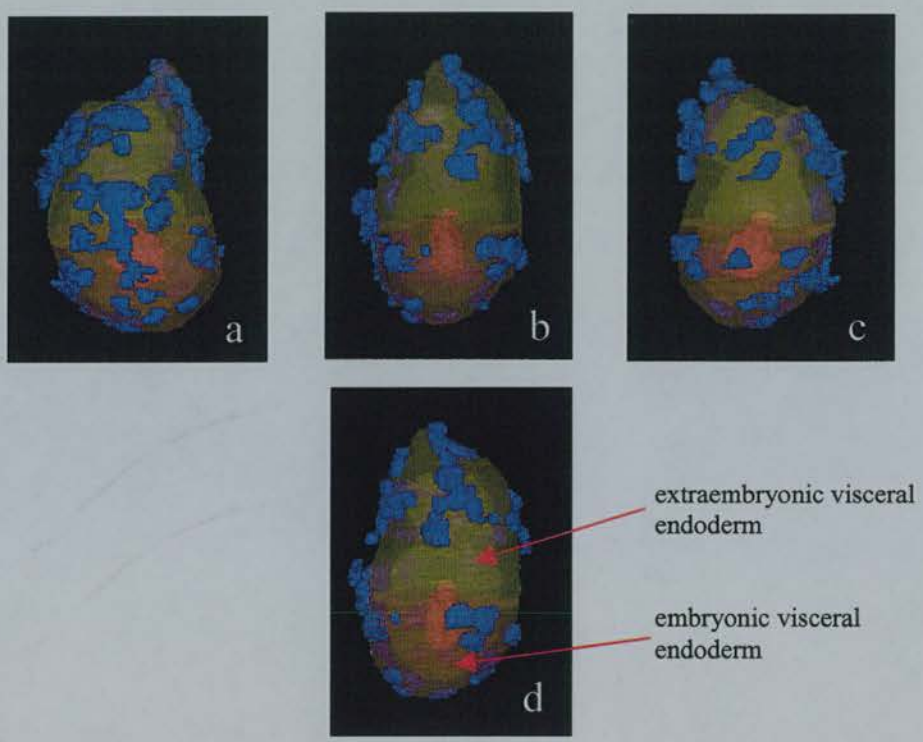

Figure 3.6: Four views of the E5.5 egg cylinder to show the distribution of parietal endoderm. (a), (b) are presumed lateral views and (c), (d) are presumed posterior and anterior views of the embryo (see text). Parietal endoderm (dark blue) extra-embryonic visceral endoderm (transparent yellow), embryonic visceral endoderm (transparent dark yellow), proamniotic cavity (red).

Do the cells of the visceral yolk sac endoderm have membrane bound vacuoles as opposed to the embryonic endoderm? (Gupta *et al.*, 1982; Kaufman, 1983), and is there a hole in the anterior visceral yolk sac just above the border between embryonic and extraembryonic ectoderm (Kaufman, 1984, 1992)

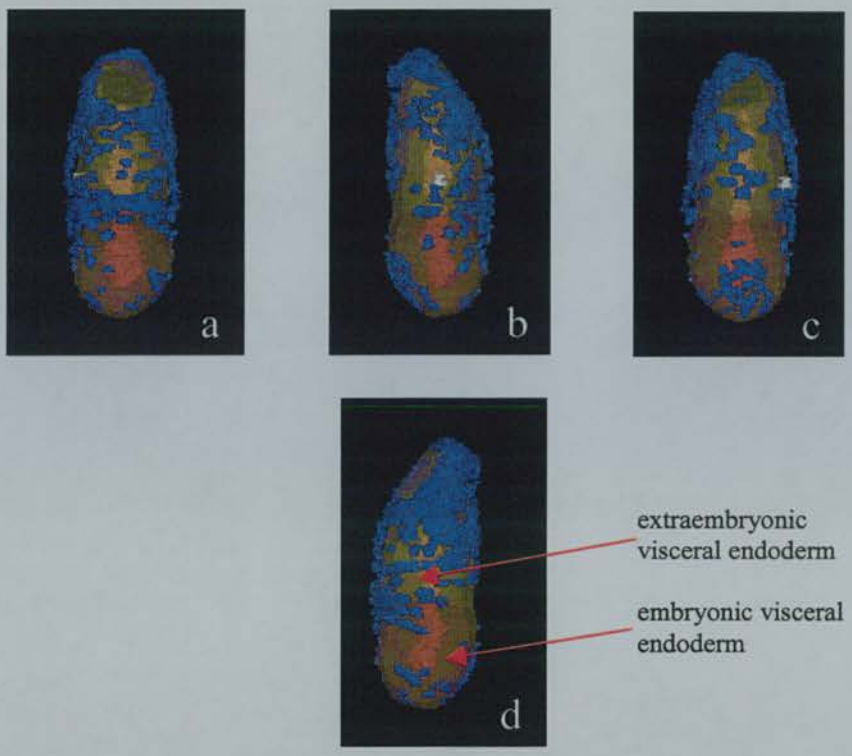

Figures 3.7: Four views of the E6 egg cylinder to show the distribution of parietal endoderm. (a) is a presumed frontal view, (b) is a presumed right view,(c) is a presumed posterior view and (d) is a presumed left view of the embryo. Parietal endoderm (dark blue) extra-embryonic visceral endoderm (yellow), embryonic visceral endoderm (orange), embryonic component of proamniotic cavity (red), extraembryonic component of proamniotic cavity (pink) and necrotic cells (white).

Is there a sign of hydrostatic pressure in the allantois and does it have more mitotic figure than other tissues in the embryo at this stage of development (Ellington, 1985)? Does the ectodermal component of the chorion have twice as many mitotic figures as the mesodermal component Ellington (1985)

3.3.3.2 Comparison with the literature

Egg cylinder formation

There is no sign of necrotic cells in the early proamniotic cavity of the E5.5 embryo (figure 3.6a,b) which is not consistent with Coucouvanis and Martin's (1996, 1999) description. There are necrotic cells, however, in both the embryonic and extra-embryonic proamniotic cavities of the E6 and the E6.5 embryos (figures 3.10a and 3.12a), although, for the E6.5 embryo, the amount of necrotic cells is higher in the extra-embryonic than in the embryonic region of the proamniotic cavity. The fact that there are more necrotic cells in the extraembryonic component of the proamniotic cavity than in the embryonic component of the cavity of the early streak embryo

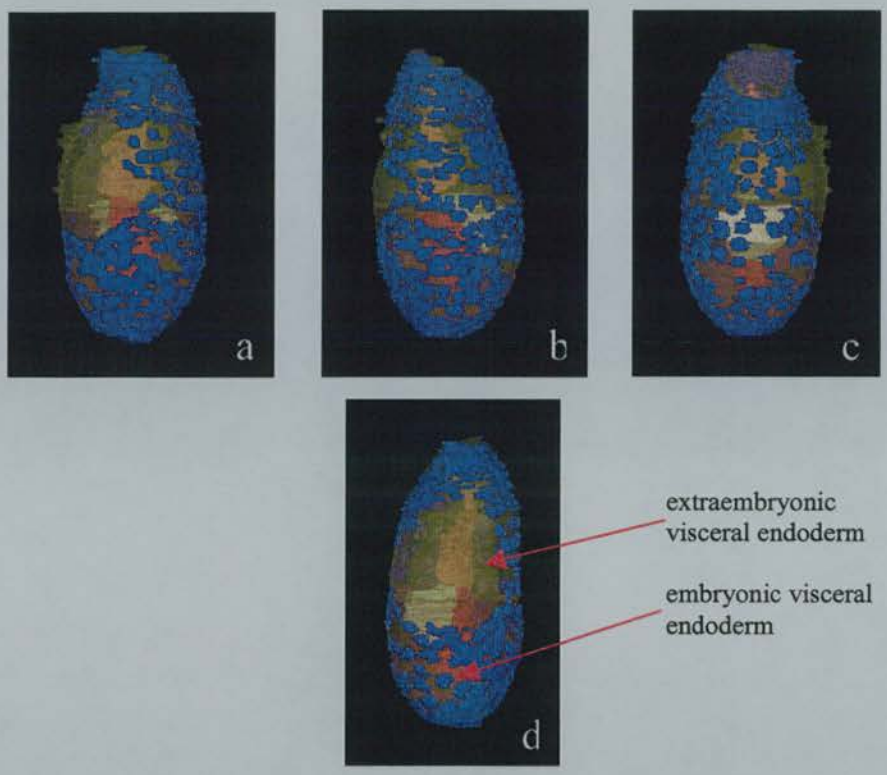

Figure 3.8: Four views of the E6.5 egg cylinder to show the distribution of parietal endoderm. (a) – frontal, (b) – right; (c) – back; and (d) - left Parietal endoderm (dark blue) extra-embryonic visceral endoderm (yellow), embryonic visceral endoderm (orange), embryonic component of proamniotic cavity (red), extraembryonic component of proamniotic cavity (pink) and primitive streak (white).

consistent with their theory because of the spread of the process of cavitation: it is to be expected that this process is in these stages in the embryonic part of the conceptus. The E7 and E7.5 embryos do not show any apoptosis in any of their cavities (figures 3.13a and 3.14a).

Visceral and parietal endodermIn none of the surface renderings of the visceral endoderm of any of the embryos studied can the ridge at the distal border of the marginal zone of the visceral endoderm be discerned (*e.g.*, see figure 3.11a-c) as described by Hogan and Newman (1984). This is probably because the combination of the resolution of the reconstruction and the rendering software is too low to distinguish such a fine difference in cell width.

The spread of the parietal endoderm on the yolk sac is more or less even in the E6.5 embryo (figure 3.8) with an increased density near the border with the visceral endoderm. The gap in the parietal yolk sac of the E6.5 is because of a dissection artefact: part of the sac was accidentally removed when dissecting the embryo. These

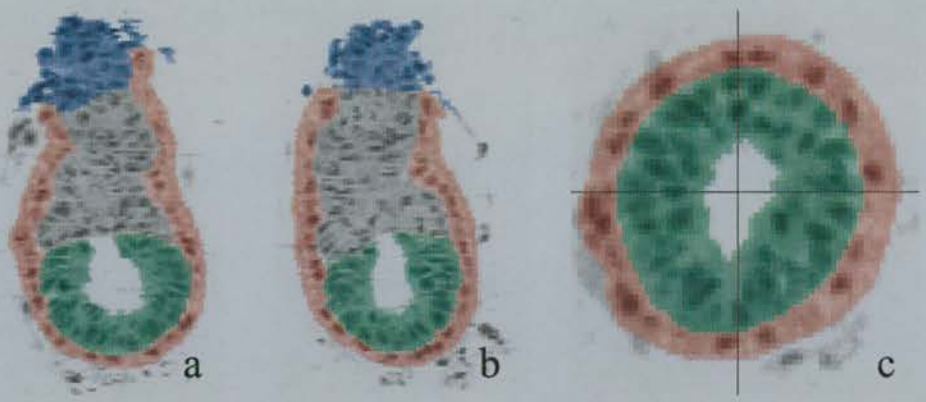

Figures 3.9: Two sagittal (a) and (b) and a transverse (c) section through the E5.5 reconstruction. (a) is parallel to the longest transverse axis through the proamnitotic cavity, and therefore presumed coronal. (a) also displays the steepest angle of the ectoplacental cone. (b) is perpendicular to the previous view and therefore presumed to be sectioned in the anterior-posterior direction. (c) is through the mid-embryonic region. The two lines indicate the planes of section of views (a - vertical) and (b - horizontal). Visceral endoderm (pink), epiblast (green) and ectoplacental cone (blue).

results are in line with the consensus that the parietal endoderm moves onto the yolk sac from the visceral endoderm (Lehtonen *et al.*, 1983; Lawson *et al.*, 1986; Hogan and Tilly, 1981). The E7 embryo was dissected free from its parietal yolk sac and therefore has no parietal endoderm. The E7.5 embryo was dissected with its parietal yolk sac, but the parietal endoderm was not delineated separately from the rest of the parietal yolk sac due to shortage of time.

The E 5.5 and E6 embryo showed a non-random distribution of parietal endoderm (figures 3.6 and 3.7). For the E6 embryo, there seem to be relatively few cells in the embryonic region apart from the left and right sides of the embryo (anterior side

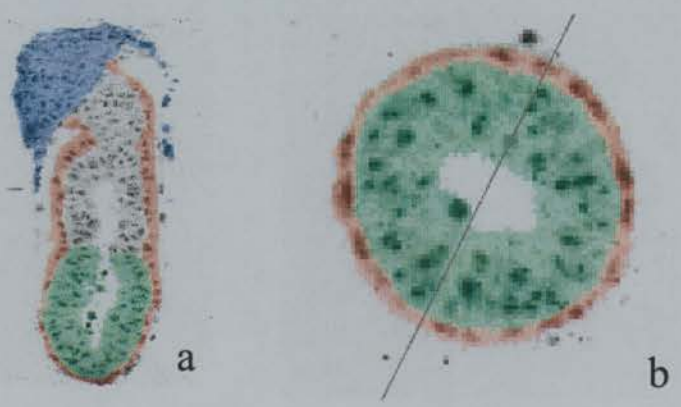

Figures 3.10: Sagittal (a) and transverse (b) section through the E6 reconstruction. View (a) is parallel to the shortest transverse axis through the proamniotic cavity, and therefore presumed in the anterior-posterior direction. (b) is through the mid-embryonic region. The line indicates the planes of section of view (a). Visceral endoderm (pink), epiblast (green) and ectoplacental cone (blue).

identified on the basis of groove in endoderm and orientation of proamniotic cavity – see next section). There is a concentration of cells in the caudal region of the embryo and around the anterior part of the border between the embryonic and the extraembryonic regions of the embryo. The extraembryonic region is more or less evenly covered, again, with a concentration of parietal cells near the border with the visceral endoderm.

The E5.5 embryo has very few parietal endoderm cells and the distribution is not even. If the assumption that the cavity indicates the anterior-posterior axis is correct, then there are hardly any cells down the left, right, and either anterior or posterior side of the embryo (since we cannot tell which side is which). There is also not a particular concentration apparent towards the border with the visceral endoderm. This pattern is not like the pattern in the E6 embryo and it might be that the pattern of distribution of parietal cells is random until the entire yolk sac has been lined with these cells (at E6.5).

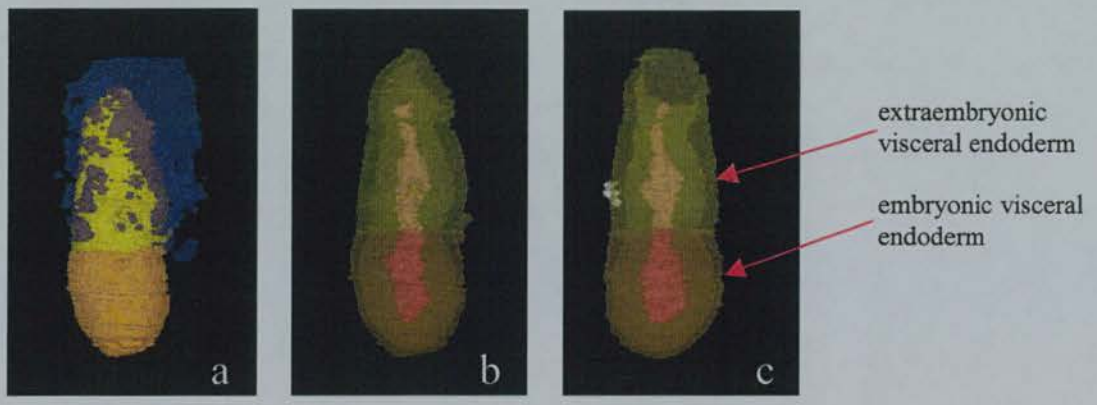

Figures 3.11: Presumed lateral (a and b) and presumed frontal views (c) of the E6 embryo, showing the anterior groove at the right hand side (a & b) and front (c). (c) also shows two necrotic cells. Extra-embryonic visceral endoderm -yellow transparent (solid in a), embryonic visceral endoderm - orange transparent (solid in a), embryonic component of the proamniotic cavity - red, extraembryonic component of the proamniotic cavity - pink, ectoplacental cone - blue and necrotic cells - white.

Asymmetry formation and axes

The E5.5 embryo

The E5.5 embryo does not have an anterior groove at the boundary between the embryonic and extraembryonic regions nor has it got heightened endoderm cells in the embryonic region just below this border (Varlet *et al.*, 1997). It does have a proamniotic cavity that is squashed in one direction, and presumably this is located in

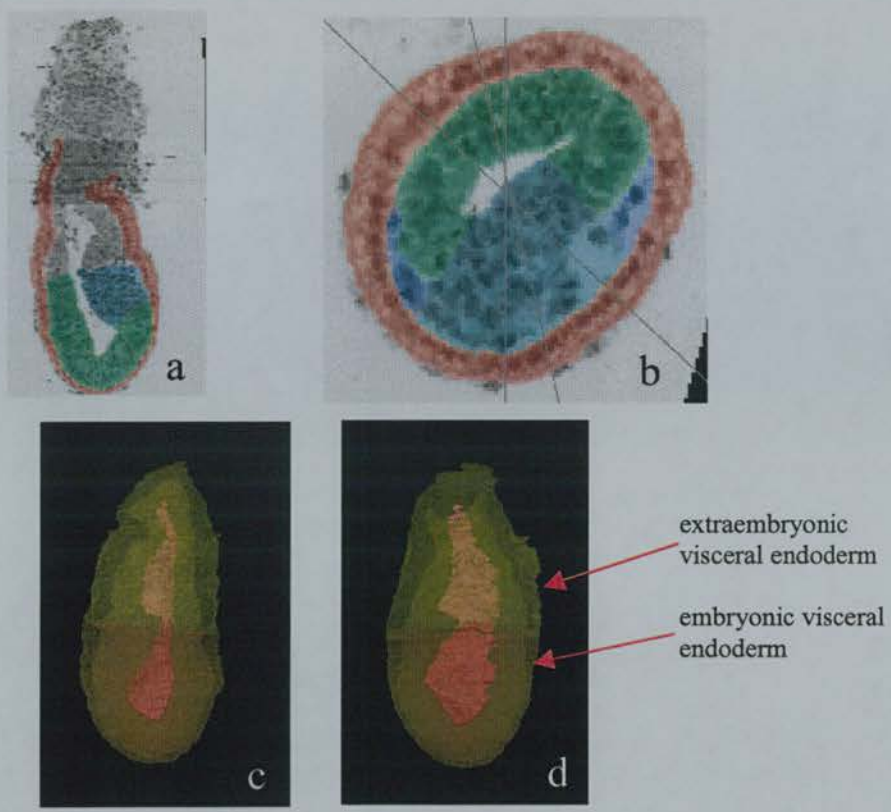

Figure 3.12: Sagittal (a) and transverse (b) sections through the E6.5 reconstruction. (a) is parallel to the steepest axis of the tilted ectoplacental cone. (b) is through the mid-embryonic region. The lines indicate the plane of section of view (a) (running from '12-6 o'clock'), the anterior-posterior axis (running from '5.30-11.30') and the shortest axis of the embryonic component of the proamniotic cavity (running from '4.30-10.30'). Visceral endoderm (pink), epiblast (green), embryonic mesoderm (blue) and primitive streak (turquoise).

Longitudinal views of the E6.5 embryo (c) - parallel to the longest (posterior to the left) and (d) shortest (posterior towards viewer) transverse axis of the proamniotic cavity. Extra-embryonic visceral endoderm (yellow transparent), embryonic visceral endoderm (orange transparent), embryonic component of the proamniotic cavity (red) and extraembryonic component of the proamniotic cavity (pink).

approximately the anterior-posterior direction. The ectoplacental cone is tilted, and the tilt is directed towards what is presumed to be the lateral side of the embryo, at an angle of 90° with the assumed anterior - posterior axis (figure 3.9). We cannot hypothesise whether this side is left or right, since there are no other asymmetries in the egg cylinder at this stage.

The E6 embryo

The E6 embryo has got an (assumed) anterior groove at the border but no heightened endodermal cells just distal to this groove (figures 3.10a and 3.11a). The proamniotic cavity in the embryonic region is squashed like that observed in the E5.5 embryo (figures 3.9c and 3.10b) and the direction of the compression is at a 20° angle with the

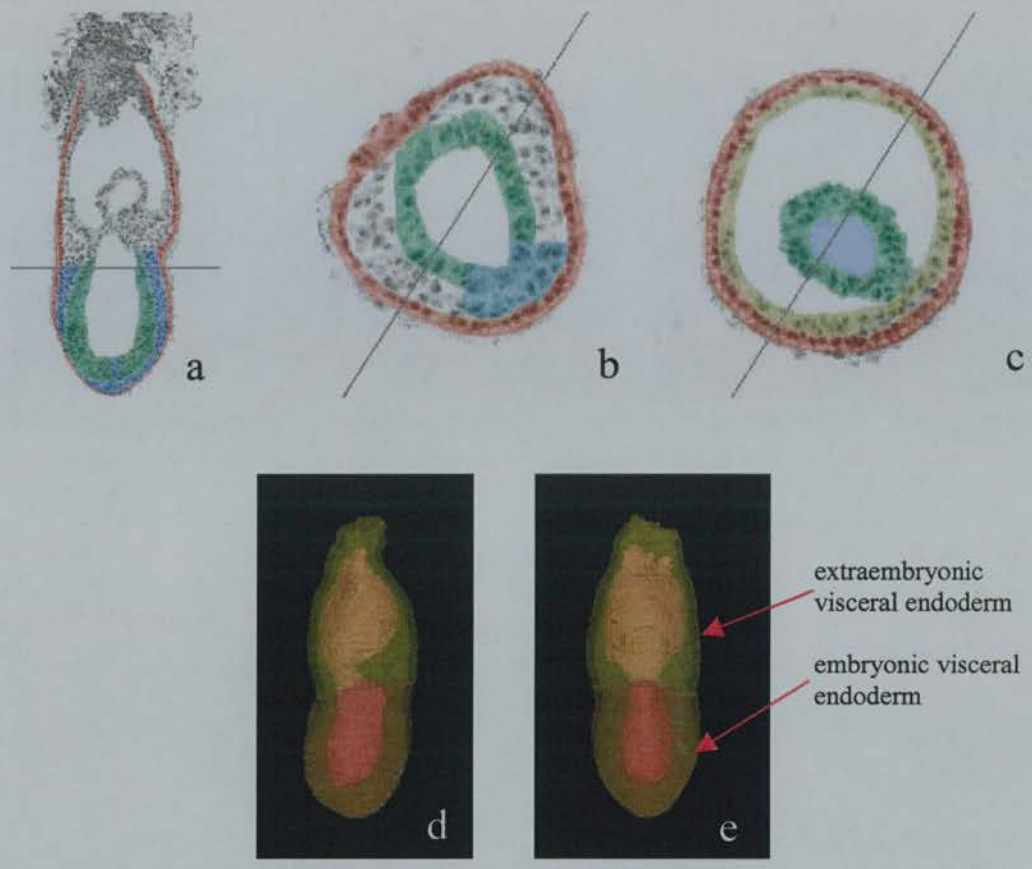

Figure 3.13: Sagittal (a) and transverse (b and c) sections through the E7 reconstruction. View (a) is parallel to the steepest axis of the tilted ectoplacental cone. (b) is through the mid-embryonic region, and shows heightened endodermal cells at the anterior region. The line indicates the plane of intersection of view (a). View (c) is through the extraembryonic region, and shows the round cavity and proamniotic fold (in this view green, with a turquoise cavity). Other colours are:visceral endoderm (pink), epiblast (green), embryonic mesoderm (blue), extraembryonic mesoderm (beige) and primitive streak (turquoise).

Lateral (d) and posterior (e) 3D views of the E7 embryo, showing the constricted proamniotic canal. Extra-embryonic visceral endoderm (yellow transparent), embryonic visceral endoderm (orange transparent), embryonic component of the proamniotic cavity (red) and extraembryonic component of the proamniotic cavity (pink).

groove. The tilt of the cone is exactly parallel to the direction of the compression of the cavity (figure 3.10a and 3.11b). If the groove is assumed anterior, then the cone is tilted towards the left anterior side of the embryo (figure 3.11a), which is according to Gardner (1992) but not to Smith (1980, 1985) who claims that the tilt of the cone is always exactly towards the posterior side of the embryo. The endodermal cells protruding around the groove (figure 3.11a,b) are not necrotic; however they do look abnormal. They have a normal nucleus but they do have irregular cytoplasmic 'outcrops' and therefore it is assumed that this morphology is likely to be a manipulation artefact.

The E6.5 embryo

The E6.5 embryo, which has an established primitive streak, has no heightened anterior endoderm cells or an anterior groove near the embryonic-extraembryonic border. The direction of the compression in the proamniotic cavity in the embryonic region is at a 30° angle with the anterior - posterior axis (figure 3.12). This is in line with the observation that the anterior-posterior direction grows faster than the lateral sides by the midstreak stage (Tam and Meier, 1982), and that the orientation of the cavity is similar to the orientation of the cavity in the early streak embryo shown by Belo *et al.* (1997). The tilt of the ectoplacental cone is directed towards the left posterior side of the embryo, at an angle of 15° with the anterior-posterior axis. This is, like the E6 embryo, according to Gardner's (1992), but not to Smith's (1980,

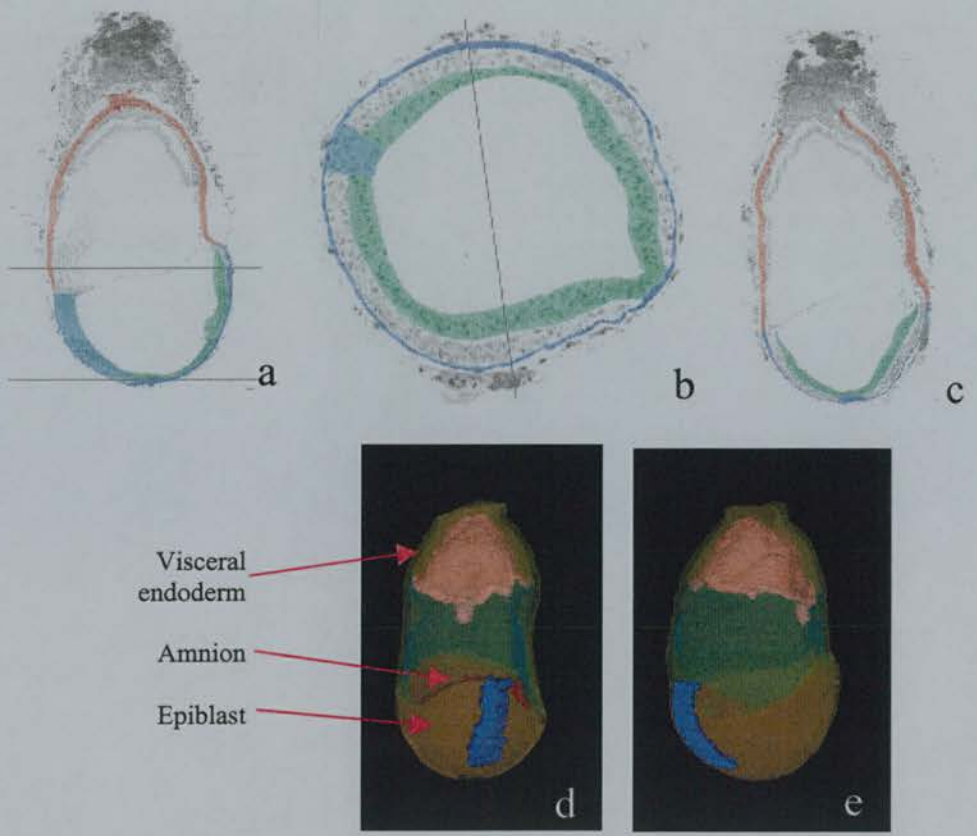

Figure 3.14: Midsagittal (a), transverse (b) and longitudinal parallel to the steepest axis of the tilted cone (c) sections of the E7.5 embryo. The transverse lines in (a) indicate the extent of the axial mesendoderm and the line in figure (b) indicates the line of intersection of view (a). Visceral extra-embryonic endoderm (pink), epiblast (green), embryonic endoderm and axial mesendoderm (blue) and primitive streak (turquoise).

3D views perpendicular (d) and parallel (e) to the steepest axis of the tilted cone of the E7.5 embryo. Visceral endoderm (yellow transparent), extra-embryonic mesoderm (turquoise), amnion (red), chorion (pink), primitive streak (blue), epiblast (brown).

1985), observations. The proximal visceral endoderm shows a manipulation artefact (figure 3.12d).

The E7 embryo

The E7 embryo, which is at the late streak stage, has no anterior groove but does have heightened cells anteriorly (figure 3.13b). The ectoplacental cone is tilted towards the anterior right side of the embryo, at an angle of 70° with the anterior-posterior direction (figure 3.13a, b). The longest direction of the cavity is now parallel to the anterior-posterior axis (figure 3.13b, d and e).

The E7.5 embryo

The E7.5 embryo has an anterior groove but no heightened cells anteriorly (figure 3.14a). The amniotic cavity is merely round (figure 3.14b) and the ectoplacental cone is tilted at an angle of 70° with the anterior-posterior direction towards the right hand anterior side of the embryo (figures 3.14b and c). This finding is not in agreement with the findings of either Gardner (1992) or Smith (1980). According to Smith (1980), the ectoplacental cone becomes symmetric between E6.75 and E7.25, but, although the tilt of the cone is less steep in the E7 and E7.5 embryos than in the developmentally less advanced embryos, the cone is still tilted in the E7.5 embryos (figure3.14d).

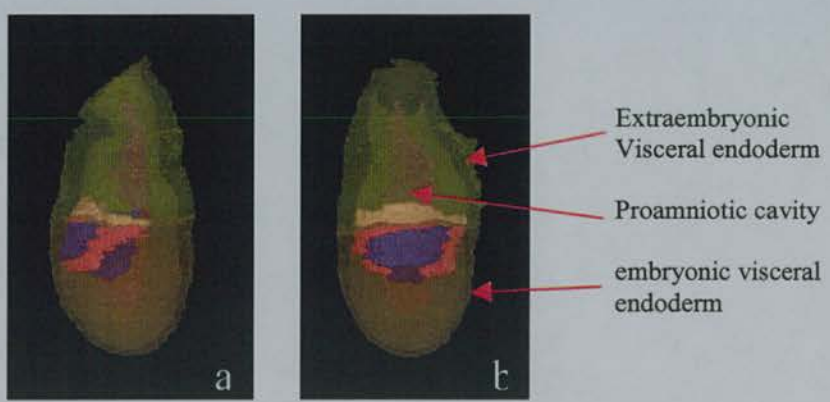

Figures 3.15: Lateral (a) and posterior (b) view of the E6.5 embryo. Extra-embryonic visceral endoderm (yellow transparent), embryonic visceral endoderm (orange transparent), embryonic mesoderm (red), extra-embryonic mesoderm (pink), primitive streak (blue) and proamniotic cavity (brown transparent).

Primitive streak and node

Mesoderm

The mesoderm in the E6.5 embryo, which has a primitive early streak, has spread laterally and posteriorly from the primitive streak (figure 3.15). The E7 embryo has mesoderm throughout the majority of the embryonic region, except for the anterior axial part of the embryo. The gap in the mesoderm is narrower towards the most distal tip of the embryo (*i.e.* the anterior end of the streak), widens towards the midembryonic region, and closes at the most rostral part of the embryo (figure 3.16). The extraembryonic region is more or less evenly covered, and the mesoderm reaches most proximally in the posterior region. By E7.5, the mesoderm has spread between the ectoderm and endoderm of the entire embryo (apart from the buccopharyngeal and cloacal membrane) and lined the visceral yolk sac. These findings agree with the description that the posterior region of the embryo grows more than the anterior region until approximately E7.5, after which the anterior region grows faster (Poelmann, 1981; Lawson and Pedersen, 1986). The facts that the extraembryonic

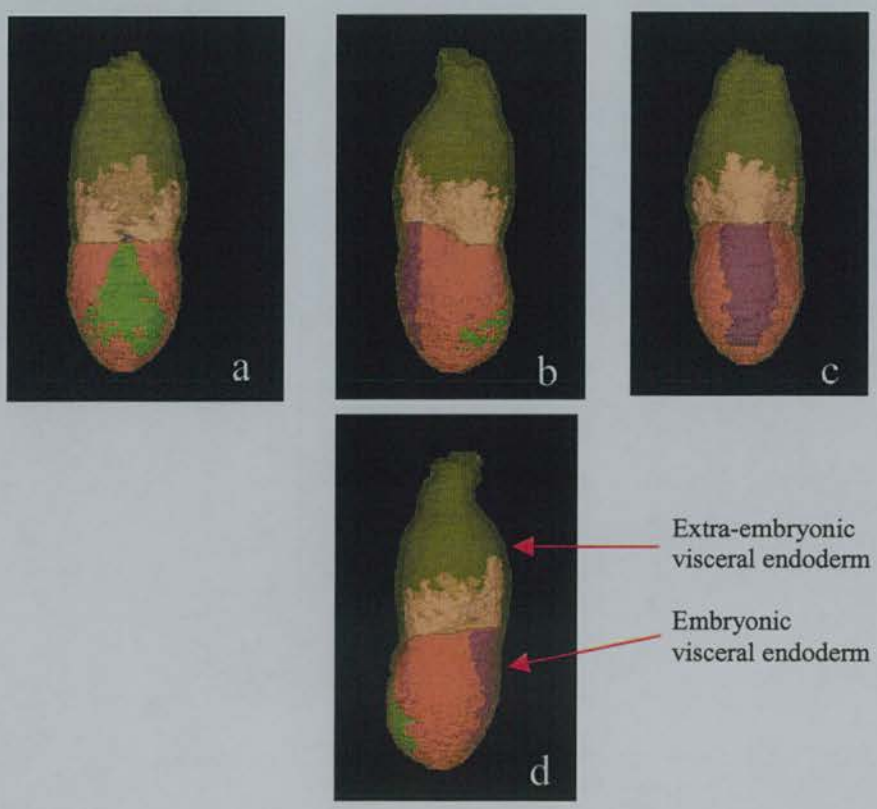

Figures 3.16: Front (a), right (b), back (c) and left (d) view of the E7 embryo. Extra-embryonic visceral endoderm (yellow transparent), embryonic visceral endoderm (orange transparent), embryonic mesoderm (orange), extra-embryonic mesoderm (pink), primitive streak (maroon) and epiblast (green).

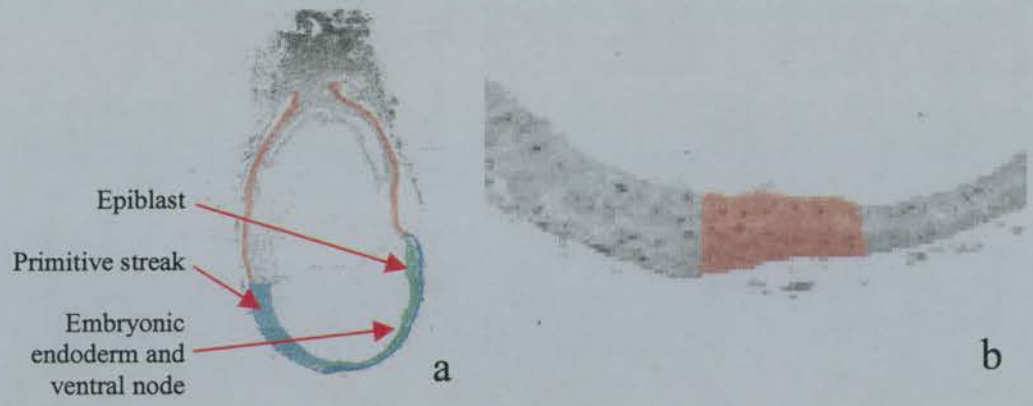

Figures 3.17: Low (a) and high (b) magnification of a midsagittal section through the node area in the reconstruction of the E7 embryo. View (a): extra-embryonic visceral endoderm (pink), epiblast (green), primitive streak (turquoise) and embryonic endoderm and ventral node area (blue). View (b): node area (pink).

mesoderm is being deposited first (Parameswaran and Tam, 1995) and that mesoderm cells move individually as well as in a cohesive sheet (Naktasuji *et al.*, 1986; Tam *et al.*, 1993), in combination with the pattern of the mesodermal spread in the E6.5 and 7 embryos, indicate that the most caudal tip of the primitive streak is the 'oldest' region (*i.e.* the part that was formed first).

Length of primitive streak

The primitive streak of the E6.5 embryo has a length of approximately 70 - 80 μm, the E7 embryo primitive streak measures 300 μm, the E7.5 embryo primitive streak measures 350 μm, the E8 streak 450 μm, the E8.5 streak 490 μm and the E9 primitive streak measures 300 μm. This finding is quite dissimilar to the report of Tam (1981) who reports that the streak reaches its maximal length at E7.5 of about 500 μm after which it regresses and only measures half this length by E8 and a third by E8.5. In the embryos used for this study the maximum length is reached a day later than he describes and this is most likely due to a difference in mouse strain since his timing schema is similar to the one used for the embryos in this study.

The node

The node has not developed in the E7 embryo, which has a posterior amniotic fold

and a continuous layer of endoderm at the most distal tip of the embryo. This is according to expectation (Bellomo *et al.*, 1996). The E7.5 embryo has a node as described by Bellomo, with a ventral and a dorsal aspect, the former forming a 'pit' in

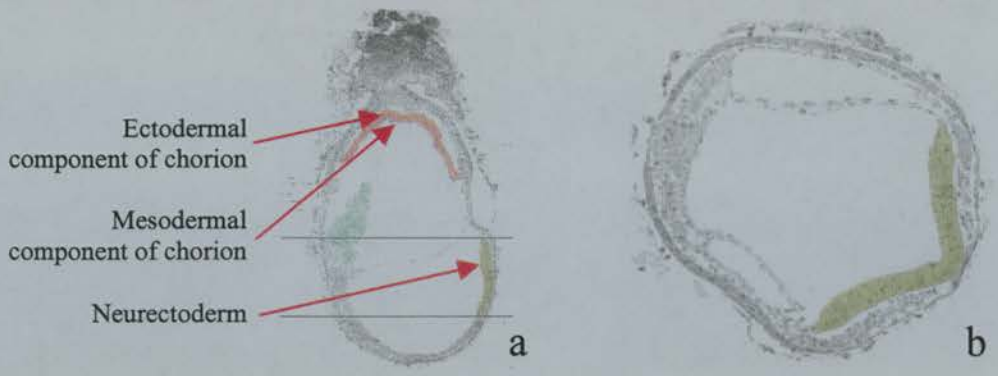

Figures 3.18: Midsagittal (a) and transverse (b) section through the neurectoderm in the reconstruction of the E7 embryo. View (a): ectodermal component of chorion (pink), allantois (green), mesodermal component of chorion (blue) and neurectoderm (beige). The two transverse lines indicate the extent of neurectoderm development. View (b): neurectoderm (beige).

the embryo, and lacking underlying endoderm (figure 3.17). Unfortunately, due to the resolution of the reconstruction it is not possible to compare mitotic indices between the dorsal and ventral aspects. Neither is it possible to distinguish the horseshoe shaped ring situated around the ventral 'pit' (Bellomo *et al.*, 1996). Anterior to the ventral aspect of the node is the axial mesendoderm or head process and posterior is the primitive streak. The axial mesendoderm reaches from the node to almost the most rostral part of the embryo (figure 3.14a).

Neurectoderm

In the E7.5 embryo, the neurectoderm has started developing in the anterior region, where a more columnar medial aspect can be distinguished from the lateral cuboidal surface ectoderm (figure 3.18b). The extent of this development stretches from almost the most proximal aspect of the embryo to about midway towards the node region (figure 3.18a).

Extraembryonic membranes

The E7 embryo

Figure 3.19 shows the posterior and left lateral view of the proamniotic fold in the egg cylinder. The figure shows that the mesodermal lining of the posterior amniotic fold stretches as far lateral as the cavity of the posterior amniotic fold, but only covers the distal side of the cavity, leaving the proximal side of the cavity covered by the extraembryonic ectodermal aspect of the fold. This aspect was not described by Ellington's account on the development of the proamniotic cavity (1987).

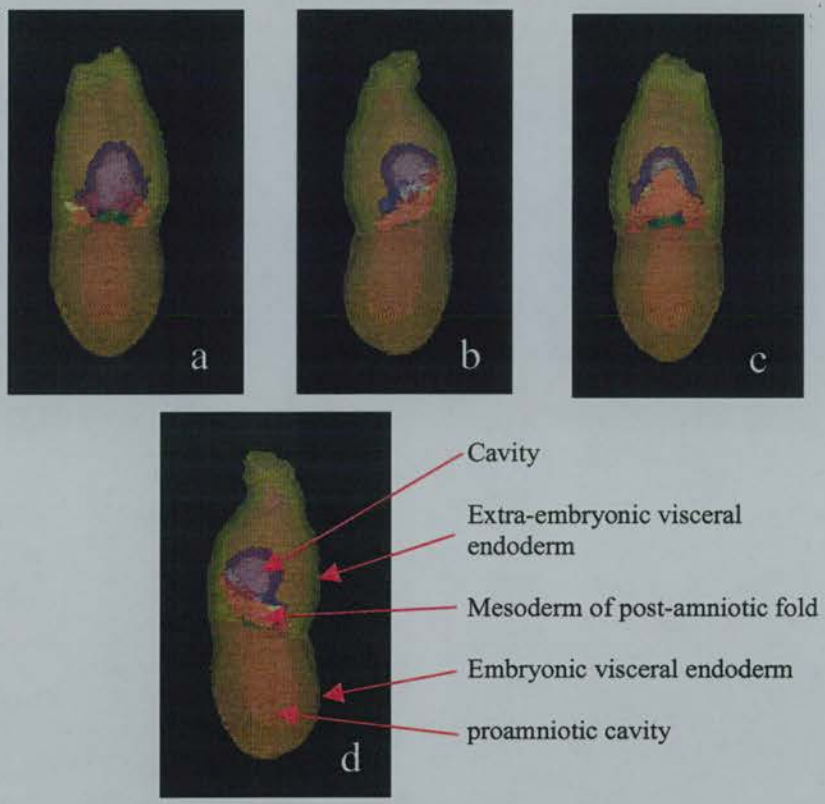

Figures 3.19: Front (a), left, (b), back (c) and right (d) view of the E7 embryo. Extra-embryonic visceral endoderm (yellow transparent), embryonic visceral endoderm (orange transparent), mesoderm in the posterior amniotic fold (red), cavity in the posterior amniotic fold (white), extra-embryonic ectodermal component of the posterior amniotic fold (blue), epiblastic component of the posterior amniotic fold (green) and proamniotic cavity (brown transparent).

The anterior proamniotic fold has not developed in this embryo. The morphology of the circumferentially constricted proamniotic canal (figure 3.13d and e), however, together with the lateral extension of the cavity of the posterior amniotic fold (figure 3.19), suggests that the proamniotic fold closes via circumferential constriction rather than a posterior and an anterior fold meeting.

The E7.5 embryo

Unfortunately mitotic indices cannot be checked in the allantois and mesodermal and ectodermal aspects of the chorion because of the resolution of the reconstruction, but what is clearly visible (figure 3.20) is the vacuolated aspect of the allantois (Ellington, 1985) and the very thinly spread mesothelium on the ectodermal aspect of the chorion (Ellington, 1985), and both observations are in agreement with her descriptions.

Yolk sac canal

Figures 3.20: Midsagittal sections of the E7.5 reconstruction showing the chorion: ectoderm (pink) and mesoderm (blue) and in (a) allantois (green).

Only the E6 embryo shows necrotic cells (2 in total, next to each other) in the extraembryonic visceral endoderm, in combination with a thin extraembryonic ectoderm at the same level. However, this does not occur at the same place as Kaufman (1984, 1992) describes: their location is not at the anterior side just above the border between epiblast and extraembryonic ectoderm, but they are situated almost 90° towards the left, above the embryonic-extraembryonic border, approximately 1/3 of the way towards the ectoplacental cone (this assumes the groove at the border between the embryonic and extraembryonic region of the egg cylinder is anterior) (figure 3.11c).

3.3.3.3 Unexpected anatomical features

Border between squamous and cuboidal endoderm

An aspect that has not been described before is the border between the squamous and the columnar endoderm in the visceral endoderm of the egg cylinder. In the E5.5 embryo, all visceral endoderm is still cuboidal (figures 3.9a and b). In the E6, E6.5, E7 and E7.5 embryos, the border between the squamous and the columnar endoderm is in the embryonic region, and as development progresses, this border becomes sharper (figures 3.10a; 3.11b and c; 3.12a, c, and d; 3.13a, d and e; 3.14a and c; and 3.17a). As described by Gupta *et al.*, 1982 and Kaufman, 1983, the cuboidal endoderm in the extraembryonic region contains more membrane-bound vacuoles than the embryonic aspect.

Irregularities in the extraembryonic ectoderm

The tilt of the ectoplacental cone seems to evoke an irregularity in the extraembryonic ectoderm of all egg cylinders, which is more exaggerated than the irregularity in the covering visceral endoderm. The extra-embryonic ectoderm in the younger embryos is more irregular than in the older ones, and by E7.5, this irregularity has almost gone, suggesting, that possibly, the ectoplacental cone is becoming symmetrical (Smith, 1980) (figures 3.6d, 3.11b, 3.12c, 3.19 and 3.14d and e).

Anterior vs. posterior epiblast

The posterior aspect of the epiblast seems to extend further proximally than the anterior epiblast as the embryo develops. If the assumption that the proamniotic cavity is compressed in the anterior-posterior direction in the E5.5 embryo is true, then there is an interesting relationship between the extent of the anterior epiblast and the extent of the posterior epiblast. In the E6 and the E6.5 embryos, these are level (figures 3.11b and 3.12b,d). In the E7 embryo however, the posterior epiblast becomes increasingly more proximal compared to the anterior epiblast (figures 3.16b,d). The epiblast of the E5.5 embryo is extending more proximal at either the anterior or posterior side (figure 3.9b). If both the compression of the cavity and the epiblast extending further on one side of the short axis through the cavity are consistent, then the polarity has become morphologically clear by this stage. Given the tendency for the posterior border to become more proximal with increasing developmental age, (except for the E7.5 (figure 3.14a)), it may well be that the anterior border of the epiblast is more proximal in the E5.5 embryo.

3.3.4 Early organogenesis (E8, E8.5 and E9)

3.3.4.1 Descriptions from the literature to be checked in the models

Neural tissue

General

The headfold or cranial flexure starts to form just before E8 at the most rostral tip of the embryo, and then progresses caudally until it reaches the mesencephalon between E9 and E10 (Jacobson and Tam, 1981). Can the neural fold be seen to be progressing caudally in the E8, E8.5 and E9 embryos? Does the increase of the angle of the cranial

flexure indeed seem to pause during neural tube formation in this area, *i.e.* between E8 and E9 (Tam, 1981)?

Is the division visible between the fore-, mid-, hindbrain in the E8 reconstruction, as expected?

Does occlusion occur before closure of the neural tube as Kaufman (1983) reports? If yes, then what is the extent of the occlusion in the three embryos studied?

Hindbrain

There is little descriptive literature available on when each of the rhombomeres develop. However, there are some pointers for the mouse: Kaufman and Bard (1999) describe two rhombomeres in the E8.5 embryo, and Murphy *et al.* (1989) describe six rhombomeres at E9.5. Do the E8.5 and E9 reconstructions comply with these findings? For the rat, seven rhombomeres have been described during the stage at which the embryo possesses between 14 and 18 pairs of somites.

In the rat, the trigeminal and facioacoustic ganglion originate from the 1st and 4th rhombomeres and are visible at (rat) E9 (Adelmann, 1925). Do the trigeminal and facioacuostic ganglia originate from the same rhombomeres in the mouse?

Sensory organs

At what level of the rhombomeres can the otic placode and pit be seen in the E8.5 and E9 embryo? Is there an otic placode in the E8 embryo? In the rat, at the stage when the embryo has 9 pairs of somites, the otic placode covers rhombomere 4 and by the stage that the embryo has 14 pairs of somites, the placode has become level with rhombomere 5 (Adelmann, 1925).

Are the optic structures visible in the E8 embryo (Kaufman, 1979) and has the brain closed cranially to the optic structures by E8.5?

Heart

General

Moorman *et al.* (1992) describe a theory of how the heart can function without valves, and a crucial component of this theory is that the cardiac jelly acts as a cushion to reduce the lumen in the heart tube to zero during a contraction. Given that no valves

are expected at these stages, is the extent of the cardiac jelly indeed such that it could fulfil such a function?

Ingalls (1926) drew an endothelial tube of a human heart that is at a similar stage of development to the E8 mouse embryo. The morphology of this heart tube is very irregular, with an irregular surface texture, in all dimensions, and the tube is lacerated with holes that allow communication between the ventral and the dorsal aspects of the endothelial tube. Does the endothelial tube of the E8 embryo resemble Ingalls drawing?

Looping

Many theories have been put forward about the mechanisms behind the looping of the heart, some of which imply differential growth of the heart myocardium (Davis, 1927; Van Praagh and De Haan; Wilens; 1955; Lepori, 1966; Stalsberg, 1969 and Patten, 1949). Is there anything visible in the reconstructions of the E8, E8.5 and E9 hearts that can support these theories? Features supporting these theories are local thinning of myocardial walls at the bending points of the looping heart, if these walls were of even thickness before looping, and a non-consistent internal and external structure of the heart, if these were consistent before the onset of looping. It has been suggested that the looping is facilitated by a lengthwise growth of the tube in combination with a ruptured dorsal mesocardium (Patten, 1922). Is the mesocardium ruptured before the onset of looping?

Vascular system

Moffat (1959) describes the vascular system of the arterial arch arteries as symmetric. Even though we can only expect two pairs of arch arteries at E9 (Theiler, 1972), can this be confirmed to be symmetric? Since the vascular system is a largely paired system, what is the difference between the progress of development in the left and right vascular structures?

The right umbilical vein has been reported to regress at about E9 (Kaufman and Bard, 1999), is there a sign of the regression in the embryonic part of this vein at this stage?

Gut

Lamers *et al.* (1987) describe that the wall of the gut is thin until the gut closes in the ventral midline, after which its cells become more columnar. Can we check this

statement in the three reconstructions and is it true for each stage? What is the topography of the hepatic diverticulum in the E8.5 and E9 embryo? Is it, as Godlewski *et al.* (1992) describe, separated ventrally from the heart and caudally from the sinus venosus by the septum transversum? Is there at either stage, a contact with the heart endothelium?

Somites

Tam (1981) finds that the somites of the upper trunk and tail are half the volume of the lumbar and sacral somites. Can this be confirmed in the reconstructions of E8-E9? He also states that the cranial border of somite 1 is just below the otic placode and Adelmann (1925) finds that in the rat, the caudal boundary of rhombomere 7 is level with the cranial boundary of somite 1. Can this topography be confirmed in the E8, E8.5 and E9 mouse?

Notochord

Jurand (1974) describes that the notochord develops from the node and gets incorporated in the gut roof until E9.5, after which the notochord separates from the roof of the gut but stays closely attached for a while to both the floor plate of the neural tube and the roof of the gut. At what stage in the E8, E8.5 and E9 does the notochord start separating from the gut roof and does it remain closely attached to both neural tissue and gut during these stages?

3.3.2.2 Comparison with the literature

Neural tissue

<u>General</u>

Little can be said to confirm the theory that the headfold moves caudally between the E8, E8.5 and E9 embryo. This is particularly the case, since in the E8 embryo, fore-, mid and hindbrain are not morphologically distinguishable (figure 3.21a,b), although it is not unlikely that the head fold is in the region of the presumptive midbrain. In the E8.5 and E9 embryos, the head fold appears to be in a similar place: *i.e.* in the middle of the midbrain (figure 3.21c-f). Therefore, in these models, the theory that the headfold starts at the most rostral tip of the embryo and then moves caudally until it

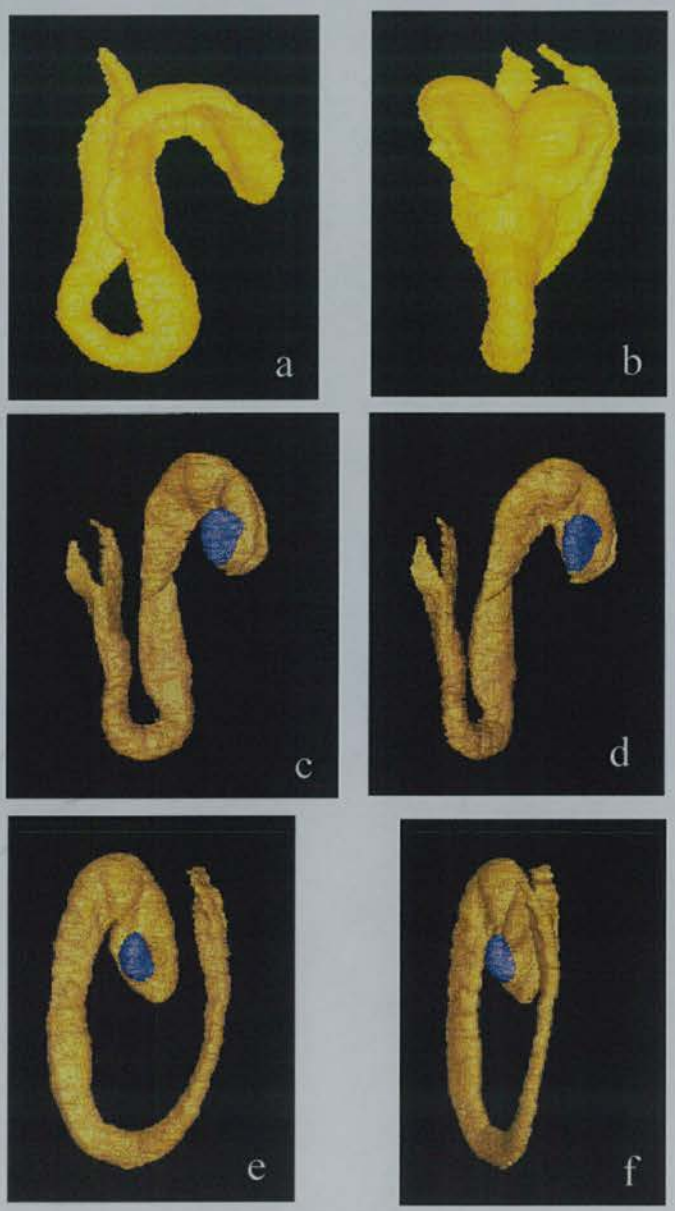

Figures 3.21: Lateral and frontal views of the neural tissue of the E8, E8.5 and E9 embryos. (a) lateral E8, (b) frontal E8, (c) lateral E8.5, (d) semi-fromtal E8.5, (e) lateral E9, (f) semi-frontal E9. Neural tissue (yellow), optic-vesicles (blue)

arrives at the midbrain (Jacobson and Tam 1981) cannot be confirmed.

The angle of the cranial flexure is difficult to quantify because of the curved aspect of the neural tissue in all directions (figure 3.21a, c and e). However, if one were to draw a line through the most rostral tip of the neural tissue and the middle of the flexure, then the angle between this line and the length axis of the hindbrain does not change much over the period of neural tube closure in this area, and varies between 20° and 30°. This finding disagrees with the finding of Jacobson and Tam (1981) that the cranial flexure pauses while tube closure occurs.

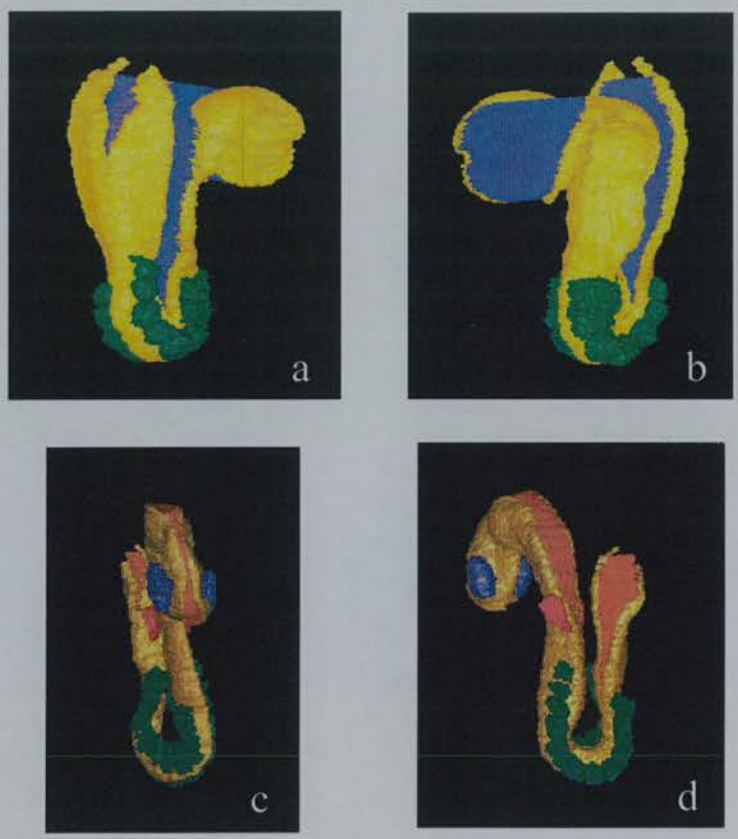

Figures 3.22: Posterior (a) and anterior (b) views of the neural tissue (yellow), lumen (blue) and somites (green) of the E8 embryo.

Anterior (c) and posterior (d) views of the neural tissue (yellow), lumen (orange), optic vesicles (blue), otic placodes (dark pink), and somites (green) of the E8.5 embryo.

The E8.5 and E9 embryo both have a morphologically distinguishable fore-, mid- and hindbrain, although in neither of the embryos studied could the hindbrain be distinguished from the future spinal cord (figure 3.21d and f). In both embryos the optic vesicles originate from the 3rd ventricle in the forebrain, caudal to which there is a smaller and more flattened vesicle. Caudal to the prosencephalon or forebrain is the

mesencephalon, which has two aspects in both embryos: rostrally there is a vesicle caudal to which there is a flattened aspect before merging into the rhombomeres.

The closure of the neural tube in the E8 embryo extends from the caudal boundary of the 2nd pair of somites to the cranial boundary of the 7th pair of somites (figure 3.22a and b). If the closure of the tube travels as fast rostrally as caudally, then the closure started at the border between the 4th and 5th pairs of somites, which is just in the cervical region, as described by Bard and Kaufman (1999) and Jascobson and Tam (1981).

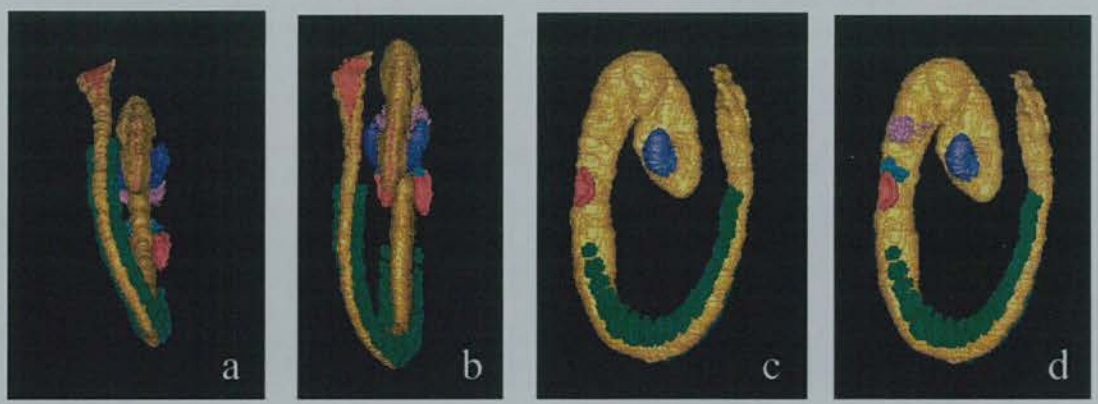

Figure 3.23: Anterior neuropore (a) and anterior (b) and lateral (c and d) views of the neural tissue (yellow), optic vesicles (blue), otic placodes (dark pink), trigeminal ganglion (lilac), facioacoustic ganglion complex (turquoise) and somites (green) of the E9 embryo.

At E8.5 the closure has progressed cranially to the mid-level of the otic placode, and caudally tube formation has progressed to the caudal boundary of the last formed somite (figures 3.22c and d). This is similar to the findings by Jacobson and Tam (1981) that an embryo with 14 pairs of somites had a fused tube up to the caudal boundary of the otic placode with an otherwise open brain region.

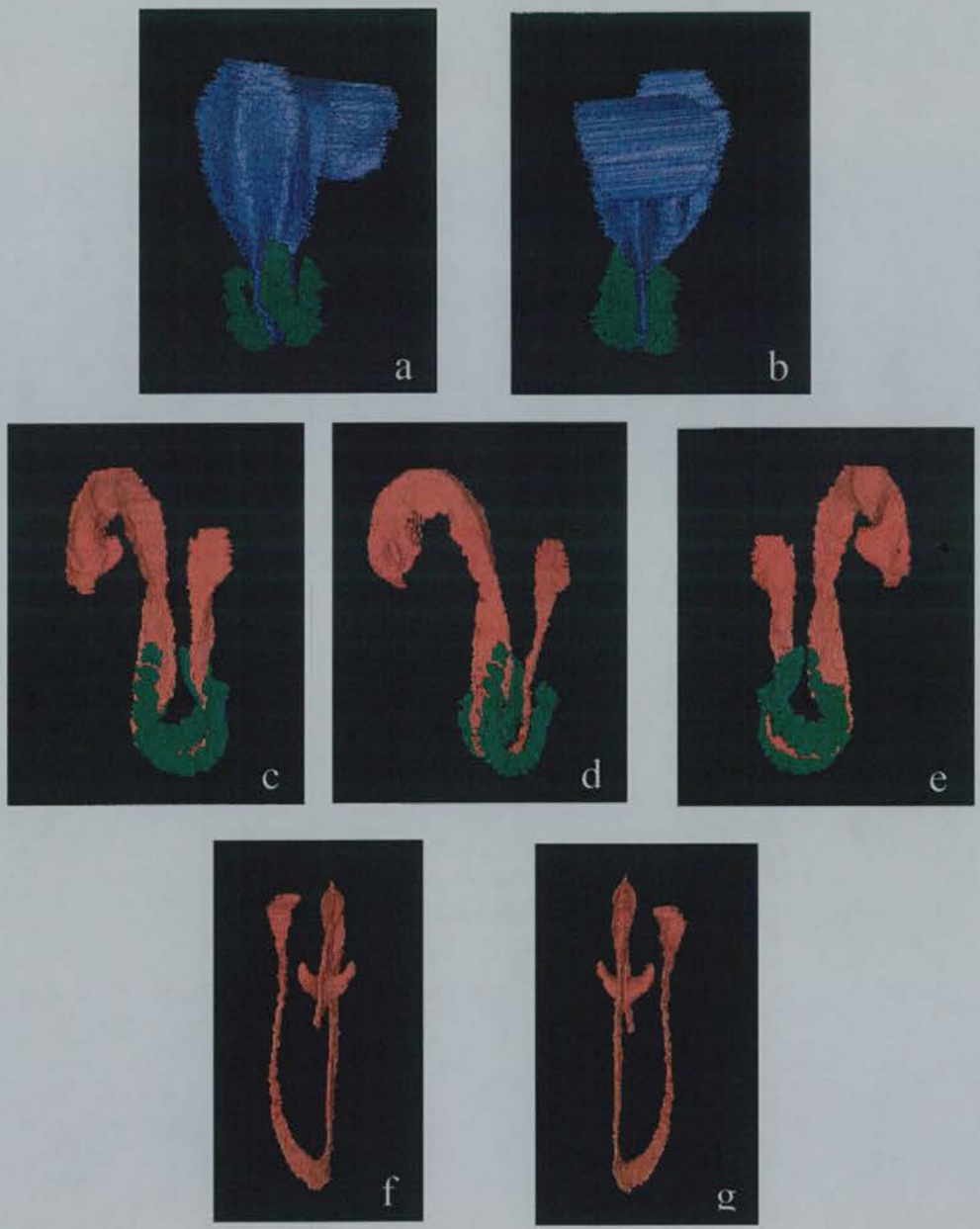

Figure 3.24: Posterior (a) and anterior (b) views of the neural lumen (blue) and somites (green) of the E8 embryo. Left lateral (c), left-anterior (d) and right lateral (e) views of the neural lumen (red) and somites (green) of the E8.5 embryo. Anterior (f) and posterior (g) views of the neural lumen (red) of the E9 embryo.

At E9 the closure is complete apart from a caudal neuropore which extents caudally from about 3 somites' length caudal to the last formed somite, and a tiny anterior neuropore (figure 3.23a and b). The line-like opening in the neural tube is an artefactual re-opening after closure of the tube due to processing of the embryo (figure 3.23a). The closure of the neural tube in this embryo is advanced compared to the findings of Kaufman (1979) and Jacobson and Tam (1981) who found that embryos with 17 pairs of somites still had open midbrains.

The occlusion of the neural tube, as presented by Kaufman (1983), occurs indeed before closure of the tube, and, moreover, is ahead of the closure of the tube in the caudal region of the embryo (figure 3.24), and in the E8 embryo, is 2 somites' length ahead of closure in the cranial direction as well. In the caudal direction, the occlusion is one somite's length ahead in the E8 embryo, 2-3 somite's lengths ahead in the E8.5, and level with the closure of the tube in the E9 embryo. In the E8.5 embryo there is no occlusion in the mid- and forebrain whereas in the E9 embryo, the occlusion includes the forebrain (apart from the optic vesicles) and the hindbrain caudal to rhombomeres 1 and 2.

Hindbrain

No rhombomeres can be distinguished in the hindbrain of the E8.5 embryo (figure 3.21d), which is not in agreement with the findings of others (Kaufman and Bard, 1999). In the E9 hindbrain, 5 rhombomeres can be distinguished (figure 3.21f) which is one less than Murphy *et al.* (1989) described for the E9.5 mouse embryo. Adelmann (1925) describes 7 rhombomeres in two rat embryos with 14 and 18 pairs of somites. It seems therefore, that the rhombomere formation is somewhat delayed in the mouse with respect to the rat, at a stage with a similar number of somites.

Sensory organs and ganglia

The optic structures can be clearly seen in the E8, E8.5 and E9 embryos (figure 3.21b-f).The optic evaginations at E8 are just slight indentations in the most rostral aspect of the forebrain, at E8.5 they have a rounded morphology and at E9 the optic vesicles are directed cranially and posteriorly, similar to the shape of horns.

The otic placodes are not present yet in the E8 embryo, and in the E8.5 embryo, the placodes are approximately 1, and in the E9, 2 somites' length apart from the 1st somite (figures 3.22d and 3.23c) This may indicate that in the E8.5 embyo, one somite has disintegrated and in the E9 embryo, 2 somites, since Tam (1981) describes the caudal boundary of the otic placode as being level with the cranial boundary of the first somite

In the E9 embryos, the otic pits are exactly level with the 5th rhombomere, which is similar to the situation observed in the rat (Adelmann, 1925), given that the 5th rhombomeres are equivalent in rat and mouse, despite the fact that the rat only forms 7 pairs and the mouse 8 pairs.

In the E9 embryo, the trigeminal and facioacoustic ganglia (figure 3.23d) are associated with the 2nd and 4th rhombomeres, respectively. This is unlike the situation in the rat, where these ganglia are associated with the 1st and 4th rhombomeres, respectively (Adelmann, 1925).

Heart

General

The reconstruction of the E8 embryo, shows, unlike that which could have been expected (Kauman and Bard, 1999), no clear demarcations between three segments that indicate a common atrium, primitive ventricle and an outflow tract of this approximately tubular heart (figure 3.25). In the E8.5 embryo, all three compartments are now clearly distinguishable (figures 3.26): there is a common atrium, separated from the primitive ventricle by the atrio-ventricular canal. There is a clear demarcation between the primitive ventricle and the outflow tract of the heart, termed the bulbo-ventricular groove. The outflow tract does not have a clear region of demarcation between the bulbus cordis region and the aortic sac region of the outflow tract, and this was described by Pexeider *et al.* (1995). The E9 heart shows a similar morphology to the E8.5 heart but with an ongoing development of the morphological features described in the E8.5 embryo (figure 3.27). In none of the three embryos can a sign of the onset of any cardiac valve formation be found.

In the E8 embryo, the cardiac jelly is more extensive than the myocardial walls of the heart and stretches both cranially and caudally beyond the rostral and caudal extents of the heart (figure 3.25). In the E8.5 embryo, the cardiac jelly still stretches beyond the rostral boundary of the outflow tract but not beyond the caudal border of the common atrium. Either the common atrium has grown whereas the cardiac jelly has not, or the cardiac jelly has disintegrated, but only part of the atrium is now lined by cardiac jelly (figure 3.26). In the E9 embryo, it can be seen that this trend has progressed: even less so than in the E8.5 embryo is the common atrium now lined by cardiac jelly (figure 3.27). Moreover, there are now parts of the outflow tract that are not lined by cardiac jelly. It needs mentioning however, that the boundaries of the myocardium with the bordering mesothelial lining of the pericardial cavity and pericardio-peritoneal canals have been based on cellular arrangement and 3D

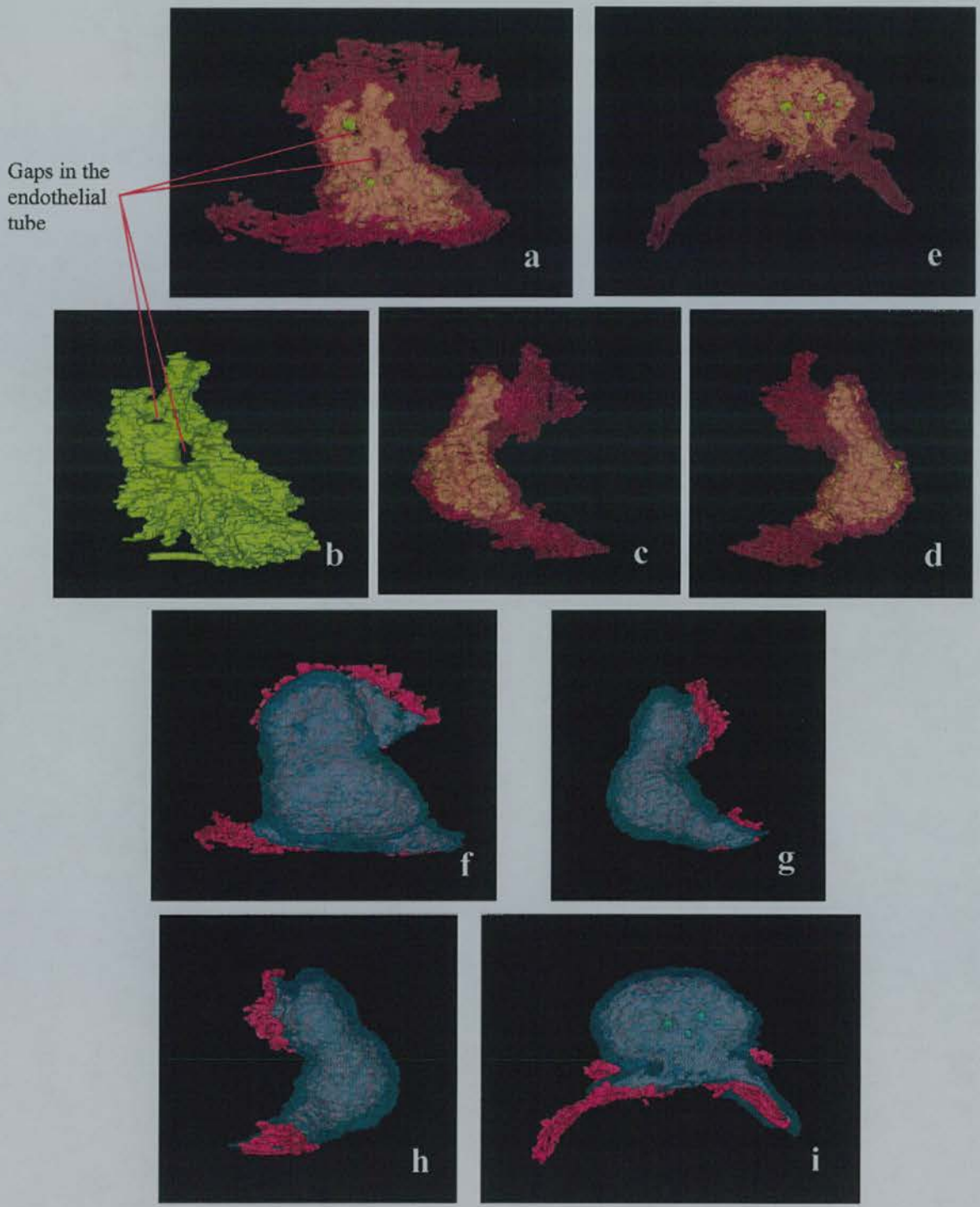

Figure 3.25: Anterior (a & b), left lateral (c), right lateral (d) and bottom (e) views of the endothelial lining (yellow) and cardiac jelly (pink transparent) of the E8 heart.

Additional views show the myocardium (turquoise transparent) with the cardiac jelly (solid pink): anterior (f), left lateral (g), right lateral (h) and bottom (i).

configuration of these tissues, and not on the presence of myosin-type filaments, since these could not be observed using the staining method employed here.

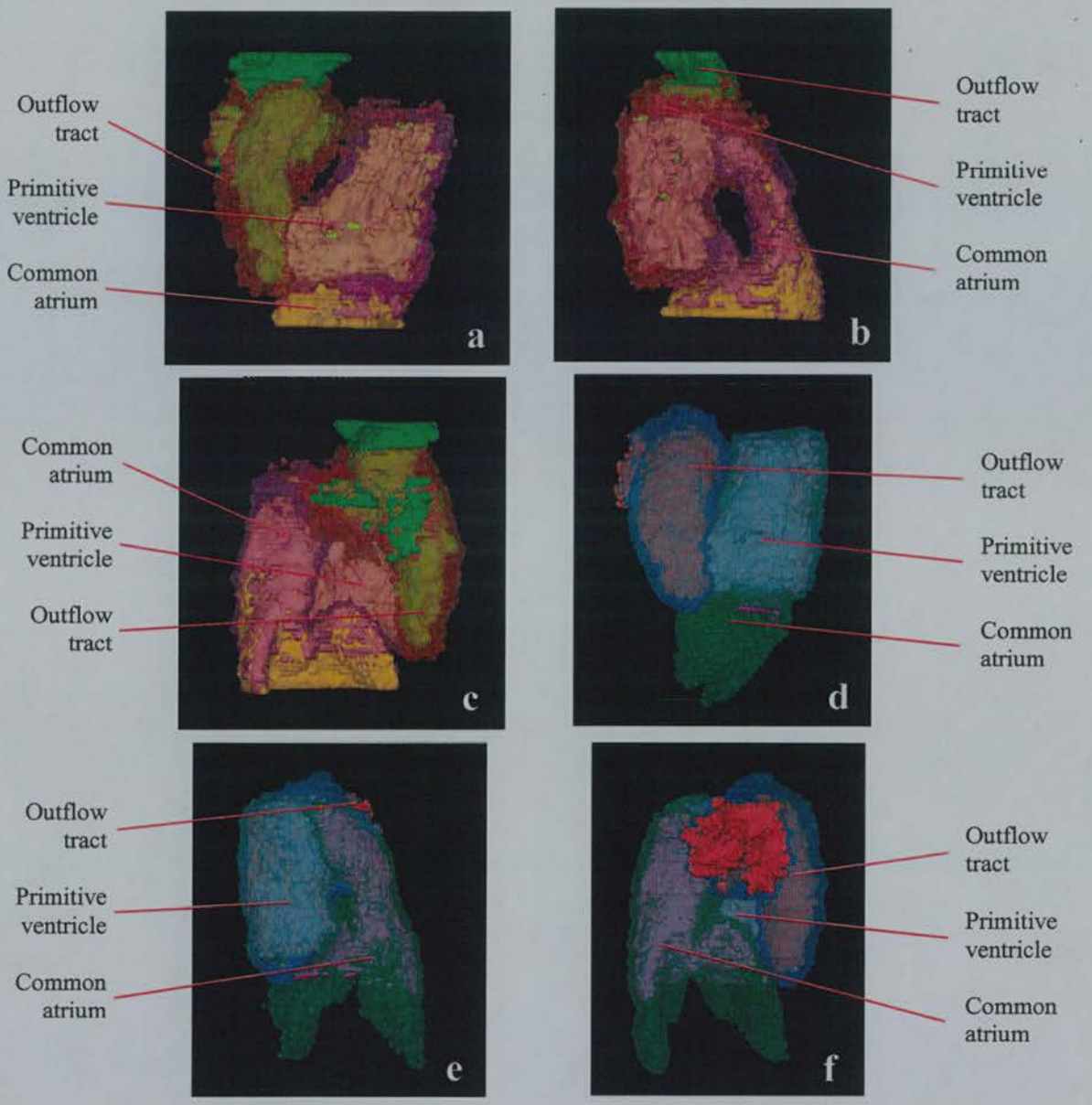

Figure 3.26: Right-anterior (a), left anterior (b), and posterior (c) views of the endodethelial lining (common atrium (yellow) primitive ventricle (lemon jellow) outflow tract (green)) and cardiac jelly (common atrium (lilac transparent); primitive ventricle (magenta transparent); outflow tract (red transparent)) of the E8.5 heart. Also right-anterior (d), left anterior (e), and posterior (f) views of the myocardium (common atrium (green transparent) primitive ventricle (turquoise transparent) outflow tract (blue transparent)) and cardiac jelly (common atrium (lilac); primitive ventricle (magenta); outflow tract (red)).

The endothelial tube of the E8 embryo is similar to the one drawn by Ingalls (1926) in the sense that the surface area is very uneven and that there are two gaps in the tube that allow communication between the dorsal and ventral aspects of the endothelial tube.

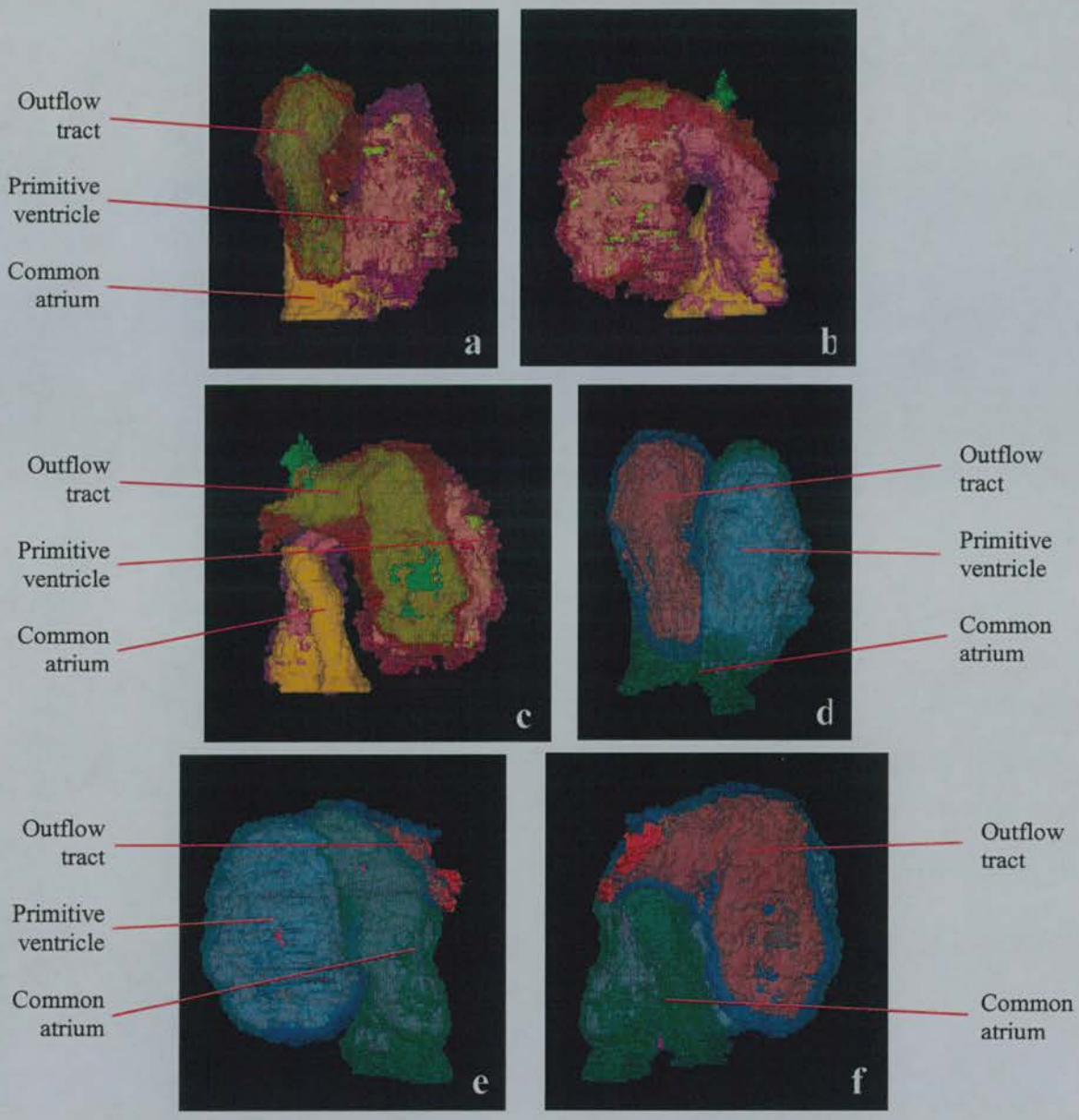

Figure 3.27: Anterior (a), left lateral (b), and right lateral (c) views of the endodethelial lining (common atrium (yellow) primitive ventricle (lemon jellow) outflow tract (green)) and cardiac jelly (common atrium (lilac transparent); primitive ventricle (magenta transparent); outflow tract (red transparent)) of the E9 heart. Also anterior (d), left lateral (e), and right lateral (f) views of the myocardium (common atrium (green transparent) primitive ventricle (turquoise transparent) outflow tract (blue transparent)) and cardiac jelly (common atrium (lilac); primitive ventricle (magenta); outflow tract (red)).

Looping

The dorsal mesocardium has ruptured in all three embryos and this is visible in figures 3.25f-h; 3.26d-g and 3.27d-g by the continuation of an intact myocardium around the dorsal side of the heart.

The E8 embryo, when viewed from the caudal side (or towards the inlet area of the heart) shows a sign of looping: the inlet area of the heart has shifted to the left and the tube area just rostral to the inlet area is extending to the right (figure 3.25f,i). The E8.5 embryo has adopted the 'S' configuration (figure 3.26), in which the common atrium is dorsal and cranially narrows to the right side of the pericardial cavity. The primitive ventricle extents from the atrioventricular canal down and to the left, whereas the bulbo-ventricular groove demarcates the caudal start of the outflow tract that projects upwards. The heart of the E9 embryo shows a compacted and elongated version of the E8.5 heart, in the sense that the outflow tract is now projecting dorsally in the most cranial part and this part is folded over the caudal half of the common atrium (figure 3.27).

There are no obvious locations throughout the heart at any of the three stages where there is a thinning or thickening of the myocardial wall. However, the start of the

Figures 3.28: left lateral views of left hand side vascular system (a) and outer surface (b) of the E8 embryo. Endothelial lining of heart (pink), 1st arch artery (orange), dorsal aorta (dark yellow), vitelline artery (yellow), internal carotid artery (lemon yellow), primary head veins (green), anterior cardinal vein (turquoise), umbilical vein (light pink) and sinus venosus (blue). Also for E8 left (c), right (d), mirrored right (e) and frontal (f) views of the vascular system. Endothelial lining of the heart (pink), venous system (blue) and arterial system (yellow).

looping at the inlet area of the heart shows a potentially interesting thickening and folding of the right hand myocardial wall, as if it is pushing the cardiac jelly and endothelial lining to the left (figure 3.25e,i). Such a sign cannot be found anywhere else in the heart or in any of the other two hearts. There are some global thickenings and thinnings but these are only slight: the myocardial wall is thinnest in the ventricular area of both the E8.5 and E9 embryos and the myocardium rostral to the atrioventricular canal is slightly thicker in both embryos (figures 3.26 and 3.27).

In all three embryos the internal (*i.e.* endothelial lining) structure more or less follows the configuration of the myocardium of the heart, which seems to suggest that the process of looping is a global process based on growth and overall change in cell

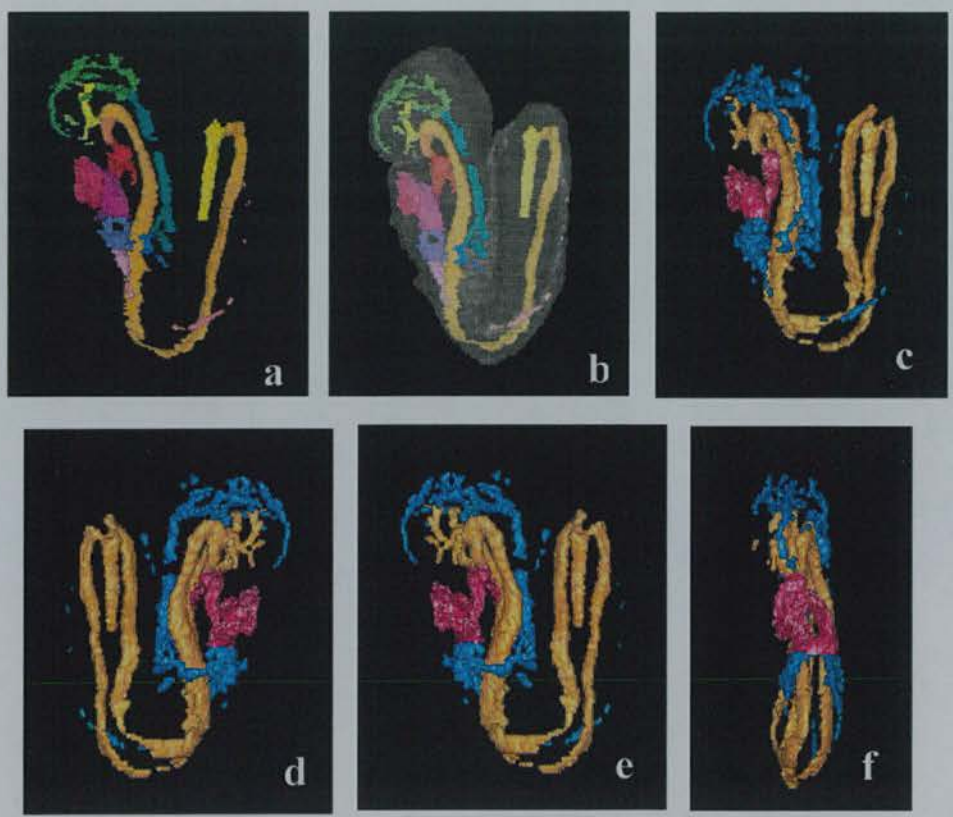

Figures 3.29: Left lateral views of left hand side vascular system (a) and outer surface (b) of the E8.5 embryo. Endothelial lining of common atrium (purple), endothelial lining of primitive ventricle (dark pink), endothelial lining of outflow tract (red), 1st arch artery (orange), dorsal aorta (dark yellow), vitelline artery (yellow), internal carotid artery (lemon yellow), vessels connecting internal carotid artery and primary head veins (lime green), primary head veins (green), anterior cardinal vein (turquoise), Posterior cardinal vein (dark blue), common cardinal vein (lilac), umbilical vein (mauve), vitelline vein (lilac) and sinus venosus (blue). Additional views of the full E8.5 vascular system: left (c), right (d), mirrored right (e) and frontal (f). Endothelial lining of the heart (pink), venous system (blue) and arterial system (yellow).

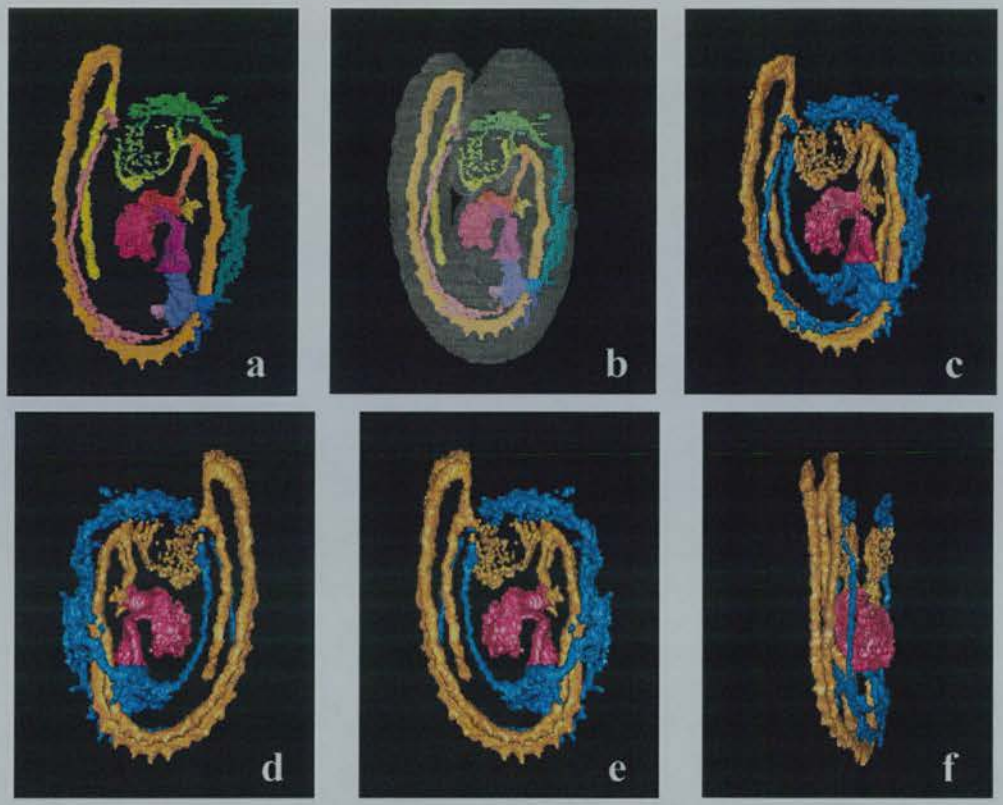

Figure 3.30: Left lateral views of left hand side vascular system (a) and outer surface (b) of the E9 embryo with colours: endothelial lining of common atrium (purple), endothelial lining of primitive ventricle (dark pink), endothelial lining of outflow tract (red), 1st arch artery (orange), 2nd arch artery (gold), dorsal aorta (dark yellow), vitelline artery (yellow), internal carotid artery (lemon yellow), vessels connecting internal carotid artery and primary head veins (lime green), primary head veins (green), anterior cardinal vein (turquoise), posterior cardinal vein (dark blue), common cardinal vein (light blue), umbilical vein (light pink), vitelline vein (mauve) and sinus venosus (lilac). Views of the E9 full vascular system: left (c), right (d), mirrored right (e) and frontal (f) with colour s: endothelial lining of the heart (pink), venous system (blue) and arterial system (yellow).

shape, more likely than to be based on certain areas that grow very rapidly and therefore put strains on the heart.

Vascular system

The arch artery system is indeed more or less symmetric, although in the E9 embryo, the left side seems slightly more advanced than the right hand side (figures 3.30a-e). In the E8.5 embryo, there is no clear evidence of the 2nd arch artery as yet, and in the E9 there is. In this embryo the angiogenesis of the 2nd arch artey originating from the rostral part of the outflow tract has not yet reached the dorsal aortae.

In the E8 embryo, it can be clearly discerned that the dorsal aortae start developing as angioblasts (Moffat, 1979) (figure 3.28). These angioblasts have yet to coalesce, as have other parts of the vascular system on both the inflow and outflow side of the heart. The statement that the internal carotid artery does not develop until E10 in the mouse (Kaufman & Bard, 1999) is untrue for the E8, E8.5 and E9 embryos in all of which a clear internal carotid artery can be discerned (figures 3.28, 3.29 and 3.30). There is no sign yet that the right umbilical vein is regressing in the E9 embryo (Kaufman & Bard, 1999).

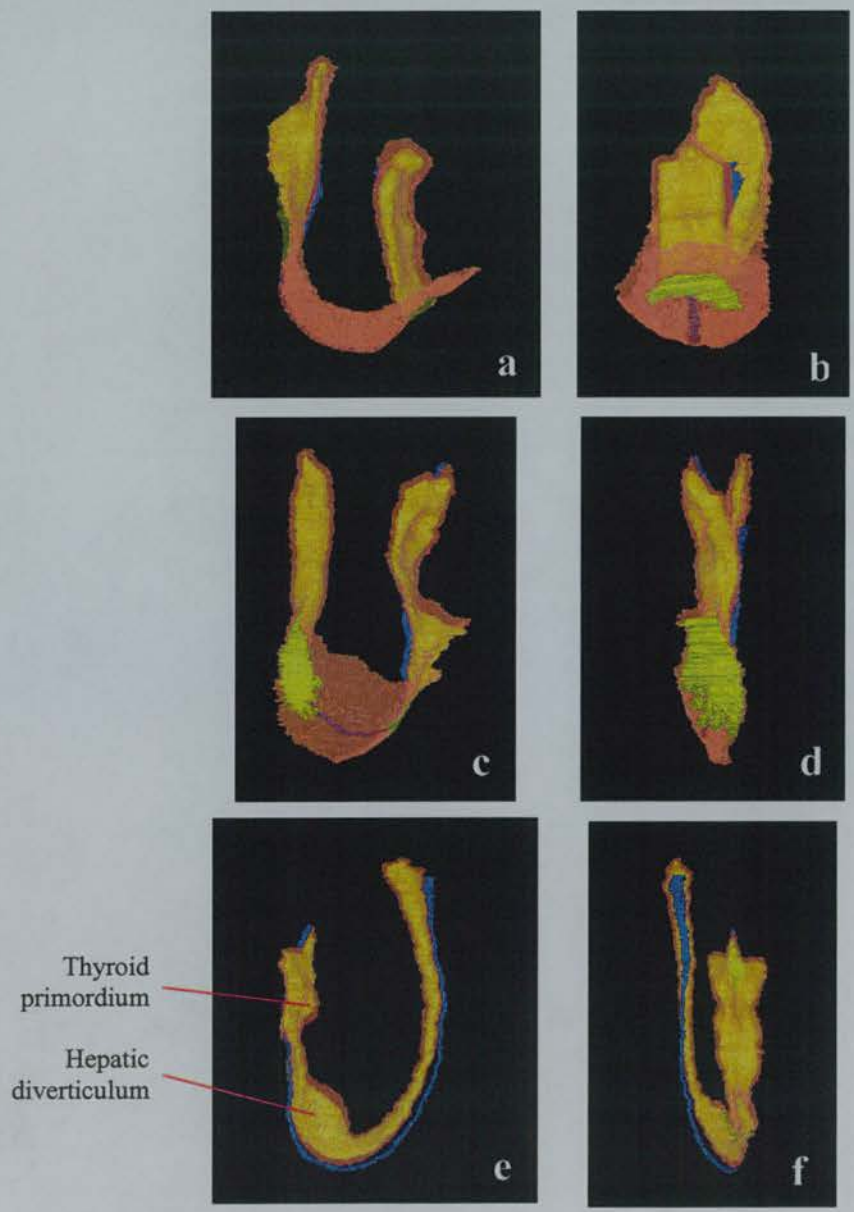

Figure 3.31: Lateral and anterior views of the gut (orange transparent), gut lumen (yellow) and notochord (blue) of the E8, E8.5 and E9 embryos. (a) E8 lateral, (b) E8 anterior, (c) E8.5 lateral, (d) E8.5 anterior, (e) E9 lateral and (f) E9 anterior.

Gut

The finding by Lamers *et al.* (1987) that, until the gut wall closes and forms a tube, the wall is thin can be confirmed in the three models (figure 3.31). The thickening of the gut wall after closure of the tube is generally even.

The hepatic diverticulum in the E9 embryo, unlike Godlewski *et al.* (1992) describe for rats at a similar stage of development, is not separated ventrally from the heart and caudally from the sinus venosus (figure 3.32). The contact between the hepatic diverticulum and the heart does not get hindered by any of the surrounding tissues. In the E8.5 embryo however, there is indeed quite an extensive contact between the region of the future hepatic diverticulum and the endothelial lining of the heart, which Godlewski claims to be the trigger for the development of the hepatic diverticulum.

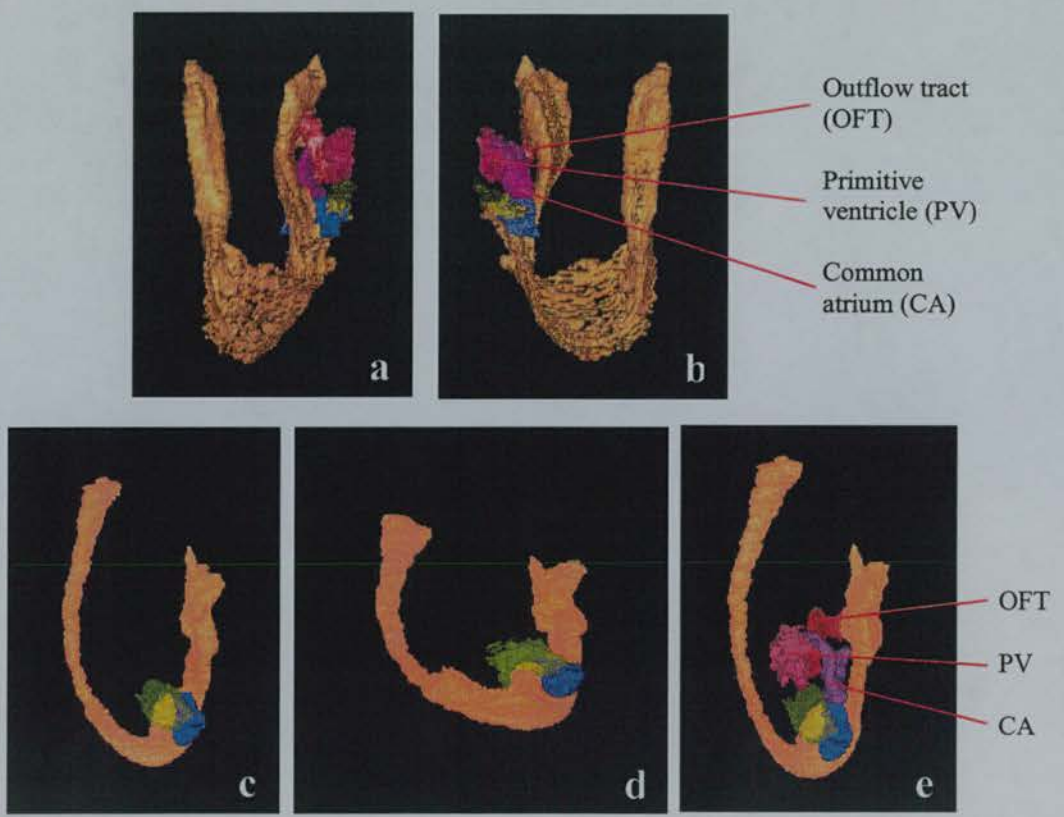

Figure 3.32: Lateral and bottom views of the gut (orange), endothelial lining of the common atrium (purple), endothelial lining of the primitive ventricle (pink), endothelial lining of the outflow tract (red), sinus venosus (blue) and septum transversum (transparent yellow) of the E8.5 and E9 embryos. (a) E8.5 right, (b) E8.5 left, (c) E9 left, (d) E9 bottom and (e) E9 left.

Somites

The statement of Tam (1981) that the somites of the upper trunk and tail are half the size of the lumbar and sacral somites, can unfortunately not be checked in the embryos used for reconstruction, since the most caudal pair of somites that has developed in the E9 embryo is probably the most caudal thoracic one (Kaufman and Bard, 1999). However, there is a clear difference between the volumes of the somites in all three reconstructions (figures 3.22, 3.23 and 3.24). However, this difference in volume is not consistent between somite numbers amongst different embryos. In the E8 embryo, the first two somites are the largest, whereas in the E8.5 and E9 embryos, the first 3 pairs of somites are the smallest. In the E8.5 embryo these are followed by approximately even sized somites for the rest of the body (and cervical region) whereas in the E9 embryo, the 4 pairs of somites following the first 3 pairs are bigger than those caudal to the first 7 pairs.

Figure 3.33: Lateral (b & c) and posterior (a & d) views of the neural tissue (yellow), gut (red), notochord (blue) and somites (green) of the E8 embryo.

Notochord

The notochord, has, unlike Jurand (1974) describes, separated morphologically from the gut roof (but is in most places still closely atttached) in all three embryos, apart from the most rostral part of the E8 embryo (figures 3.33a-b and 3.34a,c). This confirms the statement from Lamers (1987) that this separation takes place in a caudo-cranial direction. In all three embryos the notochord is adherent to the floor plate of the neural tissue, and in the E9 embryo, the notochord has started detaching

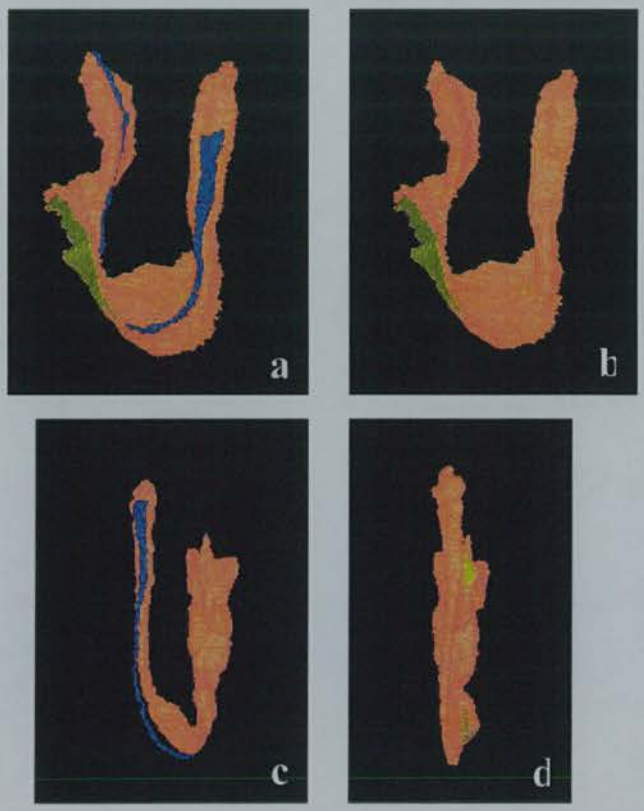

Figure 3.34: (a) & (b) - lateral views of the gut (orange), notochord (blue) and gut lumen (yellow) of the E8.5 embryo. (c) & (d) – frontal views of the gut, notochord and gut-lumen (same colours) of the E9 embryo.

from the gut roof in the midgut area of the embryo.

3.3.3.3 Unexpected anatomical features

Heart

The boundaries of the myocardial walls of the heart do not correspond with the boundaries of the endothelial structures of the hearts in the E8, E8.5 and E9 embryos. The myocardial walls and cardiac jelly cover part of the branchial arch arteries in all

three embryos, and part of the inlet area of the heart, the sinus venosus (figures 3.25, 3.26 and 3.27). This, as mentioned before, may be a genuine feature or caused by the fact that the delineation was based on cell arrangement and 3D morphology rather than distinguishing properties of cardiac muscle cells.

The trabeculation of the heart has started in the E8.5 embryo in the primitive ventricle (figure 3.26a-c). In the pictures, this is visible as a rough texture of the cardiac jelly in conjunction with gaps in the jelly, indicating direct contact between the myocardial wall and endothelial lining of the heart. In the E9 embryo, the trabeculation has spread to the bulbus cordis region of the outflow tract (figure 3.30). It is not present in the distal region of the outflow tract and the common atrium.

Vascular system

In the reconstruction of the E8 embryo, it can be seen that the vascular system is grossly incomplete (figure 3.28). Each future vessel consists of angioblasts that have yet to coalesce, and the interesting feature is that the vascular system is particularly discontinuous in the cervical region, a region that is normally advanced in embryonic development, *e.g.* with respect to neural tube closure. All angioblasts appear to be developing in line with each other.

As opposed to the much described arch artery system, there is the not described rather complicated vascular system at the inlet area of the heart. In the E9 embryo, we can see that the sinus venosus has three supplies: the medial vitelline vein, the lateral umbilical vein and the posterior common cardinal vein which is the collecting vessel of the posterior cardinal vein and anterior cardinal vein (figure 3.30). These vessels are also present in the E8.5 embryo (figure 3.29), but not in the E8 embryo: there is no sign yet of the posterior cardinal vein, and neither is there of the vitelline vein. The umbilical vein has only just started developing a few sporadic angioblasts (figures 3.28).

There is not a clear asymmetry in the development of the right and left vascular systems. To check this, figures were made of the right and left vascular system, and the right set was mirrored so they would be comparable to the left vascular system. In none of the three stages is there any obvious asymmetry during development of the vascular system (figures 3.28d-f, 3.29c-f and 3.30c-f).

Gut

In the E9 embryo (figure 3.31e and f) it can be seen that as well as the thickening of the gut wall after closure of the tube in the ventral midline, there is a thickening of the wall over the thyroid primordium and the hepatic diverticulum. This may indicate, that unlike, for example, the expansion of the ventricles in the brain, the outgrowths of the thyroid primordia and hepatic diverticulum are based on changes in cell shape rather than a local build-up of internal pressure (Coulombre and Coulombre, 1958).

Notochord

The developing notochord appears to be widening caudally in the lateral direction in all three embryos (figures 3.33a, 3.34a and c). None of the embryos show a node structure as described by Bellomo *et al.* (1996) and the E8.5 and E9 embryos have a very thin but continuous endothelium ventral to the caudal aspect of the developing notochord (figures 3.33d, 3.34b and d). It would be interesting to establish, since the notochord thins as it develops, whether this is due to cell migration away from the notochord, a stretching of the structure as the structure grows, possibly because there is only a limited amount of mitotic activity in these cells, or a reduction of the volume of the cells of the notochord.

3.4 DISCUSSION

3.4.1 Drawbacks of the system

The reconstructions have proven to be a powerful tool for describing and comparing mouse developmental anatomy. However, there are some limitations to this system. The main drawback is that we have only been able to use one embryo per Theiler stage, and although each specimen was selected for being representative of its stage, the problem is that there are no data on variation in mouse developmental anatomy. This variation does not only relate to differences in advancement of development between, say, littermates, but also to the fact there will be a degree of differentiation in the embryo's component systems. This is a particular problem when trying to compare different strains. For example, the allantoic bud in the strain used for this study (C57BLXCBA F2 hybrid embryos) appears one Theiler stage earlier than in the PO strain (Downs and Davies, 1993).

Another drawback is that the anatomy is solely based on one type of staining per embryo (Haematoxylin and eosin for the E8.5 and E9 embryos and toluidine blue for the other embryos) and therefore gives a reduced view of the anatomy. In some cases, for example, when looking at the extent of the myocardium in relation to the endocardium and cardiac jelly, additional staining methods would help to distinguish the special-case boundaries.

Despite the preservation of the original histology in relation to the 3D reconstructions of individual tissues, it has not proven possible in the reconstructions of the egg cylinders and early organogenesis embryos, to detect individual cell characteristics (for example, mitotic figures or differences in cell size, even when located on the outer surface of the embryos (Hogan and Newman, 1984)).

3.4.2 Advantages of the system

In this chapter, the particular strengths of this system have proven to be manifold: it has made anatomical assessments easier and is especially important for developmental events that require study of a large number of sections and are associated with complicated 3D topographical relationships. A good example is the assessment of multiple asymmetries in the blastocysts and egg cylinders, or when defining landmarks, such as the placement of the otic placodes in relationship to the 1st pair of somites and rhombomeres. Another good example of the value of the system is for comparison of the extents of cardiac jelly, myocardium and endocardium, and the observation that the proamniotic cavity is constricted in all directions rather than in two directions only during the development of the proamniotic folds. In addition establishing detailed 3D relationships, such as the development of the vascular system and the position of hepatic diverticulum in relationship to heart, septum transversum and sinus venosus, would otherwise not be feasible.

It is of great value to be able to refer to the underlying histology at any given angle, for example when looking at aspects of development that are beyond the boundaries of tissues. The recognition of, for example, the *node* is far easier in one plane than in others and this plane is difficult to determine before sectioning the embryo. On the other hand, it has proven of great value to assess the extent of tissues by being able to 'browse' through the embryo, for example when looking at the allantois, the extent of axial mesendoderm or the arrangement of cells in the inner cell mass.

3.4.3 General implications

The real force of this system becomes apparent when viewed with appropriate software, either as a movie of rotating images or as 3D interactive reconstructions in which the 3D aspect can be fully appreciated when wearing appropriate glasses in combination with specific software. More detail and extension of detail can be assessed using the CD-ROM that has been developed for the Edinburgh Mouse Atlas, a copy of which is included in the back of this thesis.

This system is a great aid for those without a thorough knowledge in developmental anatomy working in the field of developmental biology, particularly when trying to interpret the location of molecular or gene-expression pattern in a non-standard section. In addition to providing help for browsing through an embryo, the reconstructions also provide a framework for analysis of genetic events against anatomical events, to a degree that is much wider than has hitherto been possible.

The embryo models will form a valuable reference resource to those studying malformations, for example those of the heart, such as truncus arteriosus malformation (Yu and Hutchins (1996), double outlet right ventricle (Broekhuizen *et al.*, 1995), ventricular septal defects (Argao *et al.*, 1995), common arterial trunk (Jackson *et al.*, 1995), subaortic stenosis (Kitchiner *et al.*, 1994), aortic arch malformations, (Kurihara *et al.*, 1995). The exact onset of the abnormality can be traced and related back to underlying histology, which is accessible at any angle to fit the viewer's material. This will allow a standardisation of description of the abnormality using the standard nomenclature of the anatomy, since there now is a standard 'normal' model of development. This need for standardisation of description and descriptive terms has already been identified (Anderson, 1996; Anderson and Brown, 1996). This work, with the publication of the CD-ROM should contribute to this requirement.

3.4.4 Future work

A natural continuation of this research is to establish the consistency in location of the early morphological asymmetries, *i.e.* before the appearance of the primitive streak, in the egg cylinders. This could be attempted in different ways and at different times. *Nodal* is expressed in the E6 posterior epiblast (Varlet *et al.*, 1997), *Hex* is expressed in the E5.5 anterior endoderm (Thomas *et al.*, 1998) and *VE1* is expressed from E5.5

onwards at the anterior side of the embryo. *In situ* hybridisation for these genes over the developmental range E5-E6 should allow a conclusion about the orientation of the proamniotic cavity, tilt of the ectoplacental cone and orientation of the groove at the border between the embryonic and extraembryonic component of the egg cylinder.

The other research extension that could follow from this study is the addition (or reinforcement) of boundaries from other anatomical data sources. The boundary between the heart and the mesothelial lining of the pericardiac cavity and pericardio-peritoneal canals would benefit from additional data in serial sections that indicate myosin. Or, for another "arbitrary" boundary, the lack of morphological distinction between the hindbrain and spinal cord could be equated for studying gene expression patterns that mark this boundary in the developmental age range studied in this chapter (Holland and Hogan, 1998). The plane of the serial sections containing these data can then be found in the reconstructions after which the data can be delineated onto the reconstruction, and boundaries compared or amended.

There appears to be extensive range in the morphological appearance of the vessels of the vascular system. The appearance of the larger arteries is smooth (the vitelline artery), while some of the bigger veins are particularly branched from an early age (the anterior cardinal vein) and some vessels display a particularly uneven surface with 'spiky' extensions (the endothelial lining of parts of the heart, and the dorsal aortae forming the intersegmental arteries). There are three genes involved in the early development of the vascular system: *VE-Cadherin* (Breier *et al.*, 1996), *Hex* and *Flk-1* (Thomas *et al.*, 1998). It would be instructive to label the expression of these genes onto the time series of the mouse reconstructions and study their appearance followed by morphological shape changes in three dimensions.

3.4.5 Concluding remarks

The model embryos uniquely provide a view of the stained histological structure of a single embryo that can be explored in three dimensions and so provide a powerful tool to investigate morphogenesis. The ability to investigate discrete anatomical domains in isolation or in combination with other tissues can greatly assist us in understanding various relationships between anatomical components. Furthermore the models provide a reference for analysis of, for example, malformations at the appropriate stages of development. The reconstruction incorporates all the major anatomical

features for their stages of development, and therefore, unlike reconstructions that were produced of isolated tissues with loss of histological reference, form an extensive source of comparisons within each model. These 3D spatial relationships are clearly important for understanding the genetic control of the process of development.

CHAPTER 4: ANALYSIS OF THE PROCESS OF TURNING

4.1 INTRODUCTION

The process of turning (or axial rotation or entypy) is an extremely important one in rodents since it enables the embryo to adopt the normal mammalian or fetal arrangement with respect to its dorso-ventral axis. Before turning, the neural tube is located in the concavity of the U-shaped embryonic axis, whereas, after turning, the neural tube is then located in the convexity of the body axis. Similarly, before turning the endoderm of the gut lies in the convexity of the body axis, whereas after turning, the gut then lies in the concavity of the body axis. Only after the process of axial rotation is completed do both its amnion and yolk sac surround the embryo. Before axial rotation, neither membrane surrounds the embryo (Kaufman, 1992).

In the mouse, this process is initiated during the early somite period, at E8, and is completed when the embryo possesses about 15-20 pairs of somites, at E9 (Theiler, 1972). This process also occurs in the rat and other closely related species as well as in the guinea pig and rabbit. The 'biological value' of the unturned configuration during the egg cylinder, primitive streak and early somite stages of development is unclear. It has been suggested that in this arrangement, the embryo is very compact and accordingly occupies less space in the uterus than if it adopts the normal mammalian configuration (Snell and Stevens, 1966).

The changes that occur in the extraembryonic membranes during this process are illustrated in Hamilton and Mossman (1972). Relatively little, however, has been written on the embryonic anatomy of the process of turning but what has been observed is of particular interest, namely that in the rat the mechanism of axial rotation is opposite to that observed in the mouse embryo. During turning in the rat, its dorsal surface rotates towards its right side (Deuchar, 1971), while in the mouse its dorsal surface rotates towards its left side (Snell and Stevens, 1966; Kaufman, 1992). Why this difference should occur is unknown, but may, although unlikely, be indicative of the fact that the process of turning developed independently in the rat and the mouse. No information is currently available on the mechanism of turning in other species in which turning occurs.

In the mouse, the process of turning has recently been re-evaluated because of its link with the establishment of lateral asymmetry (Collignon *et al.*, 1996). This interest relates to the discovery of two mutations, *situs inversus viscerum* (*iv*) (Hummel and

Chapman, 1959) and *situs inversus* (*inv*) (Yokoyama *et al.*, 1993) which display a reversal of left-right asymmetry of the visceral organs and some major blood vessels feeding into or draining from these organs. A report followed that homozygous *inv* mice which display 100% *situs inversus* turn in the opposite direction to that observed in normal mice, *i.e.* the *inv* mouse turns its dorsal surface towards its right side (Collignon *et al.*, 1996). After this, a cascade of publications came out providing genetic and molecular information concerning *situs inversus* and *situs inversus viscerum.* A report of this research and model formation around these two mutations will follow in the next section.

This research has brought closer an understanding of the molecular mechanisms behind the process of turning in the mouse. However, the principal anatomical events associated with normal turning have not yet been reported in detail. Previously, these events were only comprehensible with a sequential series of diagrams associated with representative transverse histological sections taken at intervals during the turning process (Kaufman, 1992). With 3D surface rendering of internal and external relationships in turning mouse embryos, the process of turning can be clearly visualised and all 3D relationships of the embryo understood.

The aim of this study is to give a detailed anatomical account of the principal events that occur during the process of turning in the mouse with the aim of assessing whether turning is a global event or driven by a few tissues. To do this, three stages of turning will be shown in three separate sections: The onset of turning (E8.0), the middle stage of turning (E8.5) and completion of turning (E9.0). For each of these stages, the main components of the embryo that display the gross morphological internal changes that occur during turning are: the neural tissue, heart, somites, the gut, notochord and mesothelial lining of the intraembryonic coelom. The surface epithelium, neural tissue and mesothelial lining of the intraembryonic coelom are reflected by the external changes in the appearance of the embryo. All three embryos were dissected free from their membranes prior to embedding, so that we cannot display the 3D relationships of the embryonic and extraembryonic structures. However, this will at least allow us to focus on the embryonic parts, as the relationships between the extraembryonic membranes during turning have been described previously (Hamilton and Mossman, 1972).

The main conclusions from this study are that the turning process is initiated simultaneously at the head end and tail end of the embryo. The turning then progresses towards the mid-trunk region of the embryo. The last tissues to finish turning are the (still open) midgut and the closely related two rows of somites, and this remains after the neural tissue has adopted the fully turned configuration. An unexpected (but normal) element of rotation was found at the caudal tip of the neural tissue in the E9 embryo. In the three embryos used for this study there does not seem to be one single (or few) leading tissue(s) in the process of turning, and different regions of different tissues are ahead at different times.

4.2 LITERATURE REVIEW

4.2.1 Description of anatomical events during the process of turning

The most extensive report on the events associated with the process of turning in the mouse is given in Kaufman, 1992. It is stated that the embryo inverses its germ layers by rolling along its embryonic axis. This reference does not state however, where the turning process starts and neither does it give an account of the internal structure of the embryo during turning. It does however, display some clear diagrams of how the embryo rolls (figure 4.1) although there are some contradictions between diagrams and accompanying text. Three figures show how the embryo turns its dorsal side towards its left, whereas the text mentions an anticlockwise movement along the embryonic axis, when viewed towards the caudal end. Different degrees of turning for different parts of the embryo have also been mentioned, whereas the diagrams show that the entire embryo rolls along its entire length axis. One diagram is in conflict with the other three with respect to the direction of turning (figure 4.2). This is not the only conflicting source of material: Klar (1994) reports that the axial rotation in the mouse occurs counter-clockwise which is contrary to the generally accepted view.

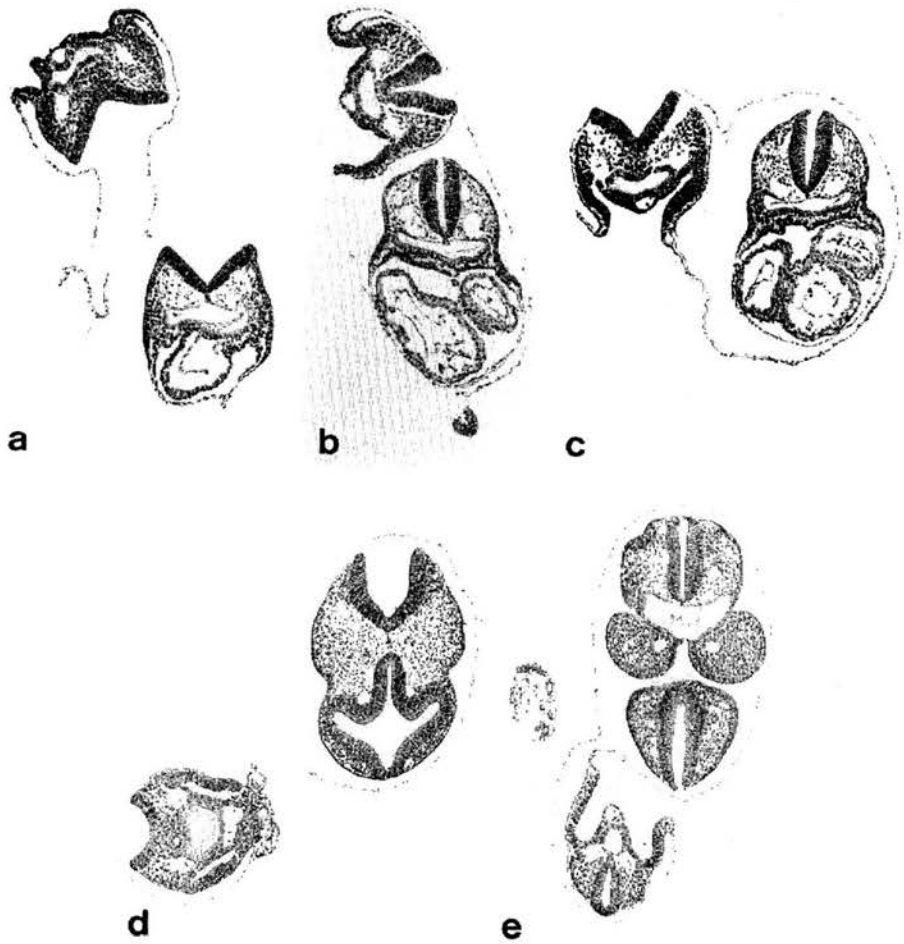

Figure 4.1: A series of representative transverse histological sections through embryos of increasing gestational ages which are proceeding through the turning sequence. (copy of figure 5 in Kaufman (1992)).

4.2.2 Turning in the rat

Turning for the rat has been more closely described even though much more work has been done on the mouse. Surprisingly, it was reported that the rat turns in the opposite direction to the mouse: the rat turns its dorsal side towards its right (Deuchar, 1971). The timing of turning is developmentally similar to the mouse and starts at the head end only. The rotation passes on caudalwards until the whole turning process is complete. Turning starts with rhythmic 'dipping' movements of the head caused by contractions of the looped heart tube. If the surrounding extra-embryonic membranes are not fully expanded they prohibit turning, yet they need to be intact as they provide anchorage and a fixed point around which the axial rotation can take place. Transections were done in

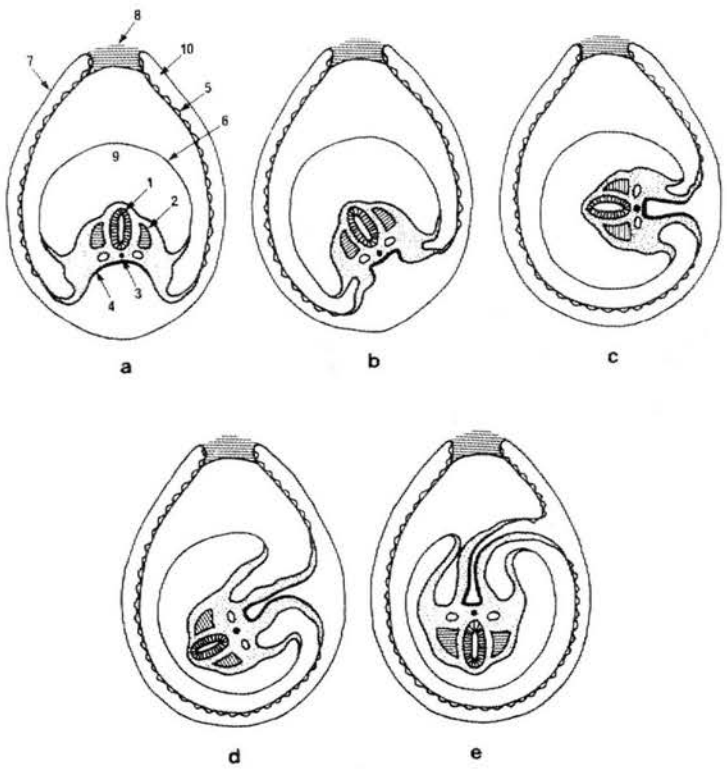

Figure 4.2: Simplified diagrammatic series illustrating the changes in the relationship between the embryo and its extra-embryonic membranes when sequential vertical sections through the mid-trunk region are viewed during fives stages of turning. (Copy of Fig. 6 in Kaufman (1992)). The number annotations are: (1) neural tube, (2) somite, (3) notochord, (4) prospective midgut endoderm, (5) yolk sac, (6) amnion, (7) parietal endoderm, (8) ectoplacental cone, (9) amniotic cavity and (10) yolk sac cavity.

the rat at day 9 and day 10 at different level of the trunk to see how the caudal stump would complete turning. The earlier and lower down the embryo the transections were done, the less able was the isolated caudal stump to complete turning (Deuchar, 1971).

4.2.3 Mouse mutants involved with the process of turning

The importance of the process of turning has recently become clear because of its relationship to the generation of asymmetry. The most well-known mouse mutant in which turning is affected is the *situs inversus* (*inv*) mutant in which homozygous mutants display 100% mirrored imaging of the visceral organs and opposite direction of turning. This mutation is located on chromosome 4 (Yokoyama *et al.*, 1993) and has, unlike the human *situs inversus* mutant Kartagener syndrome, normal cilia on all epithelia. The search for the coding sequence of this gene was slowed down by a complicated deletion and/or duplication caused by the insertion of the *inv* mutation

(Burn and Goodship, 1996) but has now been identified and cloned (Yonekawa *et al.*, 1998).

The interest that has arisen in association with the problem of laterality brought back into focus a much older mutation called *situs inversus viscerum* (*iv*) (Hummel and Chapman, 1959). This mutation causes laterality defects as well, but only 50% of homozygous mutants display mirrored imaging of the visceral organs (Hummel and Chapman, 1959; Layton, 1976). *Iv* mutants display heterotaxia, which is the phenomenon that individual organs get mirrored or not seemingly independent from each other, in a large range of possible combinations. Moreover, homozygotes exhibit 20% cardiac defects independent of *situs*, that not only stresses that looping is an independent phenomenon, but also shows that the looping itself is disorganised (Brueckner *et al.*, 1989). This mutation is non-allelic with *inv* and is located on chromosome 12 (Brueckner *et al.*, 1989) and has, like *inv*, normal cilia on all epithelia. Unfortunately, whether *iv* affects turning or not has not yet been reported.

Similarly, there is a mutation termed *no turning* (*nt*) in which homozygotes fail to turn and fail to progress beyond the forelimb bud stages (Melloy *et al.*, 1996 and 1998). Half of the homozygotes have reversed (mirrored) heart looping. Because these embryos do not progress much after E9 effects on other tissues can not be investigated.

4.2.4 Research in relation to the establishment of laterality

The 'accidental' generation of the *inv* mutant (Yokoyama *et al.*, 1993 attempted to make a pigmentation mutant) triggered considerable interest in the establishment of asymmetric laterality, since in this mouse, unlike the situation in the *iv* mouse, laterality is 100% reversed. An important breakthrough in the search for the molecular mechanisms behind the establishment of lateral asymmetry came with the publications of Collignon *et al.*, 1996 and Lowe *et al.*, 1996. Collignon *et al.*, 1996 reported that while in wild type embryos *nodal* is expressed in the left-hand only lateral plate mesenchyme (LPM) (amongst other places), in homozygous *inv* embryos the expression is on the right-hand side only (and these embryos turn in the opposite direction). Lowe *et al.*, 1996 report the same expression pattern for *inv* but do not mention their direction of turning. They also investigated *nodal* expression in *iv* homozygotes and found an unpredictable pattern of expression in these embryos. Sometimes expression was on the

right-hand side or left-hand side, but often in the middle with a slight emphasis on either side. Unfortunately, they do not link this study to the process of turning.

The research resulting from these findings led first to the cloning of the *inv* gene (Yonekawa *et al.*, 1998). This contains 15 consecutive repeats of an *ank/swi6* motif at the *inv* locus. Transgenic introduction of a minigene encoding the candidate protein restores normal left/right asymmetry. This was followed shortly afterwards by cloning and sequencing of the *inversin* gene (Morgan *et al.*, 1998) in normal embryos. This is a 47 kb region which contains only one gene. This region also contains 5.5kb cDNA and 16 exons of which numbers 3 to11 are deleted in the *inv* mutant, causing a frameshift. Reinsertion of this *inversin* gene leads to repair of normal laterality in *inv* mutants.

An array of data published on the laterality problem brings some insight into the chain of events involved with the establishment of laterality. It has been established that the FGF-β signalling proteins are primarily responsible in establishing laterality. This group comprises Nodal, Lefty 1 and –2, Activin-receptor-IIb and Smad2 and –5. However, their genetic pathways are still unclear (Chang *et al.*, 2000).

During normal development, *nodal* and *shh* are expressed asymmetrically in the node (Collignon *et al.*, 1996; Lowe *et al.*, 1996). This signal gets transferred by extracellular factors to outside the node (Yan *et al.*, 1999), where in the following order, *smad-5* (Chang *et al.*, 1999), *nodal* (Collignon *et al.*, 1996; Lowe *et al.*, 1996) and *lefty-2* (Saijoh *et al.*, 1999), ultimately lead to expression of *pitx2* in the left LPM (Ryan *et al.*, 1998). *FGF-8* and *brachyury* are expressed in mesoderm exiting the streak and are also required for *nodal* and *lefty-2* expression in the left LPM (Welsh and O'Brien, 2000). As well as *nodal*, *lefty-1* also determines expression of *lefty-2* but is not expressed in the LPM but in the left-hand side of the future neural tissue (Saijoh *et al.*, 1999; Kosaki *et al.*, 1999). *Activin* and *smad2* (Heyer *et al.*, 1999) are part of a pathway in the right LPM that leads to local expression of *snail* and hence right hand structures. Disturbance of these events anywhere in the chain leads to laterality defects. In *inv*, the chain goes wrong at the level of *nodal* expression in the left LPM, and in *iv*, at the level of expression in the node.

An important molecule in the establishment of correct *lefty-1* expression is retinoic acid (RA) (Tsukui *et al.*, 1999). RA is not part of the *shh* pathway but its absence leads to incorrect *lefty-1* expression and abnormal laterality. Raldh2 (an NAD-dependent

aldehyde dehydrogenase) is probably responsible for embryonic RA synthesis (Niederreither *et al.*, 1999).

Two other genes are involved with the establishment of asymmetric laterality, although their place in the chain of establishment events is not yet known: one of them is the *RBP-Jκ* gene. A homologous recombination of this gene leads to severe growth retardation from E8.5 with incomplete turning, defective somitogenesis and an irregularly shaped neural tube (Oka *et al.*, 1995). Later effects on laterality establishment were not reported in this mutant since embryos die after E10. The other gene is *furin* (Constam and Robertson, 2000; Roebroek *et al.*, 1998), and absence of the enzyme produced by this gene leads to incorrect expression of *lefty-2* and *pitx2*, but *nodal* expression is normal. These mutants also die soon after E10.

Tetraploidy in the mouse induces mirror- imaging of the outflow tract in males, but, interestingly, not in females (Kaufman, 1992). Other organs did not seem to be affected and unfortunately this study was not linked to an investigation in the direction of turning since the investigated embryos ranged from E12-E16, which is after the process of turning had been completed.

4.2.5 Model formation on the establishment of laterality

There have been several hypotheses advanced about the establishment of laterality. The earliest one is from Layton (1976) and concerns the establishment of laterality in the *iv* mutant. It proposes that the *iv* gene, when intact, controls the normal arrangement of the body plan, and when this gene is damaged or deleted, determination of situs is random, and moreover, that there is some rate of independence between organs establishing *situs* (heterotaxia).

The next model (Brown and Wolpert, 1990) also concerns the *iv* mutant, and splits the establishment of lateral asymmetry into three categories: establishment of lateral asymmetry through conversion at the molecular level, random establishment, and establishment through tissue-specific interpretation. Random establishment effectively is a combination of 'conversion' and 'interpretation' (see below) and only seemingly random at first glance. A good example of this category is the establishment of laterality in individual organs of *iv* mice. Establishment of laterality in the wild type mouse would happen through *conversion*: an asymmetric molecule is being laid down in non-random fashion with respect to the anterior-posterior and dorso-ventral axes and this event lies

at the root of and determines the establishment of lateral asymmetry. The *interpretation* of the *conversion* is the tissue specific response to the difference between the left and right sides: for example the left lung has only one lobe whereas the right one has four lobes; and the stomach and spleen are asymmetric and are located on the left side of the abdominal cavity (normally).

Another model appears after the generation of the *inv* mutant and is more specific (Klar,1994). It proposes that non-random distribution of mirror-image chromatids among daughter cells establishes asymmetric laterality after mitosis. Three further hypotheses were put forward: First, that *iv* and *inv* are not loss-of-function mutations since polarity (even if at the level of individual tissues) still gets established. Second, that for *inv*, the essential gene for laterality is inverted with respect to the segregation site on the chromosome required for non-random segregation. Third, the complete reversal seen in all *inv* homozygotes requires intact *iv* function. He indeed reports that mice homozygous for both *iv* and *inv* do produce 50% mirrored left-right asymmetry.

After the discovery that the expression of *nodal* is mirrored in LPM in *inv*, and random in *iv*, Okada *et al.* (1999) proposed the hypothesis that the action of the node depends on the movement of the cilia, since that is where *nodal* is still expressed normally for *inv* but not for *iv*. They found that the node has immotile cilia in *iv* mutants and a very weak leftward (normal direction) flow in *inv* mutants. They proposed that the *nodal* flow produces gradients of putative morphogen and that it triggers the first left-right determination event. Previous to this study, the same group (Nonaka *et al*, 1998) found that loss of nodal cilia in a mutant lacking KIF3B motor protein caused left-right randomisation with randomised direction of turning.

4.2.6 Discussion and conclusions

Although a considerable number of the molecular events involved in the establishment of lateral asymmetry have been placed into order, there are still a few large components of the puzzle missing. What happens between the expression of *nodal* in the node and *nodal* in the LPM and what is the role of the *inv* gene in this process? At what level do events go wrong in the *iv* mutant? The expression of *nodal* in the node is abnormal, and this may well have been caused by the immotile cilia. It would be helpful to know what other molecules of the FGF-β family are expressed abnormally in both mutants.

Currently it seems, that the *inv* gene works at the time between expression of *nodal* in the node and in the LPM. Apparently the frameshift caused by the deletions of the exons in the *inversin* gene in *inv* mutants mirrors the signal that *nodal* would have produced in wild type mice. If this is true, then Brown and Wolpert's (1990) model of *conversion* cannot be true, since the molecule from the node has been distributed correctly. If this is *conversion* in the sense that the signal subsequently gets mirrored, then this is not the first left-right asymmetric event as they were proposing for the *conversion* model. As for Klar (1994), his theory of non-random distribution of chromatids may be correct, although the cloning and sequencing of the *inv* gene does not confirm his theory of a mirror-image gene in the *inv* mutant.

The phenotype of the *iv* mutant might derive from Nodal being wrongly distributed due to immotile cilia on the node. However, one would still expect the signal to be higher at one side than the other, leading to mirrored or normal asymmetry of all visceral organs due to the cascade of signalling events in the FGF-β family of molecules. The problem is that the immotile cilia do not explain the phenomenon of heterotaxia.

4.2.7 Back to turning

Unfortunately for the study of mouse development, the reversed direction of turning in the *inv* mutant has not been the main focal point for the research groups involved, and research subsequent to the development of the mutant has focused on the problem of asymmetric laterality and not on turning. It is unfortunate that it has not been reported whether the direction of turning in *iv* mutants is randomised, since this would allow us to establish whether a normal expression pattern in the node is required for normal turning. This assumes of course, that the signalling events for laterality establishment and turning are similar. However, the fact that only one gene was found at the *inv* locus does suggest that this would be the case.

The data on the laterality problem have however spun off some useful knowledge for the process of turning in the sense that we now know more about abnormal or absent genes or proteins in relation to the process of turning. No *shh* expression in the node and a reduced signal of *brachyury* and *FGF8* in the mesoderm exiting the streak both randomise the direction of turning. An absence of RA or *furin* leads to no turning, while an absence of *smad2* or *smad5* leads to abnormal or incomplete turning. Since we do not

know the interconnections between all of these molecules, we cannot determine a cut-off point in the cascade of events below which turning will happen (or be randomised).

It is also interesting, that two reports link a failure of heart looping with a failure of turning: in the absence of RA or *furin* there is neither turning nor heart looping. Others link failure of turning with heart deformation (Chang *et al.*, 1999) or random direction of turning with random direction of heart looping (Tsukui *et al.*, 1999), but a causal link has not been established.

4.2.7 Possible mechanisms of turning

It has not become clear from the literature study what drives the process of turning. The source of the mechanism could be local, *e.g.* driven by a change in shape of a single or a small group of tissues. Alternatively, the turning might be a global event, perhaps due to the 'inside-out' configuration becoming unstable because of normal growth. It is unlikely that the extra-embryonic membranes drive the turning since these are thin compared to the mass of the embryo at these stages. If the turning is driven locally, then at a 3D level single tissues or areas would be expected to be permanently ahead in the process, or at least during the initiation. If the turning is driven at a global level, then one side of the embryo might appear squashed while the other seems more stretched out.

The aim of this study is to give a thorough and detailed account of the anatomical features of the process of turning by text and images that will subsequently be analysed for clues about the type of mechanism behind the turning. The images will be of surface rendered views of groups of tissues and histological views from the reconstruction.

4.3 MATERIALS AND METHODS

4.3.1 Biological methods

For this study, embryos of ages E8, E8.5 and E9.0 were used. The E8 embryo was embedded in plastic and cut to a nominal section thickness of 2 μm. The E8.5 and E9 embryos were embedded in paraffin and cut to a nominal thickness of approximately 7 μm.

4.3.2 Tissues considered in this study

For all three stages of development studied, identical tissues were used to observe the mechanism of turning. For the external appearance of the embryo, these were the surface epithelium, mesothelial lining of intraembryonic coelom and gut. For the internal configuration, neural tissue, notochord, gut, mesothelial lining of intraembryonic coelom, somites and heart.

For 'processing' artefacts of the original sections in the reconstruction affecting the delineation of these tissues, see appendix 1.

For the basis on which 'arbitrary' anatomical boundaries were delineated, see appendix 2.

4.3.3 Computer methods

For the figures, 3D surface renderings of individual tissues were created using the commercial software packet 'AVS'. For more details see chapter 2. The histology views are taken from the reconstructions.

4.3.4 All other methods

For all other methods (biological and computer) see chapter 2.

RESULTS

4.4.1 Introduction

4.4.1.1 Layout of the results

The process of turning takes place over E8-E9 and each developmental stage will be discussed in a separate section but to a common format. There will be a description of the internal and external configuration of tissues during the process of turning with the aid of figures accompanying the text. Figures are 3D surface views of anterior, left, right and posterior views of groups of tissues considered in this study. For the external view of the embryo, surface epithelium, gut and mesothelial lining of the intraembryonic coelom are grouped together. For internal views, figure series are presented of three groups of tissues: neural tissue, heart and somites; neural tissue, notochord and gut; and neural tissue, gut, and mesothelial lining of intraembryonic coelom.

Histological views of original sections will be shown of regions of specific interest with respect to clues to a possible mechanism of the process of turning. The histology is analysed looking for local tissue condensations which -if present- will be more clearly visible in loosely packed tissues such as the mesenchyme, and less so in denser tissues such as the neural tissue. These condensations may depending on extent and localisation form a pointer towards a local or global driven mechanism.

4.4.1.2 Tissues that are excluded from this study

The mesenchyme and the vascular system have not been used to analyse the mechanism of turning. The mesenchyme is not shown because its 3D configuration is too complicated since it is the 'tissue between all the other tissues'. Moreover, because of its morphological character, it is therefore not necessary to show it, since all the other tissues are already displayed. The vascular system has not been analysed since its structure (one-cell-layer thin endothelial tubes filled with fluid) makes it very unlikely that it has any driving force in the process of turning. For views of the heart, the endothelial lining has been shown and not the myocardial walls of the heart. The morphology of these structures is congruent (chapter 3) and the endothelial lining is the narrower structure so it is easier when viewing this to analyse the looping of the heart with respect to the process of turning.

4.4.2 E8 embryo

4.4.2.1 External view

The outline of the embryo forms a 'U'-shape in a single plane (figures 4.3a-c).

4.4.2.2 Internal view

The neural tissue does not describe a 'U'-shape in one plane (figure 4.3e). The caudal end is not in line with the rest of the body and is pointing slightly towards the left of the body. The left-hand open wall of the midbrain is slightly lower (by about one somite's length (approximately 100μm).

The two rows of somites are level (figures 4.3e and h). This is in accordance with the configuration of the neural tissue in the mid-trunk region where its dorsal midline is exactly dorsal and not directed towards one side.

The only sign of turning that the gut shows is in the hindgut region, which follows the slight out-of-one-plane configuration of the neural tissue (figures 4.4a-d). The same is true for the notochord, which is located exactly between the most medial points of the neural tissue and the gut. The mid- and foregut are in one plane.

The caudal part of the mesothelial lining has the same orientation as the caudal part of the neural tissue and the gut (figures 4.4e-h).

4.4.2.3 Histology

Analysis of the E8 histology does not yield any significant additional information to what has been described above.

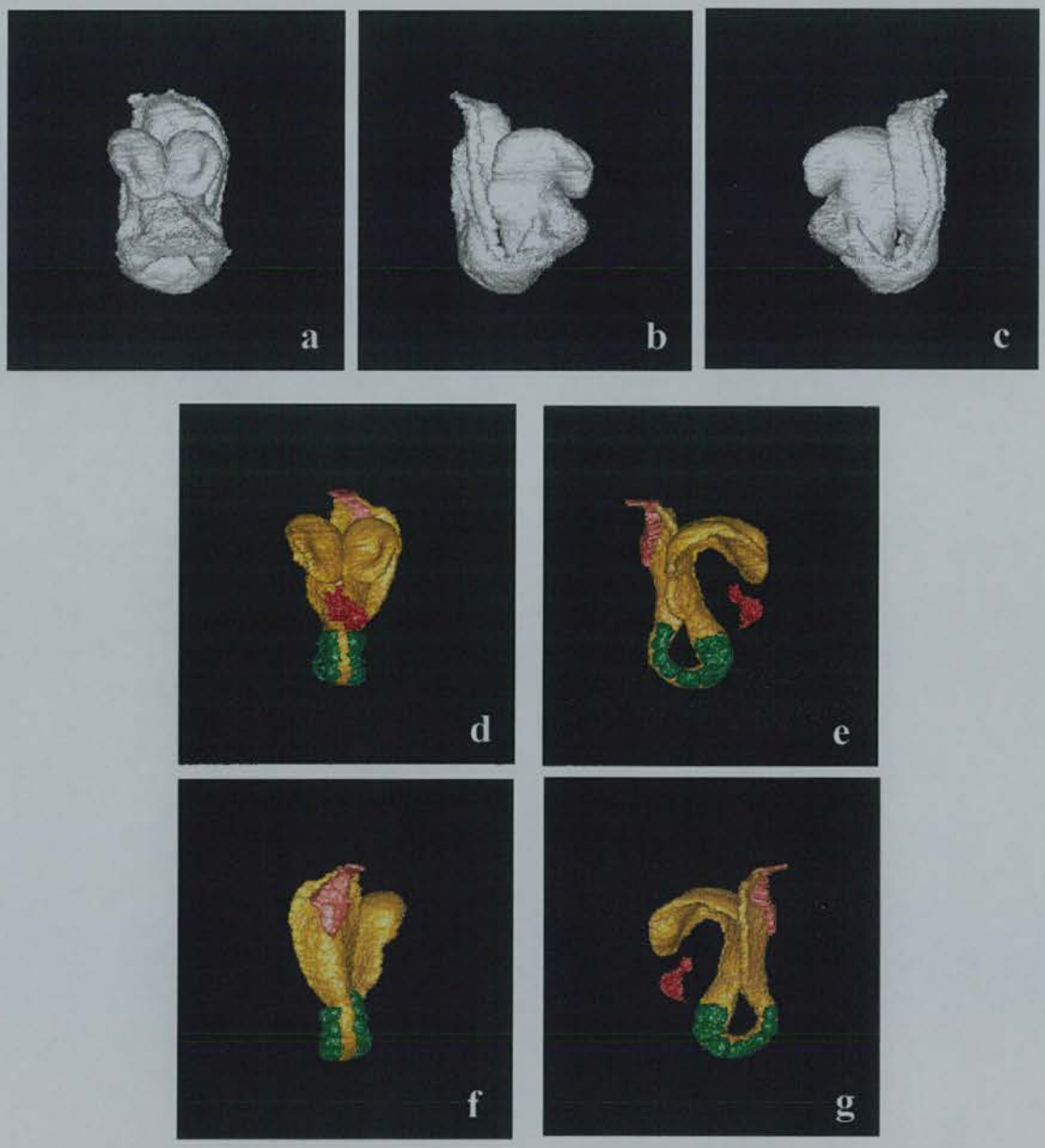

Figure 4.3: E8 embryo 3D views. (a) anterior, (b) right lateral and (c) posterior views of the outer surface. (d) anterior, (e) right lateral, (f) posterior and (g) left lateral views of the neural tissue (yellow), endothelium of the heart (red), somites (green) and primitive streak (pink).

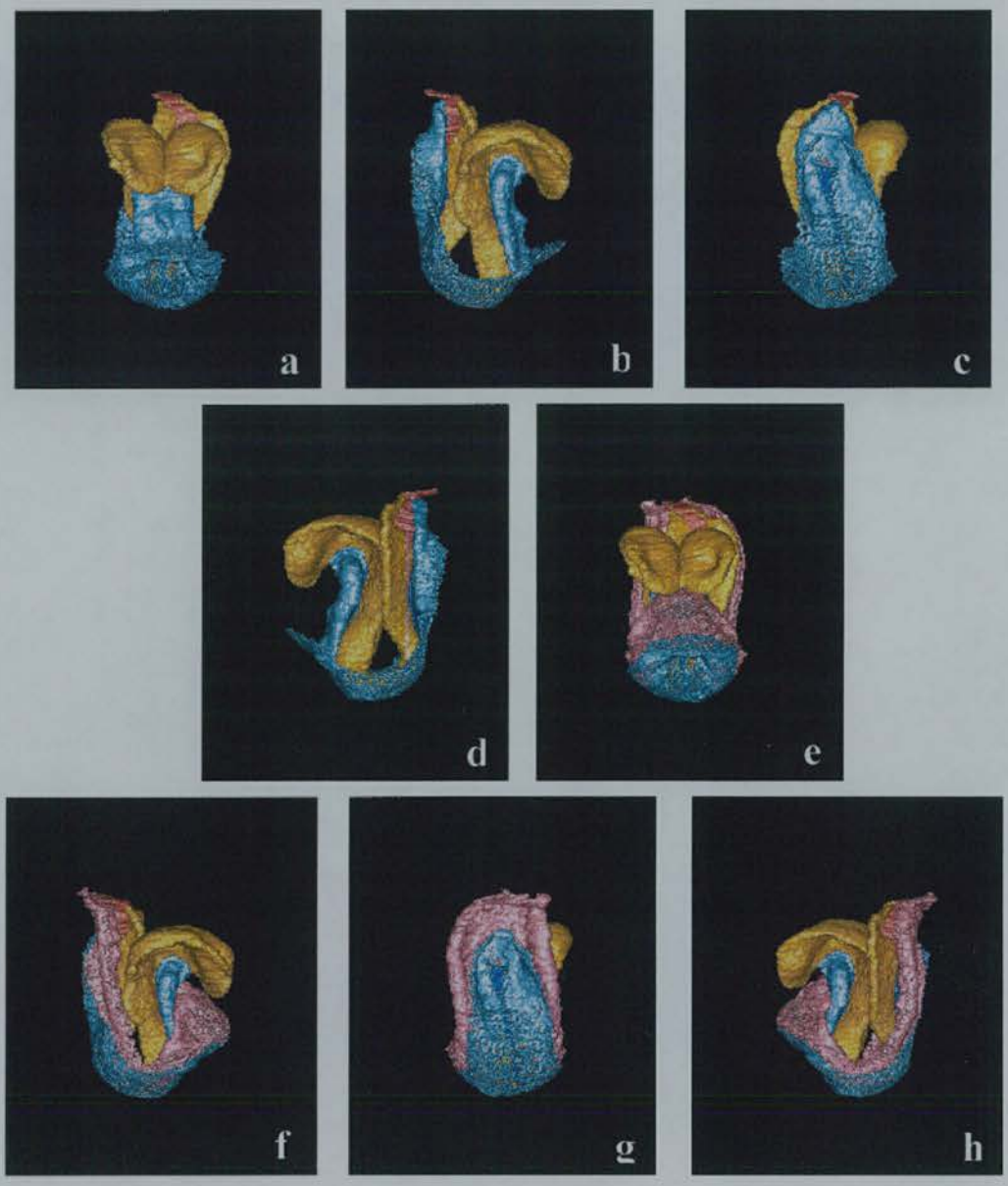

Figure 4.4: E8 embryo 3D views. (a) anterior, (b) right lateral, (c) posterior and (d) left lateral views of the neural tissue (yellow), gut (light blue), and primitive streak (pink). (e) anterior, (f) right lateral, (g) posterior and (h) left lateral views of the neural tissue (yellow), gut (light blue), mesothelial lining of the intra-embryonic coelom and primitive streak (pink).

4.4.3 The E8.5 embryo

4.4.3.1 External view

The outline of the embryo indicates a mid-turning stage. The caudal end of the embryo has rotated slightly more than 90° around its main body axis. The part caudal of the mid-region of the midbrain up till the caudal end of the hindbrain have rotated about 45° around the main body axis (figures 4.5a-d).

4.4.3.2 Internal view

The cephalic part of the neural tissue has rotated about 45°, and the most rostral tip of the forebrain points slightly towards the right of the outflow tract (figure 4.5e).

The neural tissue (figure 4.5e-h) shows that the very most caudal end has rotated nearly 180° around the main body axis. This is the most advanced region in relation to turning of the embryo. The mid-trunk region of the neural tissue has rotated about 30° around the main body axis. The left-hand open wall of the midbrain is slightly lower by less than one somite's length.

The two rows of somites are not level any more: the left row of somites is situated below the right row. This indicates a similar progress through turning as the mid-trunk region of the neural tissue (figures 4.5e-h).

The heart tube has now looped (figures 4.5e-h). The most rostral tip of the forebrain points slightly to the right of the outflow tract.

The midgut area is located to the right side of the embryo (figures 4.6a-d). The foregut region has rotated slightly towards the right compared to the situation noted at E8 and is at the same angle of rotation as the neural tissue in the region. The caudal tip of the hindgut has rotated 90° about the main body axis. The notochord is for its entire length located exactly between the midlines of the neural tissue and gut.

The mesothelial lining of the intraembryonic coelom has undergone the same degree of rotation as the gut (figures 4.6e-h).

4.4.3.3 Histology

The analysis of the histology of the E8.5 embryo shows that the left somatopleure is shorter than the right (figure 4.7).

Figure 4.5: E8.5 embryo views. (a) anterior, (b) right lateral, (c) posterior and (d) left lateral views of the outer surface. (e) anterior, (f) right lateral, (g)posterior and (h) left lateral views of the neural tissue (yellow), endothelium of the common atrium (blue), endothelium of the primitive ventricle (lilac), endothelium of the outflow tract (red), somites (green) and primitive streak (pink).

Figure 4.6: E8.5 embryo views. (a) anterior, (b) right lateral, (c) posterior and (d) left lateral views of the neural tissue (yellow), gut (light blue), and primitive streak (pink). (e) anterior, (f) right lateral, (g) posterior and (h) left lateral views of the neural tissue (yellow), gut (light blue), mesothelial lining of the intra-embryonic coelom and primitive streak (pink).

Figure 4.7: Grey-level image of a histological transverse section through the E8.5 embryo showing the shortened left somatopleure.

4.4.4 E9 embryo

4.4.4.1 External view

The outline of the embryo shows that the embryo has completed turning: the embryo has adopted the classical fetal configuration with the neural tissue being located on the outside of the curve and the gut on the inside (figures 4.8a-d).

4.4.4.2 Internal view

The neural tissue (figure 4.8e-h) confirms the external view. The length axis forms a straight line and the caudal end is situated to the right side of the head. There is, however, one important feature at the caudal end of the neural tissue. The very caudal tip has to rotate over 45° in order to finish turning (figure 4.8e-h).

The two rows of somites are not level. The left row of somites is situated below the right row. (figure 4.8e-h).

The loop of the heart tube is grossly the same as in the E8.5 embryo (figure 4.8e-h), albeit slightly more compacted. The most rostral tip of the forebrain of the embryo is situated above the junction between the primitive ventricle and the outflow tract. The right and left inflow tract of the heart (sinus venosus) are not level: the left is extending further down than the right (figure 4.8e).

The fore- and hindgut areas have completed the process of turning, but the midgut area, which is still open, is situated towards the left of the embryo (figures 4.9a-d). This area will probably not adopt a symmetric position until the midgut has closed. The notochord is located exactly between the midlines of the neural tissue and gut for its entire length of overlap with these tissues.

The mesothelial lining of the intraembryonic coelom has undergone the same degree of rotation as the gut (figures 4.9e-h).

4.4.4.3 Histology

There are no particularities in the histology other than, as for the E8.5 embryo, the left somatopleure being shorter than the right (figure 4.10).

Figure 4.8: E9 embryo views. (a) anterior, (b) right lateral, (c) posterior and (d) left lateral views of the outer surface. (e) anterior, (f) right lateral, (g) posterior and (h) left lateral views of the neural tissue (yellow), endothelium of the common atrium (blue), endothelium of the primitive ventricle (lilac), endothelium of the outflow tract (red), somites (green) and primitive streak (pink).

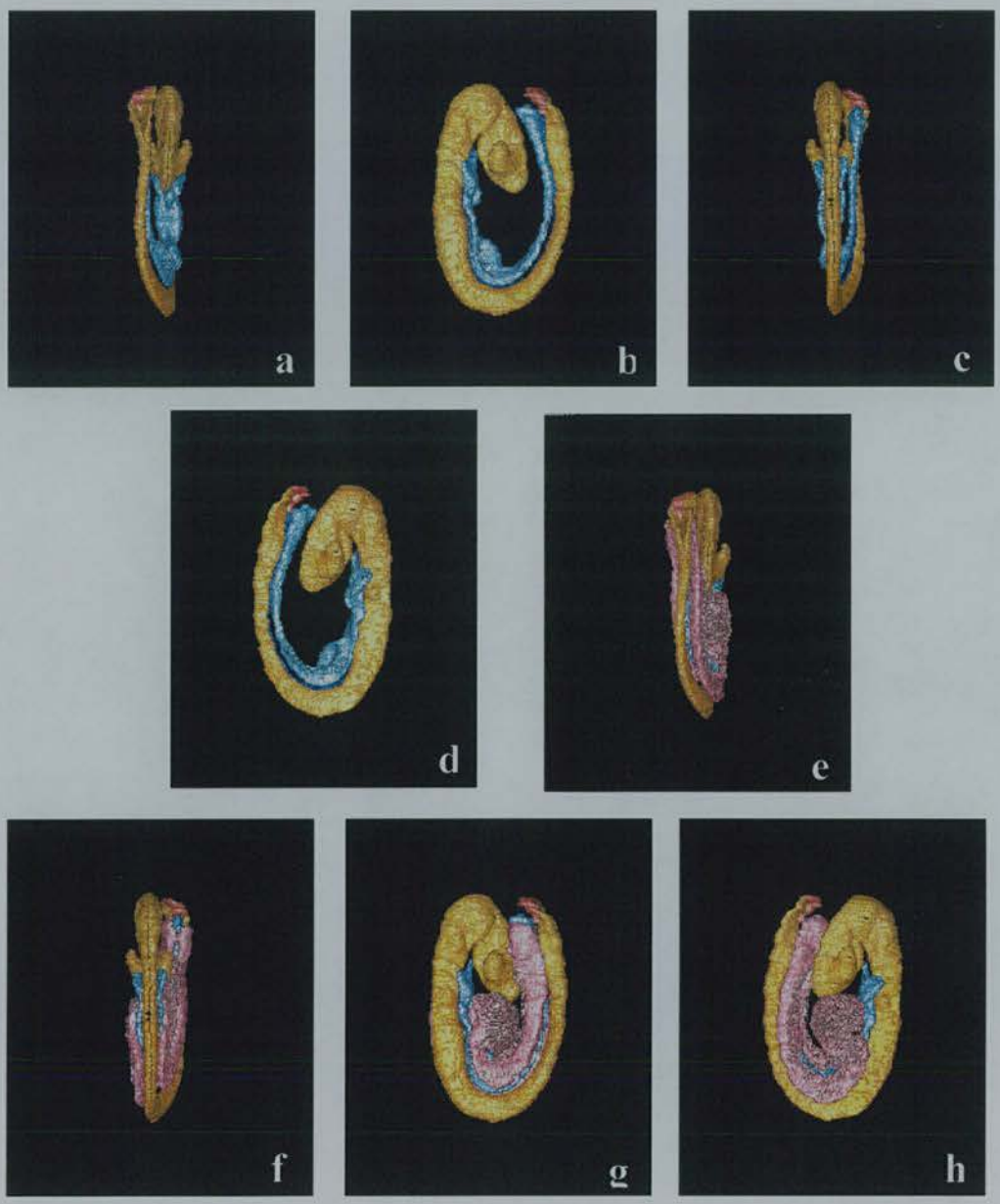

Figure 4.9: E9 embryo views. (a) anterior, (b) right lateral, (c) posterior and (d) left lateral views of the neural tissue (yellow), gut (light blue), and primitive streak (pink). (e) anterior, (f) right lateral, (g) posterior and (h) left lateral views of the neural tissue (yellow), gut (light blue), mesothelial lining of the intra-embryonic coelom and primitive streak (pink).

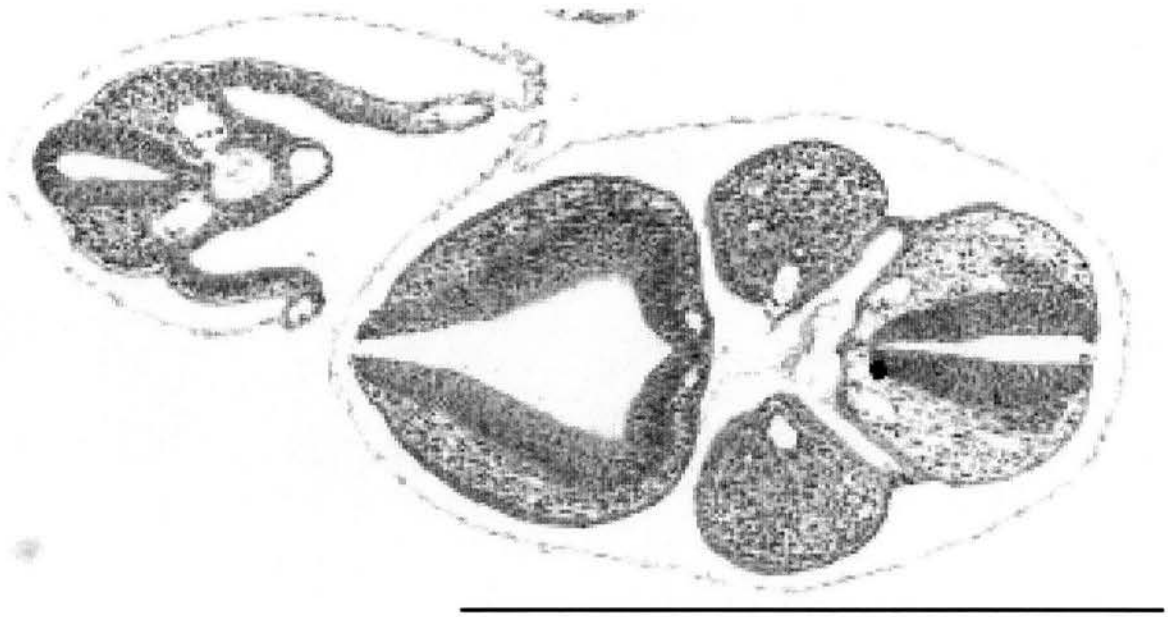

Figure 4.10: Grey-level image of a histological transverse section through the E9 embryo showing the shortened left somatopleure.

DISCUSSION

4.5.1 Discussion

4.5.1.1 Events covered in this study

The E8, E8.5 and E9 embryos used for this study display a wide range of events during the process of turning in the mouse embryo. The E8 embryo seems only just to have started turning with one side of the midbrain being slightly lower than the other side, and the caudal end of the embryo being slightly out of the plane that the rest of the embryo describes. The E8.5 embryo is at a mid-turning stage with the cranial and caudal end having progressed through respectively 45° and 90°. The E9 embryo has nearly completed turning, except in the mid-trunk region where the gut, somites and sinus venosus are still in the final stages of the process of turning.

4.5.1.2 Sequence of events during turning

From what can be observed in the three reconstructions of the E8, E8.5 and E9 embryos it appears that the turning starts at the most cranial and caudal end of the embryo and then progresses towards the midtrunk area which is the last part of the embryo to

complete turning. The direction of turning is simplest described by the embryo turning its dorsal side to its left. The part of the head rostral to the cranial flexure does not rotate around its length axis but follows the rotation of the region caudal to the cranial flexure. The latter observation is confirmed by the fact that the branchial arches and optic vesicles are level at this stage in time, and thus have not twisted with respect to each other (data not shown).

The unexpected twist in the caudal end of the E9 embryo was checked to be normal by dissecting 29 embryos free from their membranes and observing them without fixation. Fourteen of 29 embryos displayed a similar degree of rotation in the caudal tip to the E9 embryo used for this study and these were the developmentally more advanced embryos of the group that was studied. The twist is unexpected in the sense that the caudal end seems to be most advanced in the process of turning, apart from this very caudal tip that displays a degree of rotation similar to the caudal tip of the E8.5 embryo.

4.5.1.3 Heart looping and the process of turning

From this study a conclusion cannot be reached about the first event of lateral asymmetry in the embryo. In the literature there is some confusion in that some observers report that looping of the heart is the first event of lateral asymmetry while others state that the process of turning marks the first asymmetric event. In the E8.0 embryo, the process of turning and looping of the heart have both just started.

The seeming link between heart looping and turning as observed in the literature (Chang *et al.*, 1996 Tsukui *et al.*, 1996) is not apparent morphologically. By this it is meant that neither looping of the heart seemingly has an effect on the process of turning, nor does the turning process appear to have an effect on the looping of the heart. This is because the region where the main mass of the heart is located is a region of the embryo with a straight axis.

4.5.1.4 Mechanism of turning

The morphology of the three embryos during the process of turning seem to suggest that the process of turning is globally driven rather than locally driven. Morphological changes appear over large areas in the embryo and neighbouring tissues have without exception a state of progress very similar to each other. The fact, for example, that the neural tissue seems to complete axial rotation shortly before the somites, is probably more indicative of the rigidity of the neural tissue rather than the neural tissue driving

the process. If the latter would have been the case, more distortion were to be expected in surrounding loose tissue such as the body mesenchyme. What the global drive for turning is, can not be concluded from this study.

The shorter left somatopleure in the direction perpendicular to the main body axis in the E8.5 and E9 embryos might be interesting in that could provide a force that brings the configuration of the embryo before turning out of balance. It is unlikely that the left somatopleure is shortened, because the amnion in this region of the embryo is wrapping around the body as the embryo rotates around its axis (figure 4.2). This, since the amnion does not appear stretched and the cells in this region of the amnion have the same shape as elsewhere in the amnion.

The shortening of this somatopleure coincides topologically with the unilateral expression of *nodal* in this region at E8 (Collignon *et al.*, 1996; Lowe *et al.*, 1996). The interesting aspect to this coincidence is that correct expression of *nodal* is crucial to laterality establishment and, therefore, may well be crucial to turning. Whether this is indeed the case, cannot yet be established from the literature, but it might give a handle to further research.

4.5.1.5 Turning in the rat compared to the mouse

Not only the direction of turning in the mouse is different from that in the rat, but also the mechanism appears to differ (Deuchar, 1971). In the rat, turning starts in the head region only , while in the mouse the process starts in the head and tail regions. The fact that in both the mouse and rat the arrangement of the viscera is similar at the end of the process of turning indicates that the genetic control of turning and that of the establishment of *situs* might be different. This is interesting, because the data available from the literature show a very close relationship between turning and the establishment of left-right asymmetry, the latter of which involves genes that are conserved between mammals.

4.5.1.6 Shortfalls of the study

The main drawback of this study is that only one embryo per stage of turning was studied, and only three stages throughout the process. However, it needs to be said that the embryos were chosen of being representative of their stages, and that the result of this study form an uncontentious sequence of events. It is therefore not to be expected that observing more embryos would have led to a different impression.

The other drawback is that we are trying to draw conclusions about a process by looking at 'stills' and therefore we necessarily miss aspects of the process. For example, Deuchar (1971) looked at rats turning *in vitro* and found that the process of turning with 'dipping' movements of the head, triggered by starting contractions of the heart.

4.5.1.7 Strong points of the study

The system used for studying the process of turning is a very powerful one. It has been possible to look at the histology at any plane throughout the reconstruction when trying to find pointers for strains in the embryo. Moreover, the 3D surface rendering of anatomically discrete areas has enabled a detailed study of the internal geometry of the mouse embryo during the process of turning. Getting a similar overview would not have been feasible without reconstruction of the histology and delineation of the individual tissues.

4.5.1.8 Wider context

This study on turning has partly been justified by the great interest in the establishment of asymmetric laterality and the apparent link between these two events. The establishment of handedness of visceral organs in itself is key in development and this importance stretches further than the importance of a correct body plan for these organs. A study was done in which a teratogen that induces unilateral limb malformations was administered to homozygous *iv* and homozygous *inv* embryos. Importantly, these malformations were mirrored if the visceral organs were mirrored (Brown *et al.*, 1989). This seems to suggest the *situs* of the visceral organs determines the left and right hand side throughout the whole body.

4.5.1.9 Follow-up study

It would be interesting to observe mouse embryos during their process of turning and to find out whether, like in the rat (Deuchar, 1971), turning starts with dipping movements of the head seemingly caused by the contractions of the looped heart. If this is the case then this could give a handle on unravelling of the mechanisms behind turning. However, since the direction of the looping seems to cause dipping of the head in the rat in one direction and the direction of turning is opposite in the mouse, it seems unlikely that turning starts the same way in the mouse. Moreover, it would still be necessary to establish what triggers the simultaneous start of turning in the tail region.

It is furthermore important to find out whether the *iv* mice turn the opposite way if they display *situs inversus*, and turn the normal way if they display *situs solitus*. If this were the case then a natural follow-up study would be to 'clip' the left splanchnopleure just before rotation transverse to the main body axis, so to rule out the effect of the shortening in the somatopleure and to test whether the shortening is of crucial importance to the process. If it is, then the result could be confirmed by clipping the right hand somatopleure in *inv* mice.

4.5.2 Conclusions

From this study the following conclusions can be reached:

- The mouse embryo turns approximately between E8 and E9 by turning its dorsal side to its left.

- The process of turning starts at the head and tail end and progresses towards the mid-trunk area.

- Unlike the description in the literature, the process of turning was not finished in the E9 embryo.

- There is no apparent morphological relationship between the looping of the heart and the turning of the embryo.

- The process of turning appears a global process rather than driven by a confined area or set of tissues in the embryo

CHAPTER 5: THE GROWTH OF TISSUES DURING THE FIRST HALF OF GESTATION

5.1 INTRODUCTION

A detailed investigation of growth is relevant because it adds quantitative data to the existing qualitative knowledge of mouse developmental anatomy. In addition the growing interest in bioinformatics and computer modelling of development will need such baseline data. In this chapter growth was investigated in all embryonic tissues over the range of E1-E9 and in extraembryonic structures in embryos E1-E7.5. Growth rate comparisons are made between extraembryonic and embryonic structures, and also between tissues of different cell lineages. Additionally, left-right asymmetry is assessed for the appropriate structures.

Previous studies on growth of tissues were limited in that it was never possible to measure actual volumes of individual tissues and therefore estimates had to be made from combinations of mitotic numbers and cell sizes (Snow, 1977). For this study histological reconstructions of 13 embryos ranging from E1-E9 are used and all tissues in each model delineated therefore it has become possible to make quantitative intra and inter embryo comparisons that could not have been made by studying 2D histological sections or reconstructions of individual tissues.

In this study, in which a single embryo specimen was reconstructed, a key problem is to correct for shrinkage. It is assumed that for these studies the differential shrinkage is not important, in the sense that the preparation is standard and therefore for the purposes of future comparisons these effects will be common. Overall shrinkage is taken into account by normalising the absolute values with respect to the total volume. Therefore the data collected were tissue sizes (volumes) of all stages expressed as a fraction of the total embryo volume. Tissue volumes were calculated after delineation of the tissue in the model (chapter 2) using purpose-designed software (MRC HGU). Relative tissue volumes were then calculated by dividing by the total volume of tissue of (part of) the embryo. Data are presented in table format and charts and are divided in three developmental age groups: pre-implantation, egg cylinder stages and early organogenesis.

Because only one embryo per Theiler stage was used and little data is available on natural variation between whole embryos within a stage, embryos were selected to be qualitatively representative of their Theiler stages. Therefore, comparison of tissues relative to total tissue across subsequent stages to assess growth emphasis is justified. Additionally, growth rates of tissues or tissue groups were calculated by comparing absolute volumes between subsequent stages to indicate trends of tissue increase. These trends are partly justifiable because the embryos

are representative of their stages and the investigated shrinkage (see below) during processing, but confirmation of these trends will necessarily need followed-up research.

Another worry is that processing might distort structures within embryos. Where possible, embryos were processed together which reduces some unknown parameters in the comparison afterwards. Several embryos were photographed before and after processing to assess the distortion and shrinkage. Distortion was not noticeable and shrinkage was approximately 10%. All reconstructions were checked for displaying normal tissue morpholgy. The lack of multiple embryos for each stage in this study exposes some constraints and these are considered further in the discussion.

The main conclusions that can be drawn from this study are:

- a growth spurt happens simultaneously in ICM-derivatives and trophectoderm,
- this spurt happens around implantation,
- least growth in ICM-derivatives after implantation happens during organogenesis,
- during egg cylinder stages, all tissues shrink as a proportion of the whole conceptus except for the mesoderm and the ectoplacental cone (the latter shows the fastest proportionate growth),
- during organogenesis, the proportion of embryonic tissues derived from ectoderm and endoderm shrink with a corresponding gain of mesodermal structures,
- of the mesodermal structures, only half increase proportional to the embryo while the other half lessen due to differentiation,
- of the mesodermal structures, the majority remain undifferentiated and this part grows faster than the differentiated part,
- there is no left-right asymmetry in the tissue volumes,
- during organogenesis, the heart and vascular system are the fastest growing organ system,
- in the same stages, the future central nervous system is the single biggest tissue at 20% of the embryo,
- the smallest single-tissue is the gut at E9 at only 3% and

- The study provides reliable baseline results but more specimens are needed to strengthen the conclusions and to provide data on natural variation.

5.2 MATERIALS AND METHODS

5.2.1 Biological methods

The thirteen embryos used for this investigation are summarised in Table 5.1.

Table 5.1. Gestational age of embryos and dissection particulars (*italics*).

Theiler stage	Appr. age[1] [dpc]	Characteristics
2	1	2-Cell embryo, zona pellucida.
3	2	8-Cell embryo, zona pellucida.
3	2.5	12-Cell compacted embryo at the onset of cavitation, zona pellucida.
4	3	Early blastocyst, zona pellucida.
5	4	Advanced blastocyst, no zona pellucida.
7	5.5	Early egg cylinder, cavitation only in embryonic region, Reichert's membrane, ectoplacental cone starting.
8	6	Advanced egg cylinder, progressed proamniotic cavity.
9	6.5	Early primitive streak.
10	7	Late streak no bud, no node, proamniotic fold. *Dissected without Reichert's membrane, mural trophectoderm and parietal endoderm.*
11	7.5	Elongated allantois, late neural plate, no headfold.
12	8	7 Somites, primitive heart tube, no arches. *Dissected without extraembryonic membranes.*
13	8.5	13 Somites, halfway through turning, 1 arch. *Dissected without extraembryonic membranes.*
14	9	17 somites, turned, 2 arches, posterior neuropore. *Dissected without extraembryonic membranes.*

1) From table 1, chapter 2.

The embryo fixation, histological processing and staining were as described in chapter 2 (materials and methods section 2.2.1). E1-E8 embryos were plastic embedded and E8.5 and E9 embryos were paraffin embedded. E1 and E2 embryos were processed in one batch, E3 and E4 in one batch, and E5.5, E6 and E6.5 embryos in one batch.

5.2.2 Computer and calculation methods

The method of digitisation, reconstruction, warping and tissue delineation are described in chapter 2, §2.2.2 and §2.2.3. In the E6 model, the mural and polar trophectoderm were delineated as one tissue. In the E7.5 model, Reichert's membrane, parietal endoderm and mural trophectoderm were delineated as one tissue.

Purpose-built software was used to calculate the number of voxels for each tissue. This was tested by delineating five domains of known number of voxels. The program generates lists of all the tissues with the number of voxels in each. To obtain the true tissue volume the number of voxels for each tissue was multiplied by the size of a voxel in μm^3. These calculations were made by hand.

5.2.3 Calculation of voxel sizes

The E2, 3 and 4 embryos were digitised using a x20 with the result that the pixelsize of a digitised section was 0.34x0.34 μm^2; after downsizing by a factor of six and reconstruction the voxelsize becomes therefore 2.04x2.04x2.0 = 8.3μm^3.

The E1, 2.5, 5.5, 6, 6.5, 7, 7.5 and 8 embryos were digitised using a x10 objective then downsized in the original plane by a factor three which leads to the same voxelsize as above. The exception is E1 which was not downsized and therefore has a voxelsize $8.3/3^2 = 0.92\mu m^3$.

Theiler stage 13 and 14 were digitised using a x5 microscope objective which results in an original pixelsize of 1.36x1.36μm; downsizing by a factor 3 lead to a voxelsize of $4.1x4.1x7 = 1.2x10^2\mu m$.

All pixelsizes were checked with a graticule as described in chapter 2.

5.2.4 Tissues considered in this study

Tissues that were delineated in each of the reconstructions are described in chapter 2, §2.3.3. In general all tissues that were morphologically distinguishable on the sections down the microscope were delineated. All delineated structures were used for growth assessment unless the level of detail of the delineation (*e.g.* individual blood vessels in the older stages) confused the comparisons.

For comparisons between embryos, cavities volumes were discarded except for the blastocoelic cavity that is thought to be formed by a physiological action namely active pumping out of cell contents into intercellular space. Cavities were compared as individual 'tissues' between embryos. This, so that growth in total volume can be assessed separately from growth in cell mass or tissue volume.

5.2.5 Errors

There are a number of sources of error in the process from collecting the embryos through to calculating the volumes within the reconstructions, these are assessed below.

5.2.5.1 Sources of random error

For the estimation of tissue volume there are random errors arising in the histological processing – *processing errors* – and errors in the delineation or tissue identification – *interpretation errors*.

Interpretation errors arise primarily in two ways: either by mis-identifying tissue boundaries, perhaps due to poor resolution, or by errors in painting i.e. simply making a mistake in placing the boundary manually or automatically. Careful re-inspection of structural boundaries shows that the error is usually within the range ±1 pixel. For larger structures, typically with smooth boundaries the errors tend to cancel when estimating the volume. For smaller structures, the boundaries are typically delineated more accurately but errors have a proportionately greater effect. Across the range of structures the errors detected had an estimated maximum effect of 5%.

The second largest source of random error arises from processing and in particular crumpling of the tissue section. This always reduces the apparent volume. This type of error is obvious in the reconstruction and is partly corrected by the warping process. This error introduces an estimated maximum further 5% uncertainty.

5.2.5.2 Sources of systematic error

Systematic errors are errors that can be reproduced, in principle estimated and therefore may be taken into account. A good example of such an error is shrinkage during the histological processing e.g. fixation or embedding. Four specimens ranging from E7-E8 were photographed before and after processing (gradual removal of water by immersion in alcohol) for plastic embedding. All four were processed simultaneously. In all cases, the shrinkage was linear in the sense that the aspect ratios were the same before and after the processing and the shrinkage was about 10%. One of these four embryos was the E7.5; the other three were not used for reconstruction. From this it is safe to assume that non-linear shrinkage (*i.e.* distortion of the aspect ratios) is not significant. Comparing tissue sizes relative to total body size thus seems an appropriate measure although in principle absolute sizes are also important for phenotype and mutation analysis.

Another systematic error is the error in section thickness. All plastic reconstructions were compared to the photographs that were taken before sectioning and do have the same aspect ratios. Therefore, the average thickness of the sections is correct. This was not tested for the paraffin sections, since no photographs before cutting were available.

5.3 RESULTS

5.3.1 - Introduction

The 13 developmental stages covered in this chapter were divided into three groups: the preimplantation stages, the egg cylinder stages and the early organogenesis stages. Individuals were compared within each group and where relevant, comparisons were made between or across groups. The sizes of tissues will be presented in table and chart format.

The next section (5.3.2) deals with all 13 stages and compares sizes of entire conceptuses and sizes of the inner cell mass (ICM) and its derivatives between stages. In section 5.3.3 the relative sizes of all tissues in preimplantation stages are compared, in these stages there is no growth through a direct exchange of nutrients between maternal and embryonic tissue. Section 5.3.4 investigates tissue sizes of the egg cylinder stages. These tissue sizes were calculated as fractions of the whole conceptuses, as fractions of ICM-derivatives and as fractions of epiblast-derivatives. There is also a separate comparison of tissue groups from different cell lineages - the sizes relative

to the whole conceptus or group of ICM-derivatives, and the increase in tissue size between stages. The last section deals with early organogenesis and compares tissue sizes across developmental ages E8, E8.5 and E9. A summary comparison between sizes of the derivatives of the three germ layers (endoderm, mesoderm and ectoderm) relative to the embryo, from E6.5 to E9 ends this section.

All volumes, except for some in table 5.2, which are absolute, are relative to the whole conceptus, embryo or tissue group as appropriate and are expressed as a percentage. Absolute sizes, which mean the tissue sizes after processing and reconstruction, are expressed in mm^3. All growth rates or increments in tissue sizes are based on absolute sizes and mean the incremental factor of tissue size between two subsequent stages. Sometimes tissues were not present due to dissection methods or were not delineated. Where relevant, footnotes have been added to the tables indicating which values are affected and which measures were taken to minimise data distortion.

5.3.2 Sizes of reconstructions and ICM (-descendants) E1-E9

Table 5.2 and figure 5.1 compare sizes of whole reconstructions from E1 to E9 as an introduction and to create a context for further results. One drawback of comparing one reconstruction with the next is that the size of the trophoblast depends on the dissection. Therefore size comparisons between whole reconstructions are unreliable, as it is not known how much of the ectoplacental cone has been included. Hence comparisons were also made between ICM (and -derivatives) since the size of this tissue group does not depend on the dissection method. For each of these two groups, absolute sizes, growth rates and sizes relative to earliest conceptus were calculated. Sizes of whole conceptuses include all tissues of the conceptus but not the cavities within the conceptus except for the blastocoelic cavity that is thought to be formed by active pumping (Kaufman and Bard, 1999). Sizes of whole conceptuses do not include attached maternal cells. Figure 5.1 is based on table 5.1 and represents sizes of whole conceptuses and ICM or ICM-derivatives on a logarithmic scale.

Table 5.2. Absolute sizes of reconstructions E1-E9.

	E1	E2	E2.5	E3	E4	E5.5	E6	E6.5	E7[6]	E7.5[7]	E8	E8.5	E9
Total size of whole conceptus [mm^3][1]	0.08 $*10^{-3}$	0.09* 10^{-3}	0.13 $*10^{-3}$	0.16 $*10^{-3}$	0.16 $*10^{-3}$	2.0 $*10^{-3}$	5.2 $*10^{-3}$	12.4 $*10^{-3}$	30.2 $*10^{-3}$	110 $*10^{-3}$			
Total size[2,3] relative to E1	1 (3.9)	1.2 (7.5)	1.6 (4.9)	1.9 (2.8)	1.5	12.7	28.9	78.5	191	695			
Increase relative to previous stage[4]						12.7	2.61	2.38	2.44	3.63			
Total size of ICM or embryo[5] [mm^3]				0.03 $*10^{-3}$	0.02 $*10^{-3}$	1.4 $*10^{-3}$	2.7 $*10^{-3}$	6.1 $*10^{-3}$	13.8 $*10^{-3}$	45.4 $*10^{-3}$	0.16	0.24	0.44
ICM or embryo[5] size relative to E3				1	0.8	46.7	90.6	202	460	1514	5.3 $*10^{3}$	8.0 $*10^{3}$	14.7 $*10^{3}$
Increase relative to previous stage					0.8	58.3	1.94	2.2	2.3	3.3	3.5	1.5	1.8

Figure 5.1: Size of conceptus and ICM (derivatives) in E1-E9 (footnotes 1,5,6,7)

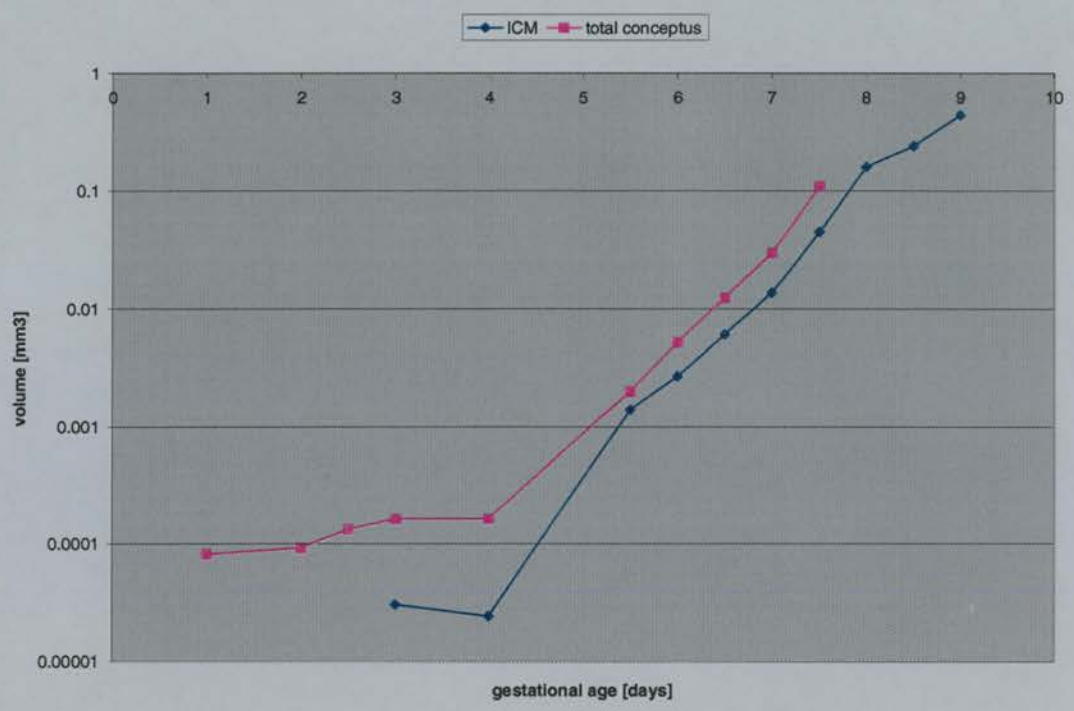

1) Values do not include zona pellucida and second polar body.

2) Between brackets the value of the perivitelline space as percentage of the whole conceptus. This part is excluded in all other calculations and only shown as indicator for shrinkage during processing.

3) Values for E5.5-E7.5 based on the average of the total size of E1 to E4 (value 0.153).

4) Value for E5.5 based on average of the total size of E1 to E4 (value 0.153).

5) Values for 'ICM' from E3-7.5 and 'embryo' from E8-E9. Therefore, values for E8-E9 for sizes relative to E1 lower than in reality since ICM contributes to extraembryonic structures as well. Similar for increment of tissue between E7.5 and E8.Values include tissues and blood but no intraembryonic cavities such as neural lumen etc.

6) E7 did not have Reichert's membrane, mural trophectoderm and parietal endoderm. Values for these respective tissues were used from E6.5 for all calculations on the whole conceptus.

7) E7.5 ICM estimate too small, as parietal endoderm not included in ICM count.

Preimplantation embryos

From table 5.1 we can conclude that the size of the 5 embryos (E1 – E4) that had yet to implant, ranges from $0.08*10^{-3}$ - $0.16*10^{-3}$ mm^3. This means that the size of the largest embryo is 1.9 times the size of the smallest embryo. All sizes fall within the range of sizes of embryos given in reference works (Theiler, 1972, Kaufman, 1994; Kaufman & Bard, 1999). This implies that after fixation sectioning and reconstruction no embryos have shrunk to an extent that comparison would not be sensible. Moreover, shrinkage does not seem to vary significantly from one batch of processing to the next, since the preimplantation embryos were processed in three batches (see §5.2.5.2). All postimplantation reconstructions get bigger as they get older which is another indicator that large random shrinkage does not occur.

Growth of ICM vs. whole conceptus

There is a large increase in the absolute size of ICM (-derivatives) and whole conceptus with implantation just before egg cylinder formation (a factor 58 over the duration of two stages, or 1.5 days (E4-E5.5)). McLaren (1976) found an acceleration in the gain of tissue volume between E6.5 – E7.5. The decelerated increment of ICM-derivatives during early organogenesis (E8-E9) could be due to the use of different fixatives for embryos E8.5 and E9. Figure 5.2 shows that 'growth-spurts' or periods of rapid growth occur simultaneously for ICM-derivatives and the whole conceptus, as found by McLaren (1976).

5.3.3 Tissue sizes in preimplantation stages

I first consider the group of preimplantation embryos. The previous section has shown that comparisons can be made between reconstructions since sizes fall within the normal range. This combined with the finding that histology is normal in any plane through the reconstruction (see chapter 2) means that any relevant non-linear shrinkage can be ruled out. Sizes are presented as percentages of the whole conceptus including the blastocoelic cavity and excluding the perivittelline space. The blastocoelic cavity was included as it is presumed to be based on active pumping out of cell contents.

Table 5.3: Relative sizes of tissues in E1-E4.

	E1	E2	E2.5	E3[2,3]	E4[2,3]
Blastomeres[1] [%]	75	63	71		
Inner cell mass[1] [%]				14 (19) [29]	22 [28]

Mural[1] trophectoderm [%]				23 (30) [45]	35 [46]
Polar[1] trophectoderm [%]				12 (17) [26]	20 [27]
Blastocoelic cavity[1] [%]				25 (34)	23
2nd Polar body [%]	2	2	1	1	
Zona pellucida [%]	23	35	28	26	

1) Conceptuses either have blastomeres or these have differentiated into inner cell mass, mural and polar trophectoderm and blastocoelic cavity.

2) Between round brackets are the values of the tissues calculated as if there is no 2nd polar body and zona pellucida. For purpose of comparison of E3 with E4.

3) Between square brackets are the values of the tissues calculated as if there is no 2nd polar body and zona pellucida *and* the blastocoelic cavity was discarded. For purpose of comparison of cell distribution of E3 with E4.

Blastomeres vs. zona pellucida +2nd polar body - variance

From table 5.3 it can be concluded that blastomeres (-derivatives) from E1-E3 make up $^{2}/_{3}$ to $^{3}/_{4}$ of the entire conceptus, with $^{1}/_{4}$ to $^{1}/_{3}$ for the remaining zona pellucida and 2nd polar body. The proportion of blastomere (-derivatives), zona pellucida and 2nd polar body relative to the whole conceptus does not differ significantly among the different embryos. This implies that the method applied for comparing relative growth of tissues amongst mouse embryos is reliable, even though embryos were not processed simultaneously. Variances that do occur fall within those of natural variation (Kaufman, 1992).

Proportions before and after loss of zona pellucida

No significant change in the proportion of tissues in the embryo occurs after the zona pellucida has been shed. The size of the blastocoelic cavity is slightly smaller in E4 but there is no redistribution in the relative sizes of ICM and mural and polar trophectoderm after the shedding. The sizes of inner cell mass, mural and polar trophectoderm are strikingly similar between E3 and E4.

The biggest tissue of the blastomere-derivatives is the mural trophectoderm that is approximately 1.5 - 2 times the size of the polar trophectoderm and inner cell mass.

5.3.4 Tissue sizes in egg cylinder stages

Egg cylinder stages are the key stages for this method to investigate tissue sizes in conceptuses. First, egg cylinder stages are interesting because there is a progressed rapid differentiation and all surrounding tissues are still present in the reconstructions. Therefore, comparisons can be drawn

all the way back to the earliest reconstruction. Second, radial symmetry has been lost so one cannot estimate tissue size by solely examining sections through the microscope.

The first available egg cylinder stage is the E5.5 embryo; E4.5-E5 (TS6) was not harvested because this is the stage of implantation and the decidual swellings are so minor that they are difficult to detect. The cut-off point for this group is E7.5. This is the last embryo in the egg cylinder phase and the last embryo that was dissected with all its surrounding membranes. E8 has clearly started organogenesis and is therefore classified in the next group.

A problem that arises in these more advanced reconstructions is that growth emphasis of a certain tissue may not be detectable at the level of the entire conceptus because of the presence of much bigger (older) tissues. Therefore, tissue sizes are compared in three ways. They are compared as part of the whole conceptus, the ICM-derivatives and the epiblast derivatives. ICM-derivatives are parietal endoderm, Reichert's membrane, visceral endoderm, epiblast and all its derivatives. Epiblast-derivatives are the primitive streak, all mesoderm and ectodermal component of the amnion (Kaufman and Bard, 1999).

There were two types of artifacts in these embryos that affect the measurements: some lacked tissues and in some it was not possible to delineate all the tissues separately. Details of these artefacts are given in table 5.4.

The shortfalls have consequences for the calculations. In the affected tables footnotes were added about lack of data and the origin of substituted values.

Table 5.4: shortfall of delineated tissues.

Gestational age	Shortfall of delineated tissue
E6	Reichert's membrane only partly delineated. Mural and polar trophectoderm were delineated as one tissue.
E6.5	Reichert's membrane not delineated.
E7	Conceptus dissected without its mural trophectoderm, parietal endoderm and Reichert's membrane
E7.5	Mural trophectoderm, parietal endoderm and Reichert's membrane and ectoplacental cone were delineated as one segment.

5.3.4.1 Sizes of individual tissues

Tables 5.5a, 5.5b, and 5.5c list relative sizes of individual tissues in the egg cylinders. The tissue sizes are expressed as part of total tissue only. Cavity sizes are expressed as part of the whole conceptus (total tissue plus cavities).

Table 5.5a: Relative volume in % of embryonic tissues in the egg cylinder reconstructions with respect to the total tissue volume.

	E5.5	E6	E6.5	E7[1]	E7.5
visceral endoderm embryonic	15 (21.3)	8.4 (16.2)	8.2 (16.6)	5.68 (12.5)	2.7 (6.6)
epiblast	17 (25.9)	20 (38.8)	17 (34.3) [79.5]	11.9 (26.1) [45.0]	7.9 (19) [30.3]
primitive streak			3.1 (6.4) [14.9]	4.0 (8.8) [15.1]	1.1 (2.6) [4.2]
embryonic mesoderm			0.7 (1.5) [3.48]	6.44 (14.1) [24.36]	7.3 (18) [28.1]
total embryo	32 (46.9)	28.4 (54)	29 (57.8) [97.9]	28 (61.5) [84.5]	19 (39.6) [62.6]

Figure 5.2: Percentage of each tissue group (whole conceptus, ICM (-derivatives) and epiblast (-derivatives) that is situated in embryonic part of conceptus (footnote 1).

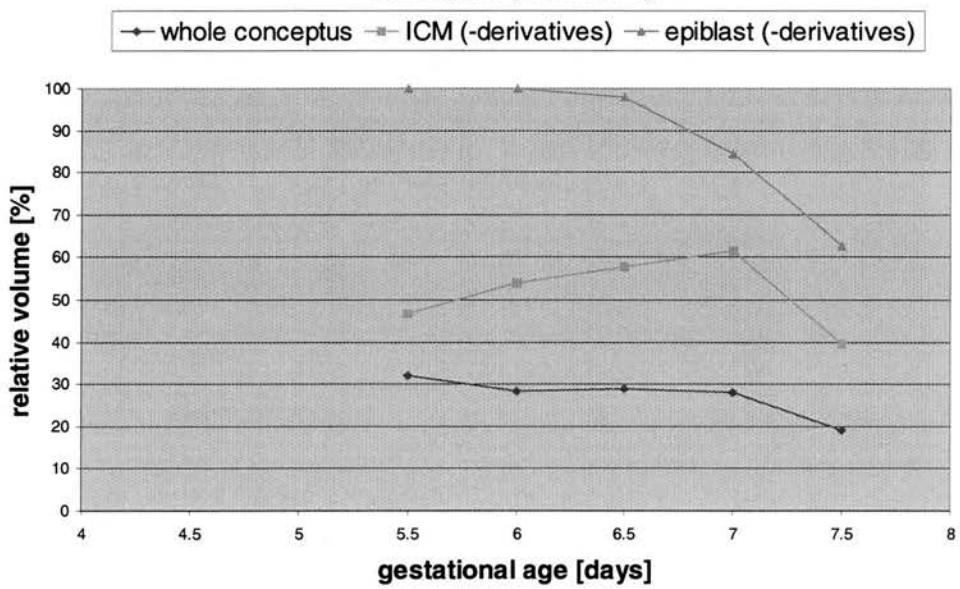

1) E7 contains borrowed values from E6.5 for mural, parietal endoderm, and Reichert's membrane in order to calculate relative tissue sizes.

Figures 5.2 and 5.3 represent the embryonic proportion of each tissue group (whole conceptus, ICM (-derivatives), epiblast (-derivatives). These data can also be found in the bottom row of tables 5.5a and 5.5b.

Round brackets indicate tissue sizes as part of the total of ICM-derivatives. Square brackets are tissue sizes as part of the total of epiblast-derivatives.

Table 5.5b: Relative size of extraembryonic tissues in the egg cylinder reconstructions.

	E5.5	E6	E6.5	E7[1]	E7.5
ectoplacental cone	10	31[2]	39		51.3[3]
mural trophectoderm	3		0.9		
parietal endoderm	6 (8.2)	6.9 (13.2)	4.3 (8.8)		
reichert's membrane	8 (11.1)	0.2 (0.48)			
visceral endoderm-extraembryonic	23 (34.3)	16.3 (31.2)	15.4 (31.5)	11.7 (25.7)	12.0 (29)
extraembryonic ectoderm	19	16	11	9.25	7.9[4]
amnion ectoderm				0.13 (0.28) [0.48]	0.64 (1.5) [2.4]
extraembryonic mesoderm			0.4 (0.91) [2.1]	2.96 (6.5)[5] [14.96]	9.1 (22.3)[6] [35.1]
total extraembryonic tissue	69 (53.6)	70.4 (44.9)	71 (41.2) [2.1]	68.2 (32.5) [15.4]	89.9 (52.8) [37.5]

1) Incorporates borrowed values from E6.5 for mural, parietal endoderm and Reichert's membrane in order to calculate for relative tissue sizes.

2) Value represents sum of mural trophectoderm and ectoplacental cone.

3) Value represents sum of ectoplacental cone, mural trophectoderm, parietal endoderm and Reichert's membrane.

4) Value represents ectoderm of visceral yolk sac and chorion.

5) Value represents extraembryonic mesoderm and mesothelium of posterior amniotic fold.

6) Value represents mesodermal component of visceral yolk sac, allantois, mesodermal component of amnion and chorion.

Figure 5.3: Percentage of each tissue group (whole conceptus, ICM (-derivatives) and epiblast (-derivatives) which is situated in extraembryonic part of conceptus (footnote 1)

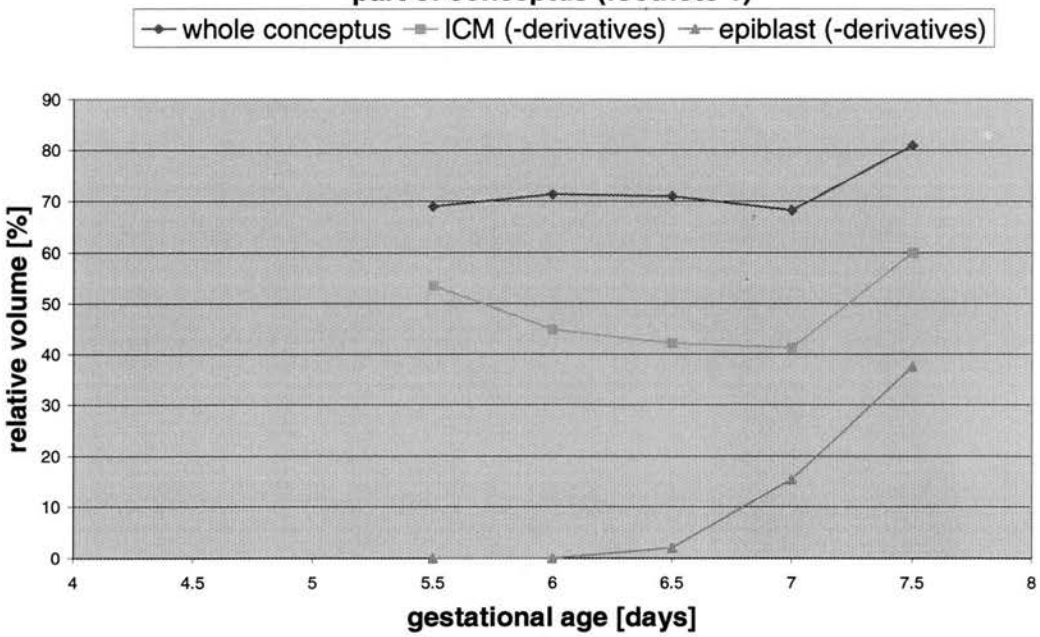

Table 5.5c: Volumes of cavities in the egg cylinder reconstructions relative to the proamniotic cavity at E5.5

	E5.5	E6	E6.5	E7[2]	E7.5
proamniotic cavity	1	2.2	1.9	14.6	
cavity in amniotic fold				1.24	
ectoplacental cavity					1.7
exocoelomic cavity					22.9
amniotic cavity					12.1
total cavity	1	2.2	1.9	15.8	36.7

1) Incorporates borrowed values from E6.5 for mural, parietal endoderm and Reichert's membrane in order to calculate for relative tissue sizes.

2) Value represents sum of mural trophectoderm and ectoplacental cone.

'Growing tissues'

The data in tables 5.5a, 5.5b and 5.5c allow the following conclusions to be drawn: The extraembryonic mesoderm is, in relative terms, the fastest growing ICM-derivative between E6.5 and E7.5 (9%, as part of the whole conceptus). The second fastest growing ICM-derivative is

embryonic mesoderm (7%). Bearing in mind that the size of the ectoplacental cone varies with dissection, the relative size of it increases with age.

'Shrinking tissues' in the embryo

The sum of the epiblast and primitive streak is diminishing relative to the whole conceptus, ICM-derivatives or epiblast-derivatives with the increase in the amount of mesoderm. Both epiblast and primitive streak proportionally increase just after they form, and then decline. There is a gradual decline in the proportion of embryonic visceral endoderm between E5.5 and E7 and then a steep decline between E7.5 and E8 which is when the majority of the visceral endoderm becomes squamous (previously columnar).

'Shrinking tissues' in the extraembryonic region

The proportion of the extraembryonic ectoderm decreases by a factor of two between E5.5 and E7.5. The visceral endoderm in the extraembryonic region as a proportion of the ICM-derivatives is more or less static and halves as part of the whole conceptus in embryos ranging from E5.5-E7.5. All other tissues in the extraembryonic region except for mesoderm and ectoplacental cone proportionally diminish with time.

Extraembryo vs embryo

For all three main tissue groups, at each point of time the majority of the tissue group is in the extraembryonic part of the conceptus.

Cavities

The proamniotic cavity, and its derivatives at E7 and E7.5, expand very rapidly with the accumulation of mesoderm in the embryonic and extraembryonic region.

5.3.4.2 Sizes of tissue groups

Table 5.6 compares relative sizes of lineage groups in the egg cylinders. For brevity 'ICM' in the table refers to ICM and ICM-derivatives. Similarly the term 'trophectoderm' refers to the mural and polar trophectoderm and the extraembryonic ectoderm.

Table 5.6: Tissues from different lineages - relative sizes and increases between stages.

	E5.5	E6	E6.5	E7	E7.5
ICM as part of whole conceptus [%]	68.3	52	49.2	43.8	41.3[5]
epiblast as part of whole conceptus [%]	17.1	20	21.1	26.4	26.1
growth rate since last stage (absolute)		3.1	2.48	3.05	3.58
epiblast derivatives as part of ICM derivatives [%]	25.1	38.8	43.1	58.0	63.1
trophectoderm[4] as part of whole conceptus [%]	32	47	51	51.25	58.9[1]
growth rate since last stage (absolute)	4.1	6.5	3.0	2.57[2]	4.41[3]

1) E7.5 trophectoderm includes parietal endoderm. Estimated component of parietal endoderm in this value: 5-10%.

2) E7 contains E6.5 mural trophectoderm value. Value of E7 trophectoderm therefore probably too low.

3) Value is too high: E7.5 trophectoderm incorporates parietal endoderm and E7 trophectoderm incorporates E6.5 mural trophectoderm.

4) Trophectoderm includes extraembryonic ectoderm.

5) Value for E7.5 ICM-derivatives contains no parietal endoderm.

Whole conceptus

From table 5.6 and figure 5.4 we find, contrary to expectation, that the relative size of ICM and ICM-derivatives with respect to the whole conceptus go down steadily over these stages at approximately 5% per Theiler stage. In contrast the size of the epiblast and derivatives, relative to the whole conceptus, increases in every stage (and much more rapidly when expressed as part of the ICM) with increments in absolute size of around a factor of three. The trophectoderm appears to be the fastest growing tissue component of the conceptus with increments in absolute volume between egg cylinder stages ranging from a factor 3 to 6.

Embryo

Figure 5.5 shows the rapid decrease of the visceral endoderm (the only ICM-derivative that is not an epiblast-derivative) in the embryo. At stage E7.5, hardly more than 10% of the entire embryo consists of visceral endoderm.

Figure 5.4: Contribution of epiblast, other ICM-derivatives and trophectoderm to the whole conceptus E5.5-E7.5 (footnotes 1-4).

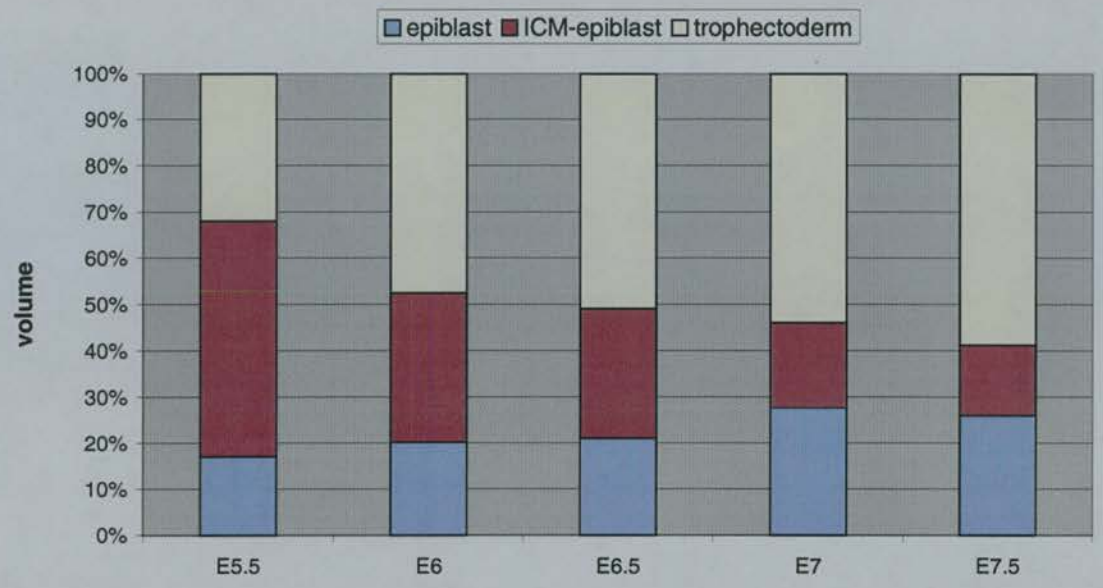

Figure 5.5: Contribution of epiblast- and other ICM-derivatives to the embryonic part of E5.5-E7.5.

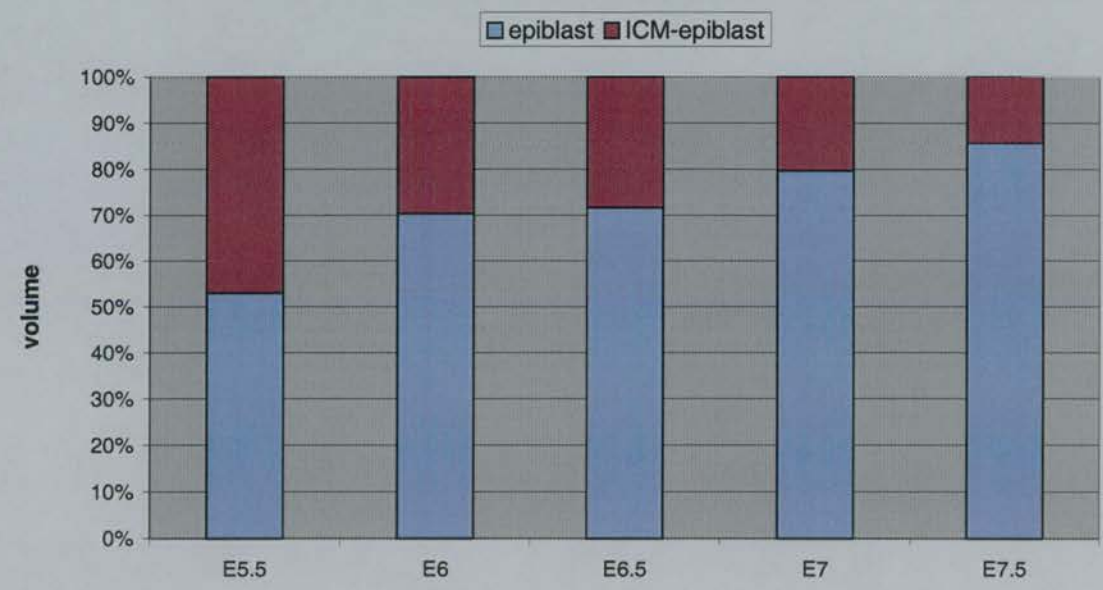

1) E7.5 trophectoderm includes parietal endoderm. Estimated component of parietal endoderm in this value: 5-10%.

2) E7 contains E6.5 mural trophectoderm value. Value of E7 trophectoderm therefore probably too low.

3) Value is too high: E7.5 trophectoderm incorporates parietal endoderm and E7 trophectoderm incorporates E6.5 mural trophectoderm.

4) Trophectoderm includes extraembryonic ectoderm.

5.3.5 Tissue sizes in stages of early organogenesis

The last set of embryos to be investigated comprises the first three stages of organogenesis: E8, E8.5 and E9. There is a rapid increase in the amount of tissues in these stages and it is now possible to investigate the tissue emphasis in this growth. As these embryos were dissected without their surrounding membranes only embryonic tissues can be considered.

In this analysis we first look at relative sizes and growth rates of individual tissues then investigate the distribution of all tissues amongst the three germ layers, again by means of looking at relative volume and growth rates. When tissues were too small or could not sensibly be considered separately, they were clustered together. For example, all vessels were divided into four main groups: left hand veins, left hand arteries, right hand veins and right hand arteries. Gut, surface epithelium, heart, coelom, branchial arches and lateral plate mesenchyme were calculated as single tissues rather than subdivided. This has led to (parts of) several tissues occuring twice in the table so therefore all sizes cannot be added up to the sum of 100%. Footnotes of the tables 5.7a, 5.7b and 5.7c indicate which tissues have been grouped together.

5.3.5.1 sizes of individual tissues

Tables 5.7a, 5.7b, 5.7c and 5.7d list the sizes of individual tissues in the early stages of organogenesis. Tissue sizes are expressed as a percentage of the total tissue. Cavity sizes are expressed as a pecentage of the whole conceptus (total tissue plus cavities). The tables are split in four tissue groups: 1) mesenchyme and somites, 2) cardiovascular system, 3) cavities and 4) other tissues.

Since over 93% of the volume of each of these reconstructions is epiblast-derived volumes were only expressed as part of the whole embryo and not as part of epiblast-derivatives. The only remaining non-epiblast-derived structure is the gut, and by E8, this may have been replaced by cells from the epiblast (Lawson and Pedersen, 1996) however epiblast-derived and primitive endoderm cannot be distinguished in our models. The table also presents growth rates between stages.

Table 5.7a: Relative sizes and growth rates of different parts of mesenchyme in E8-E9

	E8 %	E8.5 %	E9 %	growth rate E7.5-E8	growth rate E8-E8.5	growth rate E8.5-E9
Head somites	2.0	1.0	0.6		0.75	1.38
Body somites	1.1	3.4	3.6		4.91	2.46
Head mesenchyme	17.4	14.8	13.6	11.3[1]	1.30	1.97
Body mesenchyme		0.6	1.2			4.45
Intermediate mesenchyme	0.13	0.65	0.68		7.6	2.26
Lateral plate mesenchyme	2.9	2.7	3.6		1.42	3.14
Paraxial mesenchyme	8.3	5.2	3.1		0.97	1.27
First branchial arch		4.0	4.2			1.9
Second branchial arch			1.0			
Mesothelial lining of intraembryonic coelom	13.5	11.3	8.4		1.29	1.33
Urogenital system			0.21			
Notochord	0.4	0.4	0.3		1.3	1.2

1) Value represents all mesodermal derivatives.

Proportionally increasing mesenchymal structures

About half of the mesenchymal structures get proportionally bigger over the stage range E8-E9 namely: body mesenchyme and somites; intermediate and lateral plate mesenchyme; the branchial arches; and the urogenital system. A few have a very high growth rate namely: body somites, mesenchyme and intermediate mesenchyme. Their high increase is due to segregation from other tissues as well as mitotic growth. The growth rate of 1.4 for the head somites was unexpected. The E8.5 embryo has the same number of head somites as the E9 embryo but one would expect these to have started disintegration and therefore to be smaller by E9. This number is therefore an indication of natural variation in somite volume, in disintegration progress, or shrinkage during processing.

Proportionally decreasing mesenchymal structures

Head somites and head-mesenchyme, notochord, paraxial mesenchyme and mesothelial lining proportionally all decrease over the stage range E8-E9. This is due to low mitotic activity (notochord and mesothelial lining) or disintegration and differentiation. The fact that the paraxial mesenchyme proportionally decreases means that the increase in body somites is higher than the generation of paraxial mesenchyme cells by the primitive streak.

Tissues decreasing in absolute size

Over the stage range E8-E9 the head somites, paraxial mesenchyme and primitive streak all decrease in actual volume. The first two tissues shrink because of differentiation. The evidence here could be consistent with this finding if we assume shrinkage and/or natural variation.

Table 5.7b: Relative sizes and growth rates of the cardiovascular system in E8-9

	E8	E8.5	E9	growth rate E7.5-E8	growth rate E8-E8.5	growth rate E8.5-E9
Vessels left arterial[1]	1.35	3.0	2.8		3.37	1.70
Vessels right arterial[1]	1.68	3.5	2.8		3.21	1.43
Vessels left venous[1]	0.49	0.98	1.3		3.03	2.42
Vessels right venous[1]	0.42	0.97	1.2		3.55	2.21
Heart[1]	5.1	8.2	8.6		2.49	1.87
Septum transversum	0.54	0.46	0.71		1.31	3.34

1) All parts of vascular system include their volume (*i.e.* blood).

Vascular system

The only tissue that has a clear left and right component, the vascular system, does not exhibit a significant volume difference between the left part and right part.

The vascular system is proportionally increasing for all structures over E8-E9 except right - and left hand arteries between E8.5 and E9. This may indicate that the development of the arteries occurs at an earlier age than the development of the drainage.

Segregation or high mitotic speed does not explain the high growth rate in the vascular system. The hollow tubes are formed by cells and the content is blood. This gets formed in the extraembryonic region of the conceptus (blood islands in the visceral yolk sac) and since we have only dissected embryonic parts of

these stages, we cannot trace the nature of the high increase in this system. The main volume of the heart is also blood, with the second major component of cardiac jelly, which consists of very loosely packed mesenchymal cells (Kaufman and Bard, 1999). It is likely therefore that part of the high growth factor of the heart is due to non-mitotic expansion.

Table 5.7c: Relative sizes and growth rates of other tissues in E8-E9

	E8	E8.5	E9	growth rate E7.5-E8	growth rate E8-E8.5	growth rate E8.5-E9
Surface epithelium	9.3	8.8	7.0		1.45	1.43
Future brain	24.9[1]	21.2[1]	12.2	6.28[3]	1.40[2]	1.87[1]
Future spinal cord			5.8			
Optic vesicles		1.5	1.5			1.79
Gut total	6.6	5.7	2.8	3.5	1.32	1.08
Primitive streak	2.1	1.7	0.6	2.8	1.3	0.63

1) Value represents future central nervous system.
2) Value represents future central nervous system plus optic vesicles.
3) Value represents surface epithelium plus neural tissue compared with epiblast of E7.5.

Ectodermally and endodermally derived structures

Proportionally, mesodermally derived structures are increasing in volume at the expense of all ecto- and endodermally derived structures (future brain, future spinal cord and gut).

Biggest and smallest tissue

The biggest single tissue is the future central nervous system, then head mesenchyme and mesothelial lining of intraembryonic coelom. The smallest is the urogenital tissue followed by the notochord.

Table 5.7d: Relative sizes and growth rates of body cavities in E8-E9

	E8	E8.5	E9	growth rate E8-E8.5	growth rate E8.5-E9
Intraembryonic coelom	3.9	6.6	9.0	2.5	2.49

Neural lumen	8.1	6.1	6.3	1.11	1.89
Gut lumen	7.6	4.0	2.7	0.79	1.23

Body cavities

Intraembryonic coelom and neural lumen increase proportionally whereas gut lumen is relatively reduced. This, almost certainly, is the result of mechanical compression or squashing of the gut lumen during the process of turning of the embryo.

5.3.5.2 Sizes and growth rates of germ layers in E6.5-E9.

For this analysis tissues of E6.5-E9 were divided into the descendants of the three germ layers: the endoderm, mesoderm and ectoderm. Embryos younger than E6.5 were omitted from this study since they have no mesoderm. Mesoderm was split in two groups: differentiated and undifferentiated. Undifferentiated includes mesoderm, head mesenchyme, head somites, branchial arch mesenchyme, body mesenchyme, body somites, intermediate mesoderm, lateral plate mesenchyme, paraxial mesenchyme and the mesothelial lining of the intraembryonic coelom. Differentiated mesoderm includes the cardiovascular system, septum transversum, urogenital system and notochord. Ectodermal derivatives include the epiblast, surface epithelium, future brain and spinal cord, optic vesicles, primitive streak. Endodermal derivatives include visceral (embryonic) endoderm and the primitive gut. Sizes are relative to total tissue, apart from undifferentiated mesoderm that is as percentage of total mesoderm.

Table 5.8: Relative sizes of germ layers and absolute tissue increments in embryos stages E8-E9.

	E6.5	**E7**	**E75**	**E8**	**E8.5**	**E9**
endodermal tissues [%]	28.2	20.26	14.40	6.6	5.7	3.43
increment from previous stage	2.29	1.70	1.76	3.50	1.32	1.09
ectodermal tissues [%]	69.2	56.77	47.16	36.3	33.6	31.60

increment from previous stage	2.34	1.95	2.05	5.86	1.42	1.70
mesodermal tissues [%]	2.55	22.97	38.43	57.1	60.7	64.96
increment from previous stage		21.35	4.13	11.33	1.63	1.93
undifferentiated mesoderm [%]	100	100	100	82.41	71.06	71.2
increment from previous stage		21.35	4.13	9.33	1.41	1.82

Tissue gain E7.5-E8

Table 5.8 shows that there is a large increase in embryonic tissue between E7.5 and E8. This increase is mainly taking place in both differentiated and undifferentiated mesodermal tissue.

Figure 5.6: Proportions of endodermally, mesodermally and ectodermally derived tissues in embryos E6.5-E9

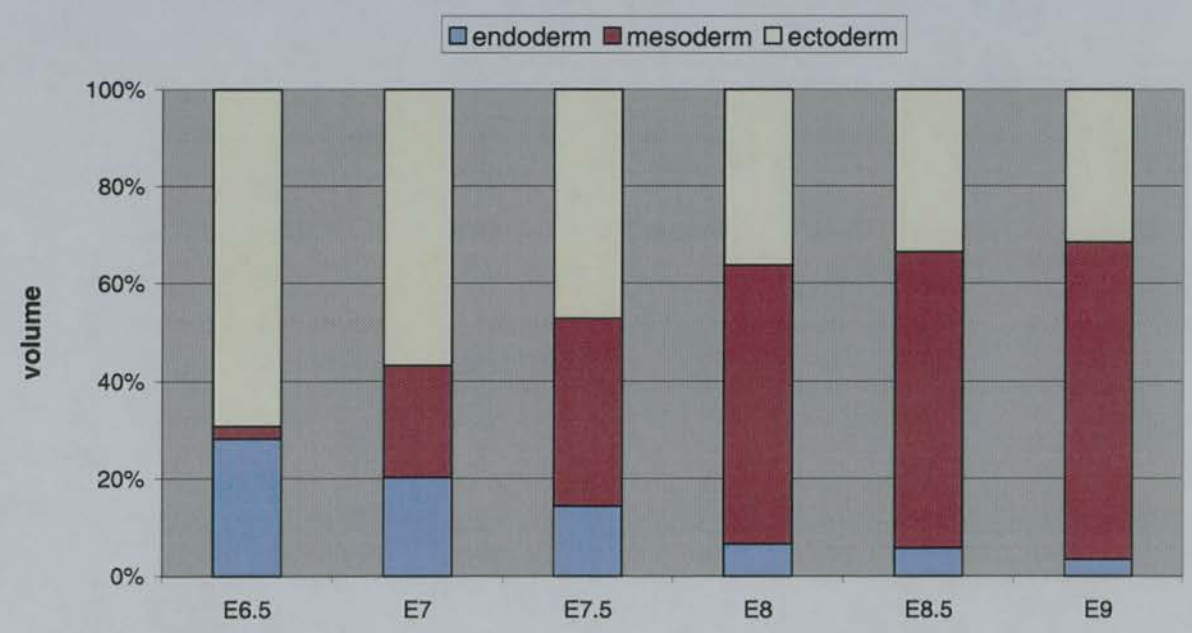

Proportional mesoderm increase

Ectodermal and endodermal tissues decline relatively over the stage range E6.5-E9 at the gain of mesodermal tissues. Mesoderm gain is highest just after the onset of mesoderm formation and this is due to the fact that the mesoderm originates from the primitive streak which has very a high mitotic activity. The proportional increase in mesoderm is non-linear over E6.5-E9 clearly shown in figure 5.6. Although endodermal derivatives have declined to less than 5% at E9, the ectodermal derivatives seem to be levelling out at just above 30% of the total embryo.

Undifferentiated vs. differentiated mesenchyme

From table 5.8 we can also see that over the range E8-E9, the differentiated mesoderm has a higher incremental factor between stages than the undifferentiated mesoderm, although the bulk of mesoderm derived tissue for those stages remains undifferentiated.

5.4 DISCUSSION

5.4.1 Conclusions

In summary the findings of this chapter are:

- A growth spurt occurs simultaneously in ICM - derivatives and trophectoderm
- This period of enhanced growth occurs around implantation
- Least growth in ICM-derivatives after implantation is during organogenesis
- During egg cylinder stages, all tissues shrink proportional to the whole conceptus to the gain of the mesoderm and the ectoplacental cone (the latter shows the fastest growth)
- During organogenesis, embryonic tissues derived from ectoderm and endoderm shrink at the gain of mesodermal structures
- The mesodermal structures, half increase proportionately to the embryo whilst the other half are reduced, mainly due to differentiation
- Of these structures, the majority remains undifferentiated and this part grows faster than the differentiated part
- There is no left-right asymmetry in the sizes of tissues
- During organogenesis, the heart and vascular system are the fastest growing organ system
- In the same stages, the future central nervous system is the single biggest tissue at 20% of the embryo
- The single smallest tissue is the gut at E9 at only 3%
- The study has shown to give reliable results but needs more specimen to strengthen its conclusions and establish variances.

5.4.2 Discussion

5.4.2.1 Enhanced growth rate

An enhanced rate of growth has been detected just after implantation. This spurt occurs throughout the entire conceptus which could indicate that either we have wrongly staged the embryo or are dealing with a large specimen (but within the normal range of variation). The former is unlikely. In the case of the E5.5 embryo it is unlikely, given the small epiblast, proamniotic cavity and ectoplacental cone, to be older (on average) than 5.5 days. What this could indicate (apart from a growth spurt) is the natural variation. Although embryos were selected to be representative of their stage, they were not selected to be of average size. The lessened activity after the onset of organogenesis is most likely due to ongoing differentiation.

McLaren found a growth spurt between E6.5 and E7.5 but uses a different mouse (Q) strain. Snow (1977) reports an increased mitotic rate in the mouse embryo in-between the two growth spurts found in this study: in his study, there is an enhanced growth at the onset of streak formation (approximately E6.5) and organogenesis (approximately E8). If these data are comparable despite the use of different mouse strains, then this means that the increased mitotic rate is not immediately linked to growth. Goedbloed (1976, 1977, 1980) investigated growth rates in mouse embryos unfortunately these are not comparable to our results as the developmental stages were not comparable.

5.4.2.2 Mesoderm vs. endoderm and ectoderm

Perhaps the most striking result is the slow gain in mass from the ectodermally and endodermally derived tissues over E8-E9. This is despite a lessening of the primitive streak (see increase in paraxial mesoderm, table 5.7a). Interesting too is the fact that undifferentiated mesenchyme continues to exhibit the fastest growth. This means that the mitotic rate is higher than the differentiation rate during early organogenesis.

5.4.2.3 Justification

Despite the fact that the size of the ectoplacental cone depends on dissection it was included in this study. The reason is that if the ectoplacental cone was omitted, no study into sizes relative to whole conceptuses could have been done. Although some of the ectoplacental cone may have been omitted during dissection, a bigger amount of ectoplacental cone present in our study probably

invariably means a bigger amount of ectoplacental cone having been present originally, therefore warranting its inclusion in the study.

The largest error in our conclusions arises from natural variation with the possibility that the embryos used for reconstruction are at either end of the size range. Since we only used one embryo per stage this could have a significant effect. Another error might be that tissues shrink differently during processing in embryos from different stages. However, such gross distortions would be visible morphologically and were not found after processing. These considerations could affect the conclusions of the overall growth rates, but the results arising from consideration of proportional volumes and the overall growth rate trends are unaffected.

There are three observations that strengthen this study: The first is the fact that the five non-implanted embryos gave highly consistent results (see table 5.3). The second strength is the earlier studies in processing and reconstruction distortion. Lastly, the fact that embryos were selected to be representative of their stage, which was checked again after reconstruction. For these reasons the study (especially the investigation in volumes proportional the conceptus or embryo, is viable and the conclusions are valid even with only one sample per stage.

5.4.2.4 Future work

Only one embryo was used per Theiler stage. This means that there is no data on natural variance between stages. The most obvious follow-up study is to repeat with more samples per stage, and investigate variance in absolute and relative sizes of tissues. To complete this study, it would be useful to put this variance in the light of developmental progress - are bigger tissues more developmentally advanced? From this study, the answer seems that this is not the case.

Another follow-up study would be to confirm the decelerated growth found in this study around organogenesis. This will have to involve consistent fixatives and will have to be measured over an amount of embryos that is probably too large for this system of measurement and therefore cruder ways will have to be designed to first establish the validity of the trend found here.

In table 5.3, it shows that the blastocoelic cavity lessens after shedding of the zona pellucida. It would be interesting to repeat a few specimens around this stage to see if the cavity is just squashed because the rigid outer shell has gone, or the cavity actually drains out a little perhaps because of a lack of counter pressure from the zona.

More work would be involved to repeat measuring the volumes to check if indeed the development of the arterial system is ahead of the venous system (table 5.7b) in more than one

specimen. Older embryos will have more paired organs and it would be worth checking for lateral asymmetry in developmental progress in more systems than was possible in this study.

CHAPTER 6: CONCLUSIONS AND DISCUSSION

6.1 CONCLUSIONS SUMMARY

This thesis set out to add to the existing description of E1-E9 mouse developmental anatomy via the use of computer-generated reconstructions of serial sections of 13 mouse embryos in this age range. The histological reconstructions include all tissue delineations of the major anatomical features characteristic of their developmental stages and can be sectioned at any arbitrary angle to match the required view. The histological views including transparent anatomical overlays, 3D surface renderings of isolated or combined tissues and all segmented anatomy have been used to assess the standard literature on developmental anatomy, the internal and external morphology during the process of 'turning' and the emphases of growth of individual tissues during these stages. Conclusions from each of the results chapters have been discussed already, in this chapter the conclusions are summarized in "bullet point" form.

6.1.1 Comparison of the reconstructions to anatomy literature

Thirteen reconstructions including their delineated anatomy ranging from E1-E9 were compared to the standard literature on mouse developmental anatomy and the results of this comparison demonstrated a considerable amount of disagreement with the literature, the most important points of which are summarised below:

- the two blastocysts used for this study (E3 and E4) can not be matched consistently to Nadijcka *et al.*'s (1974) developmental staging system,

- Gardner *et al.*'s (1992) observations of asymmetries in the blastocysts and egg cylinders are not confirmed for 4 out of 7 embryos,

- Smith's (1980,1985) reported asymmetries in blastocysts and egg cylinders are not detectable here for 6 embryos and in the 7th embryo very small effects.

- Tam's (1981) measurements of the length of the primitive streak are not consistent with this study and appear to be one day "out of sync".

- The looping of the heart seems to occur before the segmentation of the heart, in contrast to the claim of Kaufman and Bard (1999).

- The internal carotid artery was observed at E8, rather than at E10 (Kaufman and Bard, 1999).

- Mouse development is not as parallel to rat development as is usually claimed: the internal organisation at midgut-level (Godlewski *et al.*, 1992) and the development of the hindbrain (Adelmann, 1925) are different.

6.1.2 Conclusions on the process of turning

Three embryo reconstructions (E8, E8.5 and E9) were used to study the internal and external anatomy during the process in which the mouse embryo inverses its germ layers. The conclusions in summary are:

- The mouse embryo 'turns' between E8-E9.5 by turning it dorsal side to its left.
- The process of turning initiates at the head and tail end of the embryo and progresses towards the mid-trunk area.
- The process of turning is not finished by E9.
- There is no apparent mechanical relation between the looping of the heart and the process of turning.
- The process of 'turning' appears as a global process throughout the entire rather than driven by a few tissues. A possible exception to this is suggested by a shortened left splanchnopleure during the process.

6.1.3 Tissue volumes

The delineated anatomy in all 13 reconstructions of embryos ranging from E1-E9 was used to assess growth emphasis during this developmental age range.

- A period of enhanced growth rate or "spurt" occurs simultaneously in ICM - derivatives and trophectoderm at the blastocysts and egg cylinder stages
- This spurt occurs around implantation.
- Growth in ICM-derivatives after implantation is slowest during organogenesis.
- During egg cylinder stages, all tissues shrink relative to the whole conceptus except the mesoderm and the ectoplacental cone (the latter is the fastest grower).

- During organogenesis, embryonic tissues derived from ectoderm and endoderm shrink allometrically to the gain of mesodermal structures.

- Of the mesodermal structures, roughly half increase allometrically while the remainder lessen, primarily due to differentiation.

- There is left-right symmetry in the sizes of paired tissues.

- During organogenesis, the heart and vascular system are the fastest growing organ system.

- During organogenesis, the future central nervous system is the biggest tissue and comprises 20% of the embryo.

- The smallest tissue at E9 is the gut at only 3% of the volume.

6.2 DISCUSSION

6.2.1 Drawbacks

Although the system used in this thesis for exploring early mouse developmental anatomy has proven a very useful resource, it has some drawbacks, of which the most important is that only one embryo was used per Theiler stage. An additional problem is that no studies have been published on the variation amongst embryos of similar developmental stages. However, the embryos in this study were selected to be representative of their Theiler stage. Studies have been done on the amount of shrinkage during processing which is approximately 10% by length for embryos in the range studied here.

Another drawback is that the histological staining, haematoxylin and eosin for the E8.5 and E9 embryos and toluidine blue staining for the remaining embryos, does not reveal all the anatomical structures that could be delineated. This would add more detail which may be of interest, especially for tracking the onset of subtle abnormalities and mutations.

A limitation rather than a drawback of these models is that it has proven not possible to discern fine histological detail such as mitotic figures, or slight variations in individual cell sizes, even when the bigger cells are at the edge of the reconstruction. These data however, could be added from additional research to the reconstructions since they form part of a database.

Although during the process of delineation of the anatomy the general aim was to only label what could be distinguished by looking down the microscope, necessarily some "arbitrary" decisions had to be made on the tissue. For example, although there was no clear morphological distinction between the mesothelial lining of the pericardiac cavity and myocardium, a decision was made in order to delineate the myocardium (see appendix 2).

6.2.1 Strengths

In this thesis, the advantages of the used system have proven to be many. The ability to browse through the reconstruction with the delineated anatomy displayed as transparent overlays at any arbitrary angle, facilitates a simultaneous comprehension of more anatomical processes including their histological detail (within the range of resolution as described above) than has hitherto been possible. The 3D views of surface rendered individual or combined anatomical detail are particularly helpful in displaying topological relationships and proportional sizes of components.

It has proven possible using these reconstructions to critically analyse the standard literature on mouse developmental anatomy. This would not have been as straightforward using any other method of reconstruction, since it has proven valuable to be able to refer back to the histology underlying the 3D views. The process of 'turning' in the mouse has been described using the 3D views of various tissues accounting for detailed internal anatomical relationships in a way that would have been simply impossible without the method of reconstruction.

For the first time, there has been the opportunity to look at sizes of individual tissues, facilitated by the delineation of all anatomy in each of the 13 reconstructions ranging from E1-E9. Because the anatomy was segmented as volumes, it was a simple step to convert these segments into tissue sizes and this has offered a first-time and valuable look at growth emphasis during this age range, considered the limitations about variance as described above.

6.2.3 General context

Thankfully these reconstructions including the delineated anatomy will not die a slow death in this thesis that hardly anybody will ever read, but they are part of a database that is publicly accessible. When fully operable, this database will hold spatial data not only on gene-expression but on all developmental aspects of the embryos. This is particularly valuable to the developmental biologist because experimental data typically do not adhere to exact tissue boundaries and therefore, to be able to view these data in three dimensions against the histological background will be of invaluable importance.

Besides the use of the reconstructions in holding and displaying data from experiments, the reconstructions will provide a useful teaching aid for the researcher trying to locate his or her data, the student trying to comprehend tissue relationships during development or indeed anybody wishing to understand mouse development. This function is of critical importance for two reasons. First, there seems little likelihood that sufficient numbers of individuals will ever be available who are capable of interpreting the histological material from which the gene-expression data must be delineated. Second, textbooks of embryology can only provide standard views whereas the interactive computer-aided methodology described here allow the user to explore the exact anatomical details in planes and volumes that mesh with their work.

6.2.4 Future work

The most serious limitation of these reconstructions is the lack of data on variance and hence the inability to know how representative these reconstructions are. This has to be complemented by research on variation in embryos of this age range, and I propose this to be done by cutting representative sections of sufficient similarly staged embryos. The reconstructions can be sectioned arbitrarily to fit the angle of the sections, after which it is feasible to make an analysis of shape and size variance.

A second requirement is the further assessment of arbitrary boundaries by gene-expression or immunohistochemistry studies. This would hopefully solidify, amend, or add to, boundaries that have been made on arbitrary grounds and so make the anatomical models more valuable.

6.2.1 Concluding remark

The system presented in this study has not only contributed to the existing knowledge about mouse developmental anatomy but also forms an easily accessible resource since the reconstructions plus delineated anatomy are publicly available. Hopefully this will make accessible detailed and standardised anatomical definitions which will help a broad range of researchers to use a common spatial and ontological framework which in turn may form a fertile ground for many inspirational thoughts and collaborations. It is hoped that these reconstructions including their anatomy and nomenclature will to some extent satisfy an expressed requirement (Anderson, 1996, Anderson and Brown, 1996) for a standard embryo description.

REFERENCES

Adachi, H., Saijoh, Y., Mochida, K., Ohishi, S., Hashiguchi, H., Hirao, A., Hamada, H. (1999). Determination of left/right asymmetric expression of nodal by a left side-specific enhancer with sequence similarity to a lefty-2 enhancer. *Genes Dev.* **13(12)**, 1589-600.

Adelmann, H.B. (1925). The development of the neural folds and cranial ganglia of the rat. *J. Comp. Neur.* **39**, 19-171.

Allan, L.D., Santos, R. & Pexieder, T. (1997). Anatomical and echocardiographic correlates of normal cardiac morphology in the late first trimester fetus. *Heart,* **77**, 68-72.

Anderson, R.H. (1996). How should we optimally describe complex congenitally malformed hearts?. *Ann. Thor. Sur.* **62**, 710-716.

Anderson, R.H. & Brown, N.A. (1996). The anatomy of the heart revisited. *Anat. Rec.* **246**, 1-7.

Anderson, R.H., Webb, S. & Brown, N.A. (1996). Establishing the anatomic hallmarks of congenitally malformed hearts. *Tr. Cardiovasc. Med.* **6**, 10-15.

Argao, E.A., Kern, M.J., Branford, W.W., Scott, W.J. jr. and Potter, S.S. (1995). Malformations of the heart, kidney, palate, and skeleton in alpha-MHC-Hoxb-7 transgenic mice. *Mech. Dev.* **52**; **2-3**, 291-303.

Baldock, R., Bard, J., Kaufman, M.H. and Davidson, D. (1992). A real mouse for your computer. *Bioessays*, **14**, 501-502.

Baldock, R., Bard, J., Brune, R., Hill, B., Kaufman, M.H., Opstad, K., Smith, D., Stark, M., Waterhouse, A., Yang, Y. and Davidson, D. (2001). The Edinburgh Mouse Atlas: Using the CD. *Brief. In Bioinf.* **2**, 159-169.

Bard, J.B.L., Kaufman, M.H., Dubreuil, C., Brune, R.M., Burger, A., Baldock, R. and Davidson, D. (1998). An internet-accessible database of mouse developmental anatomy based on a systematic nomenclature. *Mech. Dev.* **74**, 111-120.

Beddington, R.S.P. (1994). Induction of a second neural axis by the mouse node. *Development*, **120**, 613-620.

Beddington, R.S.P. & Robertson, E.J. (1998). Anterior patterning in mouse. *Trends in Genetics.* **14(7)**, 277-284.

Bellomo, D., Lander, A., Harragan, I. & Brown, N.A. (1996). Cell proliferation in mammalian gastrulation: the ventral node and notochord are relatively quiescent. *Developmental Dynamics*. **205**, 471-485.

Belo, J.A., Bouwmeester, T., Leyns, L., Kertesz, N., Gallo, M., Follettie, M. & De Robertis, E.M. (1997). Cerberus-like is a secreted factor with neuralizing activity expressed in the anterior primitive endoderm of the mouse gastrula. *Mechanisms of Development*, **68**, 45-57.

Biben, C., Stanley, E., Fabri, L., Kotecha, S., Rhinn, M., Drinkwater, C., Lah, M., Wang, C-C., Nash, A., Hilton, d., Ang, S-L., Mohun, T. & Harvey, R.P. (1998). Murine Cerberus homologue mCer-1: A candidate anterior patterning molecule. *Developmental Biology*, **194**, 135-151.

Bodmer, R. (1995). Heart development in Drosophila and its relationship to vertebrates. *Tr. Cardiovasc. Med.* **5**, 21-28.

Breier, G., Breviario, F., Caveda, L., Berthier, R., Schnurch, H., Gotsch, U., Vestweber, D., Risau, W. and Dejana, E. (1996). Molecular cloning and expression of murine vascular endothelial-cadherin in early stage development of cardiovascular system. *Blood* **87**; **2**, 630-641.

Broekhuizen, M.L.A., Bouman, H.G.A., Mast, F., Mulder, P.G.H., Gittenberger-De Groot, A.C. & Wladimiroff, J.W. (1995). Haemodynamic changes in HH stage 34 chick embryos after treatment with all- trans-retinoic acid. *Ped. Res.* **38**, 342-348.

Brown, N., Hoyle, C.I., McCarthy, A. and Wolpert, L. (1989). The development of asymmetry: the sidedness of drug-induced limb abnormalities is reversed in situs inversus mice. *Dev.* **107**, 637-642.

Brown, N. and Wolpert, L. (1990). The development of handedness in left/right asymmetry. *Dev.* **109**, 1-9.

Brueckner, M., D'Eustachio, P. and Horwich, A.L. (1989). Linkage mapping of a mouse gene, *iv*, that controls left-right asymmetry of the heart and viscera. *Gen.* **86**, 5035-5038.

Brune, R.M., Bard, J.B.L., Dubreuil, C., Guest, E., Hill, W., Kaufman, M.H. Stark, M., Davidson, D. and Baldock, R.A. (1999). A three-dimensional model of the mouse at embryonic day 9. *Dev. Biol.*, **216**, 457-468.

Brutsaert, D.L., De, Keulenaer, G.W., Fransen, P., Mohan, P., Kaluza, G.L., Andries, L.J., Rouleau, J.L. & Sys, S.U. (1996). The cardiac endothelium: Functional morphology, development, and physiology. *Progr. Cardiovasc. Dis.* **39**, 239-262.

Burn, J. and Goodship, J. (1996). Developmental genetics of the heart. *Curr. Op. Gen. Dev.* **6**, 322-326.

Campbell, K.A. & Hutchins, G.M. (1995). Outflow tract abnormalities in atrioventricular canal malformations. *Ped. Path. Lab. Med.* **15**, 11-21.

Chang, H., Huylebroeck, D., Verschueren, K., Guo, Q., Matzuk, M.M., Zwijsen, A. (1999). Smad5 knockout mice die at mid-gestation due to multiple embryonic and extraembryonic defects. *Dev.* **126(8)**, 1631-42.

Chang, H., Zwijsen, A., Vogel, H., Huylebroeck, D., Matzuk, M.M. (2000). Smad5 is essential for left-right asymmetry in mice. *Dev. Biol.*, **219(1)**, 71-78.

Clark, E.B., Rooney, P.R., Martini, D.R. and Rosenquist, G.L. (1979). Plastic casts of embryonic respiratory and cardiovascular system: a technique. *Ter.* **19(3)**, 357-360.

Cole, R.J. (1967). Cinemicrographic observations on the trophoblast and zona pellucida of the mouse blastocyst. *J. Emb. Exp. Morph.* **17**, 481-490.

Collignon, J., Varlet, I. and Robertson, E.J. (1996). Relationship between asymmetric *nodal* expression and the direction of embryonic turning. *Nature* **381**, 155-158.

Constam, D.B., Robertson, E.J. (2000). Tissue-specific requirements for the proprotein convertase furin/SPC1 during embryonic turning and heart looping. *Dev.* **127(2)**, 245-254.

Copp, A.J. (1978). Interaction between inner cell mass and trophectoderm of the mouse blastocyst. I. A study of cellular proliferation. *J. Embryol. Exp. Morph.* **48**, 109-125.

Copp, A.J. (1981). The mechansism of mouse egg-cylinder morphogenesis in vitro. *J. Embryol. Exp. Morph.* **61**, 277-287.

Coucouvanis, E. & Martin, G.R. (1995). Signals for death and survival: A two-step mechanism for cavitation in the vertebrate embryo. *Cell.* **83**, 279-287.

Coucouvanis, E. & Martin, G.R. (1999). BMP signalling plays a role in visceral endoderm differentiation and cavitation in the early mouse embryo. *Development.* **126**, 535-546.

Coulombre, A.J. and Coulombre, J. (1958). The role of mechanical factors in brain morphogenesis. *Anat. Rec.* **130**, 289-290.

David, K.M., McLachlan, J.C., Aiton, J.F., Whiten, S.C., Smart, S.S., Thorogood, P.V. and Crockard, H.A. (1998). Cartilaginous development of the human

craniovertebral junction as visualised by a new three-dimensional computer reconstruction technique. *J. Anat.* **192**, 269-277.

Davidson, D., Bard, J., Brune, R., Burger, A., Dubreuil, C., Hill, W., Kaufman, M., Quinn, J., Stark, M. and Baldock, R. (1997). The mouse atlas and graphical gene-expression database. **8**, 509-517.

Davis, C.L. (1927). Development of the human heart from its first appearance to the stage found in embryos of 20 pairs of somites. *Contrib. Embryol. Carnegie Inst.* **19**, 245-284.

Deuchar, E.M. (1971). The mechanism of axial rotation in the rat embryo: an experimental study *in vitro*. *J. Embryol. Exp. Morph.* **25**, 189-201.

Dickson, A.D. (1966). The form of the mouse blastocyst. *J. Anat.* **100**, 335-348.

Ducibella, T. (1997). Surface changes of the developing trophoblast cell. In: Development in mammals, ed. M.H. Johnson. Amsterdam: North-Holland.

Dunwoodie, S.L., Rodriguez, T.A. & Beddington, R.S.P. (1998). Msg1 and Mrg1, founding members of a gene family, show distinct patterns of gene expression during mouse embryogenesis. *Mechanisms of Development.* **72**, 27-40.

Dziadek, M. (1979). Cell differentiation in isolated inner cell masses of mouse blastocysts *in vitro*: onset of specific gene-expression. *J. Embryol.Exp. Morpol.* **53**, 367-379.

Gardner, R. and Papaioannou, V.E. (1975). Differentiation in the trophectoderm and inner cell mass. In: the early development of mammals, eds. M. Balls and A.E. Wild. Cambrdige: Cambridge University Press.

Effman, E.L. (1982). Development of the right and left pulmonary arteries. A microangiographic study in the mouse. *Invest. Radiol.* **17**, 529-538.

Eisenberg, C.A. & Bader, D.M. (1996). Establishment of the mesodermal cell line QCE-6: A model system for cardiac cell differentiation. *Circ. Res.* **78**, 205-216.

Ellington, S.K. (1985). A morphological study of the development of the allantois of rat embryos *in vivo*. *J. Anat.* **142**, 1-11.

Ellington, S.K. (1987). A morphological study of the development of the chorion of rat embryos. *J. Anat.* **150**, 247-263.

Enders, A.C. and Schlafke, S.J. (1965). The fine structure of the blastocyst: some comparative studies. In: Preimplantation stages of pregnancy.: A CIBA

Foundation symposium, ed. G.E.W. Wolstenholme and M. O'Connor. London: J. and A. Churchill.

Fishmen, M.C. and Chien, K.R. (1997). Fashioning the vertebrate heart: earliest embryonic decisions. *Dev.* **124**, 2099-117.

Fraser, S., Keynes, R. and Lumsden, A.(1990). Segmentation in the chick embryo hindbrain is defined by cell lineage restrictions. *Nature* **344**, 431-435.

Gardner, R.L. (1972). An investigation of inner cell mass and trophoblast tissues following their isolation from the mouse blastocyst. *J. Embryol. Exp. Morph.* **28, 2**, 279-312.

Gardner, R.L. (1978). Lineage analysis of inner cell mass and trophectoderm using microsurgically reconstituted mouse blastocysts. *J. Embryol. Exp. Morphol.* **68**,199-209.

Gardner, R.L. (1982). Investigation of cell lineage and differentiation in the extraembryonic endoderm of the mouse embryo. *J. Embryol. Exp. Morph.* **68**, 175-198.

Gardner, R.L. (1984). An *In situ* cell marker for clonal analysis of the development of the extraembryonic endoderm in the mouse. *J. Embryol. Exp. Morph.* **80**, 251-288.

Gardner, R.L. (1997). The early blastocyst is bilaterally symmetrical and its axis of symmetry is aligned with the animal-vegetal axis of the zygote in the mouse. *Development.* **124**, 289-301.

Gardner, R.L., Papaioannou, V.E. & Barton, S.C. (1973). Origin of the ectoplacental cone and secondary giant cells in mouse blastocysts reconstituted from isolated trophoblast and inner cell mass. *J. Embryol. Exp. Morph.* **30, 3**, 561-572.

Gardner, R.L., Meredith, M.R. & Altman, D.G. (1992). Is the anterior-posterior axis specified before implantation in the mouse? *J. Exp. Zool.* **264**, 437-443.

Ginsburg, M., Snow, M.H.L. & McLaren, A. (1990). Primordial germ cells in the mouse during gastrulation. *Dev.* **110**, 521-528.

Godlewski, G., Gaubert-Cristol, R. and Rouy, S. (1992). Liver development in rats during the embryonic period (Carnegie stages 11-14). *Acta Anat.* **144(1)**, 45-50.

Goedbloed, J.F. (1976). Embryonic and postnatal growth of the rat and mouse. IV.

Prenatal growth of organs and tissues: age determination, and general growth pattern. *Acta Anat.* **95**, 8-33.

Goedbloed, J.F. (1977). Embryonic and postnatal growth of the rat and mouse. V. Prenatal growth of organs and tissues, general principles: allometric growth, absence of growth, and the genetic regulation of the growth process. *Acta Anat.* **98**, 162-182.

Goedbloed, J.F. (1980). Embryonic and postnatal growth of the rat and mouse. VI. Prenatal growth of organs and tissues: individual organs; final remarks on parts I-VI, phase transitions. *Acta Anat.* **106**, 108-128.

Goss, C.M. (1938). The first contractions in the heart of rat embryos. *Anat. Rec.* **70**, 505-524.

Gupta, M., Gulamhusein, A.P. and Beck, F. (1982). Morphometric analysis of the visceral yolk sac endoderm in the rat *in vivo* and *in vitro. J. Reprod. Fert.* ***65,*** 39-245.

Halpern, M.N. (1953). The azygos vein system in the rat. *Anat. Rec.* **116**, 83-93.

Hamilton, W.J. and Mossman, H.W. (1972). Hamilton, Boyd and Mossman's human embryology. Prenatal Development of form and function, 4th edn. Cambridge: W. Heffer and Sons Ltd.

Harary, I. And Farley, B. (1963). *In vitro* studies on single beating rat heart cells II. Intercellular communication. *Exp. Cell. Res.* **29**, 466-474.

Henkemeyer, M., Rossi, D.J., Holmyard, D.P., Puri, M.C., Mbamalu,G., Harpal, K., Shih, T.S., Jacks, T. and Pawson, T. (1995). Vascular system defects and neuronal apoptosis in mice lacking Ras GTP-ase activating protein. *Nature* **377**; **6551**, 695-701.

Heyer, J., Escalante-Alcalde, D., Lia, M., Boettinger, E., Edelmann, W., Stewart, C.L. and Kucherlapati, R. (1999). Postgastrulation Smad2-deficient mouse embryos show defects in embryo turning and anterior morphogenesis. *Proc. Natl. Acad. Sci. U.S.A.* **96(22)**, 12595-12600.

Hiruma, T. and Hirakow, R. (1989). Epicardial formation in embryonic chick heart: computer-aided reconstruction, scanning, and transmission electron microscopic studies. *Am. J. Anat.* **184**, 129-138.

Hogan, B.L. and Tilly, M. (1981). Cell interactions and endoderm differentiation in cultured mouse embryos. *J. Embryol. Exp. Morphol.* **62**, 379-94.

Hogan, B.L.M. & Newman, R. (1984). Scanning electron microscope study of the extraembryonic endoderm of the 8th-day mouse embryo. *Diff.* **26**, 138-143.

Holland, P.W.H. and Hogan, B.L.M. (1988). Spatially restricted patterns of expression of the homeobox-containing gene *Hox 2.1* during mouse embryogenesis. *Dev.* **102**, 159-174.

Hummel, K.P. and Chapman, D.P. (1959). Visceral inversion and associated anomalies in the mouse. *J. Her.* **50**, 9-13.

Ingalls, H.W. (1921). A human embryo at the beginning of segmentation, with special reference to the vascular system. *Contrib. Embryol. Carnegie Ins.* **11**, 61-90.

Ito, H., Iwasaki, K., Ikeda, T., Saka, H., Shimokawa, I. And Matsuo, T. (1992). HNK-1 expression pattern in normal and bis-diamine induced malformed developing rat heart: three dimensional reconstruction analysis using computer graphics. *Anat. Embryol.* **186**, 327-334.

Jackson, M., Connell, M.G., Smith, A., Drury, J. & Anderson, R.H. (1995). Common arterial trunk and pulmonary atresia: Close developmental cousins? Results from a teratogen induced animal model. *Cardiovasc. Res.* **30**, 992-1000.

Jacobson, A.G. and Tam, P.P.L. (1982). Cephalic neurulation in the mouse embryo analyzed by SEM and morphometry. *Anat. Rec.* **203**, 375-396.

Johnson, M.H. and Ziomek, C.A. (1981). the foundation of two distinct cell lineages within the mouse morula. *Cell* **24**, 71-80.

Jurand, A. (1974). Some aspects of the development of the notochord in mouse embryos. *J. Embryol. Exp. Morph.* **32 (1)**, 1-33.

Jurand, A. (1962). The development of the notochord in chick embryos. *J. Embryol. Exp. Morph.* **10 (4)**, 602-621.

Kaufman, M.H. (1979). Cephalic neurulation and optic vesicle formation in the mouse embryo. *Am. J. Anat.* **155**, 425-444.

Kaufman, M.H. and Navaratnam, V. (1980). Early differentiation of the heart in mouse embryos. *J. Anat.* **133**, 235-246.

Kaufman, M.H. (1983). The origin, properties and fate of trophoblast in the mouse. In: Biology of trophoblast, eds. Y.W. Loke and A. Whyte. Amsterdam: Elsevier/North Holland Biomedical Press.

Kaufman, M.H. (1986). Occlusion of the neural lumen in early mouse embryos

analysed by light and electron microscopy. *J. Embryol. Exp. Morph.* **78**, 211-228.

Kaufman, M.H. (1984). A re-evaluation of the morphology and function of the yolk sac in the primitive streak stage mouse embryo. *J. Anat.* **139**, 730-731.

Kaufman, M.H. (1992). Postcranial morphological features of homozygous tetraploid mouse embryos. *J. Anat.* **180**, 521-534.

Kaufman, M.H. (1992). The atlas of mouse development. Academic Press.

Kaufman, M.H., Brune, R., Baldock, R., Bard, J.B.L. and Davidson, D. (1997). Computer-aided 3D reconstruction of serially sectioned mouse embryos: its use in integrating anatomical organization. *Int. J. Dev. Biol.* **41**, 223-233.

Kaufman, M.H., Brune, R., Davidson, D. and Baldock, R., (1998). Computer-generated three-dimensional reconstructions of serially sectioned mouse embryos. *J. Anat.* **193**, 323-336.

Kaufman, M.H. and Bard, J.B.L. (1999). The anatomical basis of mouse development. Academic Press.

Kitchiner, D., Jackson, M., Malaiya, N., Walsh, K., Peart, I., Arnold, R. and Smith, A. (1994). Morphology of the left ventricular outflow tract structures in patients with subaortic stenosis and a ventricular septal defect. *Br. Heart J.* **72**; **3**, 251-260.

Klar, A.J.S. (1994). A model for specification of the left-right axis in vertebrates. *TIG.* **10(11)** 392-396.

Kosaki, K., Bassi, M.T., Kosaki, R., Lewin, M., Belmont, J., Schauer, G., Casey, B. (1999). Characterization and mutation analysis of human LEFTY A and LEFTY B, homologues of murine genes implicated in left-right axis development. *Am. J. Hum. Genet.* **64(3)**, 712-21.

Kurihara, Y., Kurihara, H., Oda, H., Maemura, K., Nagai, R., Ishikawa, T.and Yazaki, Y. (1995). Aortic arch malformations and ventricular septal defect in mice deficient in endothelin-1. *J. Clin. Inv.* **96**; **1**, 293-300.

Lamers, W.H., Spliet, W.G.M. and Langemeier, R.A.T.M. (1987). The lining of the gut in the developing rat embryo. *Anat. Embryol.* **176**, 259-265.

Lawson, K.A., Menesen, J.A. & Pedersen, R.A. (1986). Cell fate and cell lineage in the endoderm of the presomite mouse embryo, studied with an intracellular tracer. *Dev. Biol.* **115**, 325-339.

Lawson, K.A. & Pedersen, R.A. (1987). Cell fate, morphogenetic movement and population kinetics of embryonic endoderm at the time of germ layer formation in the mouse. *Dev.* 101, 627-652.

Layton, W.M. Jr. (1976). Random determination of a developmental process. *J. Her.* **67**, 336-338.

LeFurgey, A., Ingram, P., Henry, S.C., Murphy, E. and Lieberman, M. (1983). Three dimensional configuration of the mitochondria in cultured heart cells. *Scan. Electron. Micr.* 293-303.

Lehtonen, E., Lehto, V.-P., Paasivuo, R. & Virtanen, I. (1983). Parietal and visceral endoderm differ in their expression of intermediate filaments. *EMBO J.* **2(7)**, 1023-1028.

Leivo, I., Vaheri, A., Timpl, R. & Wartiovaara, J. (1980). Appearance and distribution of collagens and laminin in the early mouse embryo. *Dev. Biol.* **76**, 100-114.

Lemanski, L.F. La, France, S.M., ErginelUnaltuna, N., Luque, E.A., Ward, S.M., Fransen, M.E., Mangiacapra, F.J., Nakatsugawa, M., Lemanski, S.L., Capone, R.B., Goggins, KJ, Nash, B.P., Bhatia, R., Dube, A., Gaur, A., Zajdel, R.W., Zhu, Y., Spinner, B.J. & Pietras, K.M. (1995). The cardiac mutant gene c in axolotls: Cellular, developmental,and molecular studies. *Cell. Mol. Biol. Res.* **41**, 293-305.

Lin, I.E. & Taber, L.A. (1994). Mechanical effects of looping in the embryonic chick heart. *J. of Biomech.* **27**, 311-321.

Lowe, L.A., Supp, D.M., Sampath, K., Yokoyama, T., Wright, C.V.E., Potter, S.S., Overbeek, P. & Kuehn, M.R. (1996). Conserved left-right asymmetry of *nodal* expression and alterations in murine *situs inversus. Nature*, **381**, 158-161.

Lumsden, A. and Wilkinson, D. (1990). The promise of gene ablation. *Nature,* **347**, 335-336.

McLaren, A. (1976). Growth from fertilization to birth in the mouse. *In* Embryogenesis in Mammals. CIBA Symposium Vol 40 (new series), Ed. McLaren, A. (Elsevier, Excerpta Medica, North-Holland, Amsterdam) 47-51.

Manasek, F.J. and Monroe, R.G. (1972) Early cardiac morphogenesis is independent of function. *Dev. Biol.* 27, 584-588.

Manasek, F.J., Burnside, M.B. and Waterman, R.E. (1972). Myocardial cell shape change as a mechanism of embryonic heart looping. *Dev. Biol.* **29**, 349-371.

Manning, A. and McLachlan, J.C. (1990). Looping of chick embryo hearts *in vitro*. *J. Anat.* **168**, 257-263.

Meier, S. (1984). Somite formation and its relationship to metameric patterning of the mesoderm. *Cell Diff.* **14(4)**, 235-243.

Meier, S. and Tam, P.P.L. (1982). Metameric pattern development in the embryonic axis of the mouse. I. Differentiation of the cranial segments. *Differentiation,* **21**, 95-108.

Melloy, P.G., Ewart, J.L., Desmond, M.E. and Lo, C.W. (1996). *No Turning*, a novel mutation causing laterality defects in mouse embryos. *Dev. Biol.* **175**, 72.

Melloy, P.G., Ewart, J.L., Cohen, M.F., Desmond, M.E., Kuehn, M.R. and Lo, CW. (1998). *No turning*, a mouse mutation causing left-right and axial patterning defects. *Dev. Biol.*, **193(1)**, 77-89.

Mochizuki, T., Saijoh, Y., Tsuchiya, K., Shirayoshi, Y., Takai, S., Taya, C., Yonekawa, H., Yamada, K., Nihei, H., Nakatsuji, N., Overbeek, P.A., Hamada, H. and Yokoyama T. (1998). Cloning of inv, a gene that controls left/right asymmetry and kidney development. *Nature*, **395(6698)**, 177-181

Moffat, D.B. (1959). Developmental changes in the aortic arch system of the rat. *Am. J. Anat.* **105**, 1-35.

Moorman, A.F.M. and Lamers, W.H. (1992). Nieuwe ontwikkelingen in de cardiovasculaire embryologie. I. Hoe het embryonale hart kan werken zonder kleppen en zonder geleidingssysteem. Ned. Tijdschr. Geneesk. **136, 51**, 2503-2508.

Morgan, D., Turnpenny, L., Goodship, J., Dai, W., Majumder, K., Matthews, L., Gardner, A., Schuster, G., Vien, L., Harrison, W., Elder, F.F., Penman-Splitt, M., Overbeek, P., Strachan, T. (1998). *Inversin*, a novel gene in the vertebrate left-right axis pathway, is partially deleted in the *inv* mouse. *Nat. Genet.* **20(2)**, 149-56.

Murphy, P., Davidson, D.R. and Hill, R.E. (1989). Segment-specific expression of homeobox-containing gene in the mouse hindbrain. *Nature,* 341, 156-159.

Nadijcka, M and Hillman, N. (1974). Ultrastructural studies of the mouse blastocyst substages. *J. Embryol. Exp. Morph.* **32**, 675-695.

Nakagawa, M., Price, R.L., Chintanawonges, C., Simpson, D.G., Horacek, M.J., Borg, T.K. & Terracio, L. (1997). Analysis of heart development in cultured rat embryos. *J. Mol. Cell. Card.* **29**, 369-379.

Nakatsuji N., Snow M.H and Wylie, C.C. (1986). Cinemicrographic study of the cell movement in the primitive-streak-stage mouse embryo. *J. Embryol. Exp. Morphol.* **96**, 99-109.

Navaratnam, V. (1965). Development of the nerve supply to the human heart. *Br. Heart J.* **27**, 640-650.

Navaratnam, V. Kaufman, M.H., Skepper, J.N., Barton, S. and Guttridge, K.M. (1986). Differentiation of the myocardial rudiment of mouse embryos: an ultrastructural study including freeze-fracture replication. *J. Anat.* **146**, 65-85.

Niederreither K, Subbarayan V, Dolle P, Chambon P. (1999). Embryonic retinoic acid synthesis is essential for early mouse post-implantation development. *Nat. Genet.* **21(4)**, 444-8.

Nonaka, S., Tanaka, Y., Okada, Y., Takeda, S., Harada, A., Kanai, Y., Kido, M., Hirokawa, N. (1998). Randomization of left-right asymmetry due to loss of nodal cilia generating leftward flow of extraembryonic fluid in mice lacking KIF3B motor protein. *Cell* **11;95(6)**, 829-37.

Oka, C., Nakano, T., Wakeham, A., de la Pompa, J.L., Mori, C., Sakai, T., Okazaki, S., Kawaichi, M., Shiota, K., Mak, T.W. and Honjo, T. (1995). Disruption of the mouse RBP-Jκ gene results in early embryonic death. *Dev.* **121**, 3291-3301.

Okada, Y., Nonaka, S., Tanaka, Y., Saijoh, Y., Hamada, H. and Hirokawa, N. (1999). Abnormal nodal flow precedes situs inversus in *iv* and *inv* mice. *Mol. Cell.* **4**, 459-468.

Padget, D.H. (1948). The development of the cranial arteries in the human embryo. *Contrib. Embryol. Carnegie Inst.* **32**, 205-261.

Papaioannou, V.E. (1982) Lineage analysis of inner cell mass and trophectoderm using microsurgically reconstituted mouse blastocysts. *J. Embryol. Exp. Morphol.* **68**,199-209.

Paramaswaran, M. & Tam, P.P.L. (1995). Regionalisation of cell fate and morphogenetic movement of the mesoderm during mouse gastrulation. *Dev. Gen.* **17**, 16-28.

Patten, B.M. (1949). Initiation and early changes in the character of the heart beat in vertebrate embryos. *Physiol. Rev.* **29**, 31-47.

Pentecost, J.O. et al. (1999). 3D computer modelling of human cardiogenesis. *Comp. Med. Imag. Graph.* **23**, 45-49.

Poelmann, R.E. (1980). Differential mitosis and degeneration patterns in relation to the alterations in the shape of the embryonic ectoderm of early post-implantation mouse embryos. *J. Embryol. Exp. Morph.* **55**, 33-51.

Poelmann, R.E. (1981a). The formation of the embryonic mesoderm in the early post-implantation mouse embryo. *Anat. Embryol.* **162**, 29-40.

Poelmann, R.E. (1981b). The head-process and the formation of the definitive endoderm in the mouse embryo. *Anat. Embryol.* **162**, 41-49.

Quinlan, G.A., Williams, E.A., Tan, S. & Tam, P.P.L. (1995). Neurectodermal fate of epiblast cells in the distal region of the mouse egg cylinder: implication for body plan organization during early embryogenesis. *Dev.* **121**, 87-98.

Rappolee, D.A., Iyer, A. & Patel, Y. (1996). Hepatocyte growth factor and its receptor are expressed in cardiac myocytes during early cardiogenesis. *Circ. Res.* **78**, 1028-1036.

Ringwald, M., Baldock, R., Bard, J., Kaufman, M., Eppig, J. and Richardson, J. (1994). A Database for mouse development. *Science* **265**, 2033-2034.

Roebroek, A.J., Umans, L., Pauli, I.G., Robertson, E.J., van Leuven, F., Van de Ven, W.J., Constam, D.B. (1998). Failure of ventral closure and axial rotation in embryos lacking the proprotein convertase Furin. *Dev.* **125(24)**, 4863-76.

Rosenquist and Bergsma (199?). Morphogenesis and malformation of CVS. *New York: Alan R. Liss.*

Rosenquist, T.A. & Martin, G.R. (1995). Visceral endoderm-1 (VE-1): an antigen marker that distinguishes anterior from posterior embryonic visceral endoderm in the early post-implantation mouse embryo. *Mech. Dev.* 49, 117-121.

Rossant, J. Development of extraembryonic cell lineages in the mouse embryo. In: Concepts in mammalian embryogenesis, ed. M.I. Sherman. Cambridge, MA: MIT Press.

Rugh, R. (1968). The Mouse. Its reproduction and development. *Minneapolis: Burgess Publishing Company.*

Ryan, A.K., Blumberg, B., Rodriguez-Esteban, C., Yonei-Tamura, S., Tamura, K., Tsukui, T., de la Pena, J., Sabbagh, W., Greenwald, J., Choe, S., Norris, D.P., Robertson, E.J., Evans, R.M., Rosenfeld, M.G. and Izpisua

Belmonte, J.C. (1998). Pitx2 determines left-right asymmetry of internal organs in vertebrates. *Nature* **394**, 545-551.

Saijoh, Y., Adachi, H., Mochida, K., Ohishi, S., Hirao, A., Hamada, H. (1999). Distinct transcriptional regulatory mechanisms underlie left-right asymmetric expression of lefty-1 and lefty-2. *Genes Dev.* **13(3)**, 259-69.

SanchezQuintana, D., GarciaMartinez, V., Climent, V. & Hurle, J.M. (1995). orphological changes in the normal pattern of ventricular myoarchitecture in the developing human heart. *Anat. Rec.* **243**, 483-495.

SansComa, V., Fernandez, B., Duran, A.C., Thiene, G., Arque, J.M., MunozChapuli, R. & Cardo, M. (1996). Fusion of valve cushions as a key factor in the formation of congenital bicuspid aortic valves in Syrian hamsters. *Anat. Rec.* **244**, 490-498.

Scarborough, J., Aiton, J.F., McLachlan, J.C., Smart, S.D. and Whiten, S.C. (1997). The study of early human embryos using interactive 3-dimensional computer reconstructions. *J. Anat.* **191**, 117-122.

Schneider, A., Mijalski, T., Schlange, T., Dai, W., Overbeek, P., Arnold, H.H., Brand, T. (1999). The homeobox gene NKX3.2 is a target of left-right signalling and is expressed on opposite sides in chick and mouse embryos. *Curr. Biol.* **9(16)**, 911-914.

Schoenwolf, G.C. and Delongo, J. (1980). Ultrastructure of secondary neurulation in the chick embryo. *Am. J. Anat.* **158**, 43-63.

Sherwood, R.J., McLachlan, J.C., Aiton, J.F. and Scarborough, J. (1999). The vomeronasal organ in the human embryo, studied by means of three-dimensional computer reconstruction. *J. Anat.* **195**, 413-418.

Smith, B.R. (1996). Magnetic resonance microscopy with cardiovascular applications. *Tr. Cardiovasc. Med.* **6**, 247-254.

Smith, B.R. (2001). Magnetic resonance microscopy in cardiac development. *Microsc. Res. Techn.* **52**, 323-330.

Smith, B.R., Johnson, G.A., Groman, E.V. and Linney, E. (1994). Magnetic resonance microscopy of mouse embryos. *Proc. Natl. Acad. Sci. U.S.A.* **91**, 3530-3533.

Smith, L.J. (1980). Embryonic axis orientation in the mouse and its correlation with blastocyst relationships to the uterus. Part 1. Relationships between 82 hours and 4.25 days. *J. Embryol. Exp. Morph.* **55**, 257-277.

Smith, L.J. (1985). Embryonic axis orientation in the mouse and its correlation with blastocyst relationships to the uterus. Part II. Relationships between 4.5 and 9.5 days. *J. Embryol. Exp. Morph.* **89**, 15-35.

Smith, R. and McLaren, A. (1977) Factors affecting the time of formation of the mouse blastocoele. *J. Embryol. Exp. Morphol.* **41**, 73-92.

Snow, M.H.L. (1977). Gastrulation in the mouse: growth and regionalization of the epiblast. *J.Embryol. exp. Morph.* **42**, 293-303.

Snell, G.D. and Stevens, L.C. (1966). Early embryology. In: Biology of the laboratory mouse, 2nd edn. New York: McGraw-Hill.

Stalsberg, H. (1969). The origin of heart asymmetry: right and left contributions to the early chick embryo heart. *Dev Biol.* **19**, 109-27.

Stalsberg, H. (1970). Mechanism of dextral looping of the embryonic heart. *Am. J. Card.* **25**, 265-271.

Streicher, J., Donat, M.A., Strauss, B., Sporle, R., Schughart, K. and Muller, G.B. (2000). Computer-based three-dimensional visualization of developmental gene expression. *Nature Genetics* **25,** 147-152.

Sumida, H., Akimoto, N. and Nakamura, H. (1989). Distribution of the neural crest cells in the heart of birds: a three-dimensional analysis. *Anat. Embryol.* **180**, 29-35.

Taber, L.A., Sun, H., Clark, E.B. & Keller, B.B. (1994). Epicardial strains in embryonic chick ventricle at stages 16 through 24. *Circ. Res.* **75**, 896-903.

Tam, P.P.L. and Snow, M.H.L. (1981). Proliferation and migration of primordial germ cells during compensatory growth in mouse embryos. *J. Embryol. Exp. Morph.* **64**, 133-147.

Tam, P.P.L. (1981). The control of somitogenesis in mouse embryos. *J. Embryol. Exp. Morph.* **65**(supplement), 103-128.

Tam, P.P.L. and Meier, S. (1982). The establishment of a somitomeric pattern in the mesoderm of the gastrulating mouse embryo. *Am. J. Anat.* **164**, 209-225.

Tam, P.P.L. (1989). Regionalisation of the mouse embryonic ectoderm: allocation of prospective ectodermal tissues during gastrulation. *Dev.* **107**, 55-67.

Tam, P.P.L. and Beddington, R. (1992) Establishment and organization of germ layers in the gastrulating mouse embryo. In: Postimplantation development of the mouse. *CIBA Symposium* no.165. Chichester: John Wiley.

Tam, P.P.L., Williams, E.A. and Chan, W.Y. (1993). Gastrulation in the mouse embryo: ultrastructural and molecular aspects of germ layer morphogenesis. *Microsc. Res. Techn.* **26**, 301-328.

Theiler, K. (1972). The House Mouse: Development and normal stages from fertilization to 4 weeks of age. Berlin: Springer-Verlag.

Thomas, P. and Beddington, R. (1996). Anterior primitive endoderm may be responsible for patterning the anterior neural plate in the mouse embryo. *Curr. Biol.* **6-11**, 1487-1496.

Thomas, P.Q. and Beddington, R.S.P. (1998). Hex: a homeobox gene revealing peri-implantation asymmetry in the mouse embryo and an early transient marker of endothelial cell precursors. *Dev.* **125**, 85-94.

Tonegawa, A., Moriya, M., Tada, M., Nishimatsu, S., Katagiri, C. & Ueno, N. (1996). Heart formative factor(s) is localized in the anterior endodermof early Xenopus neurula. *Roux's Arch. Dev. Biol.* **205**, 282-289.

Tsukui, T., Capdevila, J., Tamura, K., Ruiz-Lozano, P., Rodriquez-Esteban, C., Yonei-Tamura, S., Magallon, J and Chandraratna, R.A. (1999). Multiple left-right asymmetric defects is *Shh* mutant mice unveil conversion of the *Shh* and retinoic acid pathways in control of Lefty-1. *Proc. Natl. Acad. Sci. U.S.A.* **96(20)**, 11376-11381.

VanPraagh, R., and DeHaan, R.L. Morphogenesis of the heart: mechanism of curvature, Annual report of the director, Department of embryology, Washington, D.C., Carnegie Institute Washington Yearbook, 536-537.

Varlet, I., Collignon, J. and Robertson, E.J. (1997). *Nodal* expression in the primitive endoderm is required for specification of the anterior axis during mouse gastrulation. *Dev.* **124**, 1033-1044.

Verbeek, F.J., Huijsmans, D.P., Baeten, R.J., Schoutsen, N.J. and Lamers, W.H. (1995). Design and implementation of a database and program for 3D reconstruction from serial sections: a data-driven approach. *Micr. Res. Tech.* **30 (6)**, 496-512.

Viragh, S. and Challice, C.E. (1973). Origin and differentiation of cardiac muscle cells in the mouse. *J. Ultrastr. Res.* **42**, 1-24.

Vuillemin, M. and Pexeider, T. (1989). Normal stages of cardiac organogenesis in the mouse: I. Development of the external shape of the heart. *Am. J. Anat.* **184**, 101-113.

Vuillemin, M. et al. (1992). A two-step alignment method for 3D computer-aided reconstruction. *Eur. J. Morphol.* **30**, 181-193.

Welsh, I.C., O'Brien, T.P. (2000). Loss of late primitive streak mesoderm and interruption of left-right morphogenesis in the Ednrb(s-1Acrg) mutant mouse. *Dev. Biol,* **225(11)**, 151-168.

Wenink, A.C. and Chon, Y. (1984). The value of graphic reconstructions - comparison with scanning electron microscopy. *Anat. Rec.* **210 (3)**, 537-540.

Westfall, M.V., Pasyk, K.A., Yule, D.I., Samuelson, L.C. & Metzger, J.M. (1997). Ultrastructure and cell-cell coupling of cardiac myocytes differentiating in embryonic stem cell cultures. *Cell Mot. Cytoskel.* **36**, 43-54.

Whiten, S., Smart, S.D., McLachlan, J.C. and Aiton, J.F. (1998). Computer aided interactive 3D reconstruction of the embryonic human heart. *J. Anat.* **193**, 337-346.

Wilens, S. (1955). The migration of heart mesoderm and associated areas in Amblystoma punctatum. *J. Exp. Zool.* **129**, 579-605.

Wilson, V., Manson, L., Skarnes, W.C. & Beddington, R.S.P. (1995). The *T* gene is necessary for normal mesodermal morphogenetic cell movements during gastrulation. *Dev.* **121**, 877-886.

Wilting, J., Brandsaberi, B., Kurz, H. and Christ, B. (1995). Development of the embryonic vascular system. *Cell. Mol. Biol. Res.* **41**; **4**, 219-232.

Witte, D.P., Aronow, B.J., Dry, J.K. and Harmony, J.A.K. (1994). Temporally and spatially restricted expression of apolipoprotein J in the developing heart defines discrete stages of valve morphogenesis. *Dev. Dyn.* **201**; **3**, 290-296.

Wu T.-C., Wan,Y.-J, Chung, A.E. & Damjanov, I. (1983). Immunohistochemical localization of entactin and laminin in mouse embryos and fetuses. *Dev. Biol.* **100**, 496-505.

Yan, Y.T., Grittsman, K., Ding, J., Burdine, R.J., Corrales, J.D., Price, S.M., Talbot, W.S., Schier, A.F. and Shen, M.M. (1999). Conserved requirement for EGF-CFC genes in vertebrate left-right axis formation. *Genes Dev.*, **13(19)**, 2527-37.

Yokoyama, T., Copeland, N., Jenkins, N.A., Montgomery, C.A., Elder, F.F.B. and Overbeek, P. (1993). Reversal of left-right asymmetry: a situs inversus mutation. *Science*, **260**, 679-682.

Yu, I.T. & Hutchins, G.M. (1996). Truncus arteriosus malformation: A developmental arrest at Carnegie stage 14. *Teratology*, **53**, 31-37.

Zernicka-Goetz, M., Pines, J., McLean Hunter, S., Dixon, J.P.C., Siemering, K.R., Haseloff, J. & Evans, M.J. (1997). Following cell fate in the living mouse embryo. *Dev.* **124**, 1133-1137.

APPENDIX 1: ANNOTATIONS ON ARTEFACTS IN THE GREY LEVEL IMAGES AND IMPLICATIONS FOR PAINTED TISSUES

GENERAL REMARKS:

The lists in this appendix detail the sections with disrupted tissue for each of the reconstructions. The lists also specify the implication of the disruption for the delineation of the anatomy in affected sections. The disruptions include dirt and bubbles under the coverslip or section, and folds, tears or loss of tissue. The lists do not include the minor squashing and stretching that comes about from sectioning the embryo and mounting the sections.

Naturally, the disruptions or artefacts prompt a decision on how to delineate the affected tissue: delineations can follow artefacts or ignore them and follow the presumed boundary had the tissue not been damaged. In the case of loss of tissue, we typically painted across the gap, to correct for the tissue lost. In the case of displaced tissue, the decision depended on the amount of tissue and the displacement: If the displacement is relatively small and the amount of tissue affected rather large, we followed the artefact, thus maintaining the benefit of matching histology and delineation. However, if the displacement is large compared to the amount of tissue affected, we chose to draw the boundary in the presumed correct position. Systematic artefacts (i.e. artefacts expected to occur in all similarly processed material) were not corrected.

In this appendix the nature of each artefact is listed, each embryo in a table, by transverse section number ('x-y view'). Affected tissues are displayed in bold and the delineation strategy with respect to the artefact is displayed in italics. There are three types of strategies: 'not corrected', 'painted across the gap' and 'corrected'. 'Not corrected' means that the delineation matches the artefact. 'Painted across the gap' means that the delineation matches the artefact crosses the crack or tear to match up with the tissue on the other side of the gap. The delineation across the gap is always the shortest line between two edges. 'Corrected' means that the delineation does not match the artefact and follows the track of what was believed to be normal anatomy which was deduced from unaffected, neighbouring sections.

NB: This document does not give details on sections that are not part of the reconstruction i.e. those that were too thin, too damaged or lost.

THEILER STAGE 2, E1

All sections were adequate and no corrections were required

THEILER STAGE 3, E2

All sections were adequate and no corrections were required

THEILER STAGE 3, E2.5

Section 27:	**zona pellucida** and **compacted morula** affected by air bubble under section.	ignored

THEILER STAGE 4, E3

All sections were adequate and no corrections were required

THEILER STAGE 5, E4

All sections were adequate and no corrections were required

THEILER STAGE 7, E5.5

All sections were adequate and no corrections were required

THEILER STAGE 8, E6

All sections were adequate and no corrections were required

THEILER STAGE 9, E6.5

Section 45:	**polar trophectoderm** affected by air bubble under section.	ignored
Section 110-112:	**polar trophectoderm** affected by air bubble under section.	ignored
Section 143:	**parietal endoderm** affected by air bubble under section. .	ignored
Section 144:	**polar trophectoderm** affected by air bubble under section.	ignored
Section 145:	**polar trophectoderm** and **parietal endoderm** affected by air bubble under section.	ignored

THEILER STAGE 10, E7

All sections were adequate and no corrections were required

THEILER STAGE 11, E7.5

Approximately 25% of sections for this reconstruction were image enhanced using 'Photoshop' in order to remove bubbles that were trapped under the sections. However, the enhanced sections are not mentioned in this list because the bubbles were never larger than a few cells, and neither the enhancement nor the bubbles influenced the delineation of anatomy.

Section 92:	Smaller than neighbouring sections. **Affecting all tissues**	ignored
Section 204:	Smaller than neighbouring sections. **Affecting all tissues**	ignored
Section 214:	Smaller than neighbouring sections. **Affecting all tissues** .	ignored
Section 271	**extraembryonic visceral endoderm, mural** - and **polar trophectoderm** and **parietal endoderm** affected by air bubble under section.	ignored
Section 327-328:	**mural trophectoderm** affected by air bubble under section.	ignored
Section 338:	Smaller than neighbouring sections. **Affecting all tissues**	ignored

Section 387:	Smaller than neighbouring sections. **Affecting all tissues**	ignored

THEILER STAGE 12, E8

Section 267:	**mesothelial lining of intraembryonic coelom, surface ectoderm** and **unsegmented mesenchyme** folded in tail region on the lhs.	ignored
Section 275:	**neural tissue** head region and **neural tissue, unesegmented mesenchyme** and **surface ectoderm** in the tail region on the lhs folded.	ignored
Section 304-335:	tear in frontal rhs neural fold in head region, between **neural tissue** and **surface ectoderm.**	painted across gap
Section 332:	tissue lost in lhs tail region affecting **mesothelial lining of intraembryonic coelom, surface ectoderm** and **unsegmented mesenchyme.**	painted across gap
Section 350:	tissue folded in rhs frontal **neural fold** in head region	ignored
Section 358:	smeared and lost tissue in lhs tail region affecting **surface ectoderm, unsegmented mesenchyme, neural tissue** and **dorsal aorta.**	corrected
Section 490-487:	25% of lhs tail region lost affecting **surface ectoderm, unsegmented mesenchyme, neural tissue** and **dorsal aorta**.	corrected

THEILER STAGE 13, E8.5

Section 62-146:	**mesothelial lining of intraembryonic coelom** and **wall of right dorsal aorta** torn in tail region on the rhs, approximately on the dorsal boundary between somatopleure and splanchnopleure of the mesothelial lining of the intraembryonic coelom.	painted across gap
Section 65-115:	**surface epithelium** torn in tail region on the rhs next to neural tissue.	painted across gap
Section 95:	**surface epithelium, unsegmented mesenchyme** and **mesothelial lining** of intraembryonic coelom torn in body region on the lhs next to gut. **surface epithelium** and **mesothelial lining of intraembryonic coelom** forming the body wall around the pericardiac cavity torn on the rhs.	painted across gap
Section 102-104:	**Ssurface epithelium** and **mesothelial lining of intraembryonic coelom** forming the body wall around the pericardiac cavity torn in the middle.	painted across gap
Section 104-176:	Crack in the **neural tissue** on the fusion site of the neural walls in the dorsal body region.	not corrected
Section 104-154:	body wall around the **pericardiac cavity** torn on the rhs affecting **surface epithelium, mesothelial lining of intraembryonic coelom** and **unsegmented mesenchyme.** From section 151-154 tear also affects **right horn of the sinus venosus.**	painted across gap
Section 120-159:	**rest of primitive gut** torn in several places in tail region around notochord.	painted across gap
Section 124-147:	**body wall** around the **pericardiac cavity** torn on the lhs affecting **surface epithelium** and **mesothelial lining of intraembryonic coelom.**	corrected
Section 131-180:	**mesothelial lining of intraembryonic coelom** and **wall of common atrium** torn in several places around the coelomic cavity on the rhs.	painted across gap
Section 140-156:	**mesothelial lining of intraembryonic coelom** and **wall of common atrium** torn in several places around the coelomic cavity on the lhs.	painted across gap
section 147-170:	crack in the fusion site of the neural walls in the tail region.	not corrected
Section 149-188:	**rest of primitive gut** torn in several places in body region.	painted across gap or corrected
Section 172-186:	**mesothelial lining of intraembryonic coelom** torn in the rhs ventral tip of the body region.	painted across gap
Section 156-174:	right dorsal aorta torn in the body region ventral aspect.	painted across gap

THEILER STAGE 14, E9

All:	Crack along almost the entire length of the future brain and future spinal cord, on the fusion site of the neural walls:	not corrected
Section 18-20:	future spinal cord lost in the tail region:	painted across gap
Section 30 to 32:	tear in future spinal cord, posterior region.	painted across gap

Section 45-103:	tear in the mesothelial lining of peritoneal cavity of left coelomic cavity, approximately on the dorsal boundary between somatopleure and splanchnopleure.	painted across gap
Section 60-76:	tear in the mesothelial lining of peritoneal cavity of left coelomic cavity, approximately on the ventral boundary between somatopleure and splanchnopleure.	painted across gap
Section 60-96, 158-174:	tear in the mesothelial lining of peritoneal cavity of right coelomic cavity, approximately on the dorsal boundary between somatopleure and splanchnopleure.	painted across gap
Section 67-151:	tear in the gut and right dorsal aorta in dorsal region.	painted across gap
Section 70-77:	tear in floor plate of future brain.	
Section 110-111+114:	tear in prosencephalon of future brain.	corrected
Section 126-206:	tear (sometimes in two places) in the mesothelial lining of peritoneal cavity, mesenchyme and surface epithelium of right somatopleure. 126 -153 + 200-206: tear only in mesothelial lining of peritoneal cavity. 154-200: tear in mesothelial lining, mesenchyme and surface epithelium. 168: tissue between the two cracks folded over.	not corrected
Section 126-206:	tear (sometimes in two places) in the mesothelial lining of peritoneal cavity, mesenchyme and surface epithelium of right somatopleure. 126-158,185-206:	painted across gap
Section 126-206:	tear (sometimes in two places) in the mesothelial lining of peritoneal cavity, mesenchyme and surface epithelium of right somatopleure. 159-184:	corrected
Section 130-138:	tear in and loss of tissue of mesenchyme and surface epithelium of first branchial arch, left. 130-135,137-138:	painted across gap
Section 130-138:	tear in and loss of tissue of mesenchyme and surface epithelium of first branchial arch, left. 136:	corrected
Section 136-210:	body wall (mesothelial lining of pericardiac cavity and surface epithelium) torn in several places, in almost every section (of the ones mentioned above).	corrected
Section 141-144:	tissue of future brain (ventral side of rostral tip) lost.	painted across gap
Section 184:	tissue lost in wall of common atrium.	painted across gap
Section 192:	partially lost, posterior region of embryo. Affecting surface epithelium, future spinal cord, somite.	corrected
Section 209:	end of vitelline artery in model. Site of dissection of model from maternal blood flow.	
Section 221-245:	Site of dissection of embryo from supporting membrane. Affecting gut, mesothelial lining of peritoneal cavity and possibly septum transversum.	
Section 234:	folded in anterior region. Tissues affected: body and head mesenchyme, mesothelial lining of pericardio-peritoneal canal, gut, dorsal aorta, somite, surface epithelium, and right horn of sinus venosus.	sinus venosus corrected, rest not corrected.

APPENDIX 2: ANNOTATIONS ON ARBITRARY BOUNDARIES OF TISSUES

GENERAL REMARKS:

The delineation of tissue boundaries is based on cell shape and configuration as seen in the original sections under a microscope. Where it was not possible to base boundaries on these grounds, we tried to look in other planes in the digital model. In a few cases, this led to an unambiguous boundary e.g. for the somites. However, in the majority of the cases in which boundaries could not be discerned in the original sections, decisions had to be based on other criteria than cell shape and configuration; we call these arbitrary boundaries. Arbitrary boundaries are generally based on 3-dimensional shape, for example, the division between the branchial arch and the rest of the embryo.

In this document tissues are listed with arbitrary boundaries and the grounds for each decision. The tissues are listed alphabetically in bold under the main components in the anatomy nomenclature database (Bard *et al.*, 1998). Boundaries which, though based on cell shape and configuration, were doubtful are also listed.

THEILER STAGE 4, E3

Extra-embryonic component	**Trophectoderm**	Boundary between **polar** and **mural ectoderm** determined by position of **inner cell mass**

THEILER STAGE 5, E4

Extra-embryonic component	**Trophectoderm**	Boundary between **polar** and **mural ectoderm** determined by position of **inner cell mass**

THEILER STAGE 7, E5.5

Embryo	**Endoderm**	Boundary between **embryonic endoderm** and **extraembryonic (visceral) endoderm** based on extent of **epiblast**.
	Mesoderm	Boundary between **embryonic mesoderm** and **extraembryonic (visceral yolk sac) mesoderm** based on extent of **epiblast**.
	Cavities and linings	Boundary between **embryonic** and **extraembryonic component of proamniotic cavity** based on extent of **epiblast**
Extra-embryonic component	**Trophectoderm**	Boundary between **extraembryonic ectoderm** and **ectoplacental cone** determined by proximal boundary of **visceral endoderm**.

THEILER STAGE 8, E6

Embryo	**Endoderm**	Boundary between **embryonic endoderm** and **extraembryonic (visceral)**

		endoderm based on extent of **epiblast**.
	Mesoderm	Boundary between **embryonic mesoderm** and **extraembryonic (visceral yolk sac) mesoderm** based on extent of **epiblast**.
	Cavities and linings	Boundary between **embryonic** and **extraembryonic component of proamniotic cavity** based on extent of **epiblast**
Extra-embryonic component	**Trophectoderm**	Boundary between **extraembryonic ectoderm** and **ectoplacental cone** determined by proximal boundary of **visceral endoderm**.

THEILER STAGE 9, E6.5

Embryo	**Primitive streak**	If no different organisation of cells between **epiblast** and **embryonic mesoderm** can be distinguished, the area was defined as primitive streak.
	Endoderm	Boundary between **embryonic endoderm** and **extraembryonic (visceral) endoderm** based on extent of **epiblast**.
	Mesoderm	Boundary between **embryonic mesoderm** and **extraembryonic (visceral yolk sac) mesoderm** based on extent of **epiblast**.
	Cavities and linings	Boundary between **embryonic** and **extraembryonic component of proamniotic cavity** based on extent of **epiblast**
Extra-embryonic component	**Trophectoderm**	Boundary between **extraembryonic ectoderm** and **ectoplacental cone** determined by proximal boundary of **visceral endoderm**.

THEILER STAGE 10, E7

Embryo	**Primitive streak**	If no different organisation of cells between **epiblast** and **embryonic mesoderm** can be distinguished, the area was defined as primitive streak.
	Endoderm	Boundary between **embryonic endoderm** and **extraembryonic (visceral) endoderm** based on extent of **epiblast**.
	Mesoderm	Boundary between **embryonic mesoderm** and **extraembryonic (visceral yolk sac) mesoderm** based on extent of **epiblast**.
	Cavities and linings	Boundary between **embryonic** and **extraembryonic component of proamniotic cavity** based on extent of **epiblast**
Extra-embryonic component	**Amniotic fold**	Boundary between **ectodermal component of amniotic fold** and **epiblast/extraembryonic ectoderm** based on 3D shape.
	Trophectoderm	Boundary between **extraembryonic ectoderm** and **ectoplacental cone** determined by proximal boundary of **visceral endoderm**. The **ectoplacental cone** may contain some **parietal endoderm** cells
	Endoderm	All endoderm considered to be **visceral** since **parietal endoderm** was removed with **Reichert's membrane**

THEILER STAGE 11, E7.5

Embryo	**Primitive streak**	If no different organisation of cells between **epiblast** and **embryonic mesoderm** can be distinguished, the area was defined as primitive streak.
	Endoderm	Boundary between **embryonic endoderm** and **extraembryonic (visceral) endoderm** based on extent of **epiblast**.
	Mesoderm	Boundary between **embryonic mesoderm** and **extraembryonic (visceral yolk sac) mesoderm** based on extent of **epiblast**.
Extra-embryonic component	**Allantois**	Boundary between **mesodermal component of visceral yolk sac** and the **allantois** is based on 3D shape only.
	Amnion	Boundary between **ectodermal component of amnion** and **epiblast** based on 3D shape. Boundary between **mesodermal component of amnion** and **mesodermal component of visceral yolk sac** based on cell layers: cells were labelled as **mesodermal component of amnion** when there is only one cell layer present

		on top of **ectodermal component of amnion**.
	Chorion	Boundary between **ectoderm of chorion** and **ectodermal component of the egg cylinder wall** based on 3D shape.
	Trophectoderm	Boundary between **extraembryonic ectoderm** and **ectoplacental cone** determined by proximal boundary of **visceral endoderm**.

THEILER STAGE 12, E8

Embryonic /extra-embryonic boundary	**Lumina:**	*Painting was done on the basis of the original transverse sections, so the comments should be considered from that viewpoint.* Each intraembryonic lumen that is formed gradually is included in intraembryonic space from the moment that the tissues that will eventually enclose the lumen, start to rise. The lumen will thus be bordered by the shortest line (in the transverse section plane) between the tips of the tissues that will fuse to enclose it. An example is the lumen of the forming neural tube. This comment applies to: neural lumen, peritoneal cavity, gut lumen. Lumina that will never be fully enclosed are not considered to be intraembryonic.
Body cavity	**Cavities of peritoneum, pericardio-peritoneal canals and pericardiac cavity**	Division between these parts based on 3D shape and location of the **heart** and the **septum transversum.**
	Mesothelial lining of peritoneum, pericardio-peritoneal canals and pericardiac cavity	Based on the boundaries of the cavities of these components.
Head-body division	**Somites**	The first four visible somites are thought to be **occipital somites**. This assumes that the first, transient somite has disintegrated.
	Nervous tissue (future brain and future spinal cord):	Based on the division of **future brain** and **future spinal cord** according to our assessment of position in the embryo as a whole and morphology of the **neural tube**. This boundary is approximate. Correlation with gene expression patterns and other data will be required to determine the true position of the 'head/body' boundary
	Mesenchyme	Based on the division of the somites into head- and body somites
Heart	**Cardiac jelly and endothelium of different parts of the heart:**	Boundaries designed to follow the boundaries of the wall of the heart, unless otherwise state
	Wall:	Boundary with **septum transversum** based on difference in cell compaction. Boundary with **mesothelial lining of pericardio-peritoneal canals** based on 3D shape and a possible slight difference in cell compaction.
	Endothelial lining:	Boundary with **sinus venosus**: Cranial end of sinus venosus ends where the **lumen of the common atrium** splits into two parts. Boundary with **mesothelial lining of pericardiac cavity** defined by both the extension of **cardiac jelly** and 3D shape of the wall and **mesothelial lining of pericardiac cavity**
Mesenchy-me:	**Intermediate mesenchyme:**	Condensed mesenchyme between **somites** and **lateral plate mesenchyme**. Where it has differentiated into two parts, the medial part is labelled as **nephrogenic cord** and the lateral part as **presumptive nephric duct**.
	Splanchnic / somatic, lateral plate mesenchyme:	Medial extension of the **splanchnopleure-** and **somatopleure-derived mesoderm** is defined by the extension of the **mesothelial lining of the peritoneum**. We have divided the **lateral plate mesenchyme** from the **head mesenchyme** at caudal level of the **pericardial-peritoneal canal**.
	Paraxial mesenchyme:	**Mesenchyme** medial to the lateral plate mesenchyme, caudal to the **somites** and rostral and lateral to the **primitive streak**.
	Intercellular space:	Those spaces between and around **somites** and **intermediate mesoderm** that may result from shrinkage during fixation.

	Notochord:	We based the presence of a **notochord** on a distinctly different cellular organisation from the adjacent future **neural tube**. If there is no different organisation of cells the area was defined as **primitive streak**. Boundary between **notochord** and surrounding mesenchyme was based on cell arrangement.
	Somites:	Most caudal site of radial cell organisation on microscopic level defined as the **last-formed somite**.
Vascular system:		All boundaries between different parts based on 3D shape only

THEILER STAGE 13, E8.5

Embryonic /extra-embryonic boundary		*Painting was done on the basis of the original transverse sections, so the comments should be considered from that viewpoint.*
	Lumina	Each intraembryonic lumen that forms is gradually included in intraembryonic space from the moment that the tissues that will enclose the lumen start to form. The lumen will thus be bordered by the shortest line (in the transverse section plane) between the tips of the tissues that will fuse to enclose it. An example is the lumen of the forming neural tube, others are the peritoneal cavity andgut. Lumina that will never be fully enclosed are not considered to be intraembryonic.
Body cavity:	**Cavities of peritoneum, pericardio-peritoneal canals and pericardiac cavity:**	Division between these parts based on 3D shape and location of the **heart** and the **septum transversum**.
	Mesothelial lining of peritoneum, pericardio-peritoneal canals and pericardiac cavity:	Based on the boundaries of the cavities of these components.
Branchial arches:		Boundary with **head mesenchyme** based on difference in grey level density of the two tissues.
	Surface epithelium and endodermal lining of the branchial arch:	Those parts of **gut** and **surface epithelium** that touch the **mesenchyme** of the **branchial arch**. **Endoderm**: **endodermal lining** is that part of the gut lining the arch.
	Branchial pouches:	Separation from **gut** based on 3D shape only.
Head-body division:	**Somites**	The first four visible **somites** are thought to be **occipital somites**. This assumes that the first, transient somite has disintegrated.
	Nervous tissue (future brain and future spinal cord):	Based on the division of future **brain** and future **spinal cord** according to our assessment of position in the embryo as a whole and the morphology of the **neural tube**. This boundary is approximate. Correlation with gene expression patterns and other data will be required to determine the true position of the 'head/body' boundary.
	Mesenchyme	Based on the division of the **somites** into head- and body somites.
Heart:		
	Cardiac jelly and endothelium of different parts of the heart:	Boundaries designed to follow the boundaries of the walls of the **heart**, unless otherwise stated.
	Common atrium wall:	Boundary with **septum transversum** based on difference in cell compaction. Boundary with **mesothelial lining of pericardio-peritoneal canals** based on 3D shape and a possible slight difference in cell compaction. Boundary with **primitive ventricle** constructed by propagating the line connecting the **atrio-ventricular canal** and **atrio-ventricular groove** cranially.
	Endothelial lining:	Boundary with **sinus venosus**: Cranial end of **sinus venosus** ends where the lumen of the **common atrium** splits into two parts.

	Primitive ventricle wall:	Boundary with **outflow tract** constructed by extrapolating the **bulbo-ventricular groove** cranially.
	Outflow tract wall:	Boundary with **mesothelial lining of pericardiac cavity** defined by both the extension of **cardiac jelly** and 3D shape of the wall and **mesothelial lining of pericardiac cavity**. Boundary with **bulbus cordis** based on 3D shape only
Mesenchyme:	**Body mesenchyme:**	Those parts of the **body mesenchyme** that are not **paraxial, lateral plate or segmented (somites, intermediate mesoderm, nephrogenic cord, presumptive nephric duct).** Contains **sclerotome-derived** and **neural-crest-derived** cells.
	Intermediate mesenchyme:	Condensed mesenchyme between **somites** and **lateral plate mesenchyme**. Where it has differentiated into two parts, the medial part is labelled as **nephrogenic cord** and the lateral part as **presumptive nephric duct.** **Intermediate mesenchyme** may contain migrating **neural-crest-derived melanoblasts** and **somite-derived myoblasts**.
	Splanchnic / somatic, lateral plate mesenchyme:	Medial extension of the **splanchnopleure-** and **somatopleure-derived mesoderm** is defined by the extension of the **mesothelial lining of the peritoneum**. We have divided the **lateral plate mesenchyme** from the head mesenchyme at the mid level of the **pericardial-peritoneal canal**.
	Paraxial mesenchyme:	Mesenchyme medial to the **lateral plate mesenchyme,** caudal to the **somites** and rostral and lateral to the **primitive streak**.
	Intercellular space:	Those spaces between and around **somites** and **intermediate mesoderm** that may result from shrinkage during fixation.
	Notochord:	We based the presence of a **notochord** on a distinctly different cellular organisation from the adjacent **future spinal cord**. If there is no different organisation of cells the area was defined as **primitive streak**. Boundary between **notochord** and **surrounding mesenchyme** was based on cell arrangement.
	Somites:	Most caudal site of radial cell organisation on microscopic level defined as the last-formed **somite.**
Neural crest:	**Facio-acoustic and trigeminal neural crest:**	Separation from mesenchyme on the basis that the neural-crest-derived cells that form these **ganglia** are more compacted than the surrounding mesenchyme. Therefore, ganglia cells may be excluded and other head mesenchyme cells included or vice versa. **Neural crest cells** have not been painted within the branchial arches, because these could not be recognised morphologically.
Sensory organs:	**Optic vesicles:**	Separation from **future brain** based on 3D shape only.
Vascular system:		All boundaries between different parts based on 3D shape only.

THEILER STAGE 14, E9

Embryonic /extra-embryonic boundary:		Painting was done on the basis of the original transverse sections, so the comments should be considered from that viewpoint.
	Lumina:	Lumina: Each intraembryonic lumen that is formed gradually is considered to be included in intraembryonic space from the moment the tissues that will enclose the lumen start to rise. The lumen will thus be bordered by the shortest line (in the transverse section plane) between the tips of the tissues that will later fuse to enclose it. An example is the lumen of the forming neural tube. Affecting: neural lumen, peritoneal cavity, gut, otic pit. Lumina that will never be fully enclosed are not considered to be intraembryonic.
		Boundary between the embryo and the allantois is based on 3D shape.

Body cavity:	Peritoneal cavity, pericardio-peritoneal canals and pericardiac cavity:	Division between these parts based on 3D shape and location of the heart and the septum transversum.
	Mesothelial lining of peritoneum, pericardio-peritoneal canals and pericardiac cavity:	Based on the boundaries of the **cavities** of these components.
Branchial arches:	All.	Boundary with **head mesenchyme** based on 3D shape and difference in grey level density of the two tissues.
	Surface epithelium and endodermal lining of the branchial arches and branchial pouches:	Those parts of **gut** and **surface epithelium** that touch the mesenchyme of the branchial arches. For the endoderm: endodermal lining: parts of the gut that lines the arches, but excluding the **branchial pouches**. Branchial pouches are based on 3D shape.
Surface epithelium:	Rathke's pouch:	Separation from **surface epithelium** based on 3D shape only.
	Surface epithelium of the branchial arches:	See under **branchial arches**.
Gut:	Biliary bud:	Separation from **gut** based on 3D shape only.
	Thyroid primordium:	Separation from **gut** based on 3D shape only.
	Branchial pouches:	Separation from **gut** based on 3D shape only.
	Endodermal lining of branchial arches:	See under **branchial arches**.
Head-body division:	Somites:	The first four visible somites are considered to be the occipital somites. This assumes that the first, transient somite has disintegrated.
	Nervous tissue (future brain and future spinal cord):	Based on the division of future brain and future spinal cord according to our assessment of position in the embryo as a whole and morphology of the neural tube. This boundary is approximate. Correlation with gene expression patterns and other data will be required to determine the true position of the head/body boundary.
	Mesenchyme:	Based on the division of the somites into **head- and body-somites**.
Heart:	Cardiac jelly and endothelium of different parts of the heart:	Boundaries follow the boundaries of the **walls of the heart**, unless otherwise stated.
	Common atrium wall:	Boundary with **septum transversum** based on difference in cell compaction. Boundary with **mesothelial lining of pericardio-peritoneal canals** based on 3D shape and a possible slight difference in cell compaction. The laterally asymmetric shape of the embryo accords with the observation that the atrial wall extends further caudally on the left than on the right.
	Common atrium endothelial lining:	Boundary with **primitive ventricle** was constructed by extrapolating cranially the line connecting the **atrio-ventricular canal** and **atrio-ventricular groove**. Boundary with **sinus venosus**: the cranial end of sinus venosus is taken as the point where the lumen of the common atrium splits into two parts.
	Primitive ventricle:	Boundary with **outflow tract** was constructed by extrapolating the **bulbo-ventricular groove** cranially.
	Outflow tract:	Boundary with **mesothelial lining of pericardiac cavity** is defined by both the extent of cardiac jelly and 3D shape of the wall of the **pericardiac cavity**. Boundary with **bulbus cordis** is based on 3D shape.
Mesenchyme:	Body mesenchyme:	Those parts of the **body mesenchyme** that are not **paraxial**, **intermediate**, or **lateral plate mesenchyme**. Contains sclerotome-derived and neural-crest-derived cells. (Affected: ***somites*, intermediate mesoderm, *nephrogenic cord*, *presumptive nephric duct***).
	Intermediate mesenchyme:	Condensed mesenchyme between the **somites** and the **lateral plate mesenchyme**. Where it has differentiated into two parts, the medial part is labelled **nephrogenic cord** and the lateral part **presumptive nephric duct**. **Intermediate mesenchyme** may contain migrating neural-crest-derived and somite-derived cells.
	Splanchnic / somatic, lateral plate mesenchyme:	Medial limits of the **splanchnopleure**- and **somatopleure**-derived **mesoderm** are defined by the medial extension of the **mesothelial lining of the peritoneum**.

	Unsegmented paraxial mesenchyme:	Mesenchyme medial to the **lateral plate mesenchyme**, caudal to the somites and rostral and lateral to the primitive streak.
	Intercellular space:	Spaces between and around **somites** and **intermediate mesoderm** that may result from shrinkage during fixation.
	Facio-acoustic and trigeminal neural crest:	Separation from **mesenchyme** on the basis that the neural-crest-derived cells that form these ganglia are more compacted than the surrounding mesenchyme. Therefore, ganglia cells may be excluded and other head mesenchyme cells included or vice versa. Other neural-crest-derived cells have not been painted because these could not be recognised morphologically.
	Somites	Most caudal site of radial organisation in cells of the **paraxial mesenchyme**, as observed under the microscope, is defined as the last formed **somite**.
	Notochord	The presence of a notochord was based on a distinctly different cellular organisation from the adjacent **future spinal cord**. If there is no different organisation of cells the area is labelled primitive streak. Boundary between notochord and surrounding ***mesenchyme*** is based on cell arrangement.
Sensory organs:	Optic vesicles:	Separation from future brain based on 3D shape only.
Vascular system:		All boundaries between different parts based on 3D shape only.